NTNU

Norwegian University of
Science and Technology

Numerical and Experimental Analysis of General Mixed Mode I/II/III Fracture of Polymethyl Methacrylate

Haakon Lie Hokstad

Mechanical Engineering
Submission date: June 2018
Supervisor: Filippo Berto, MTP
Co-supervisor: Seyed Mohammed Javad Razavi, MTP

Norwegian University of Science and Technology
Department of Mechanical and Industrial Engineering

Preface

The presented dissertation was submitted for the degree Master of Science, M.Sc. This thesis has been carried out at the department of mechanical and industrial engineering, faculty of engineering, at the Norwegian University of Science and Technology. The thesis was written under the supervision of Professor Filippo Berto, during the spring semester of 2018. The presented dissertation was the concluding work of a M.Sc. degree in mechanical engineering.

Haakon Lie Hokstad
Trondheim, 2018-06-11

Abstract

Mixed mode loading often has a significant effect on fracture behaviour in components. Cracks is in many cases the reason for failure or fracture of a component. All of the mechanisms of cracks and fracture behaviour are still not completely known. This also applies for the three dimensional loading case of mixed mode I/II/III. This thesis will therefore study the existing theory on two dimensional, and three dimensional mixed mode loading. Mixed mode I/II/III brittle fracture behaviour of polymethyl methacrylate, PMMA, will be studied experimentally and theoretically, using pre-cracked CTS specimens. This specimens contains pre-cracks and will be subjected to different mixed mode loading conditions, ranging from pure mode I to pure mode II and pure mode III. During this thesis, a mixed mode I/II/III loading device were designed and used for the experimental procedure. Experiments were conducted on all twenty five combinations of the loading device. The presented mixed mode loading device allowed mixed mode I/II/III loading combinations in steps of 22.5°, for in and out of plane rotations. After the conducted experiments, fracture loads were obtained. In-plane crack initiation angles and out of plane crack initiation angles were measured for all of the fractured specimens. These experimentally obtained results were then compared with predictions of various fracture criteria. Maximum tangential stress criterion, MTS, generalized maximum tangential stress criterion, GMTS, and the criterion by Richard were used for numerical predictions in this thesis. Numerical analysis were conducted by obtaining results from three-dimensional finite element simulations in Abaqus, and applying them in different fracture criteria. The criteria showed a good relation with experimentally obtained angles.

Sammendrag

Flermode-last har ofte en signifikant effekt når det kommer til bruddadferd i komponenter. Sprekker er i mange tilfeller årsaken til feil eller brudd i en komponent eller struktur. Det eksisterer fortsatt mekanismer for sprekker og bruddadferd som ikke er kjent. Dette gjelder også for flermode lasttilefeller i tre dimensjoner, I/I-I/III. Denne masteroppgaven vil derfor studere eksisterende teori av flermode-last i to og tre dimensjoner. Bruddoppførsel av PMMA under tre-dimensjonal flermode-last, vil bli undersøkt ved hjelp av fysiske eksperiment og teoretiske beregninger. Prøvestykker av typen CTS, vil bli benyttet for strekktesting. Dette prøvestykket er konstruert med en påbegynt sprekk. Prøvestykket vil bli utsatt for ulike tre-dimensjonale flermode-last kombinasjoner, fra ren mode I til ren mode II og ren mode III. I denne masteroppgaven vil en test-rigg, som tillater flermode-last i tre dimensjoner, bli designet og konstruert. Denne test-riggen ble benyttet i de fysiske eksperimentene. Tester ble gjennomført i riggens tjuefem last kombinasjoner. Test-riggen kan belaste prøvestykket, med flermode-last, i steg på 22.5°, rotasjon om to akser. Etter at strekktestene var gjennomført ble bruddlaster hentet. Vinkler, og vridningsvinkler, ble målt på alle prøvestykker ved hjelp av et mikroskop. Resultater fra eksperimentene ble deretter sammenlignet med resultatene fra teoretiske kriterier og numeriske analyser. Bruddkriteriene MTS, GMTS og Richards kriteria ble benyttet for teoretisk predikering av bruddvinkler og bruddgrenser. Numeriske analyser ble gjennomført i programvaren Abaqus, ved hjelp av tre-dimensjonal elementmetode-simuleringer. Verdier fra Abaqus ble deretter implementert i de nevnte kriteriene. Kriteriene viste seg å stemme godt med de målte bruddvinklene.

Acknowledgment

I would like to thank my supervisor Professor Filippo Berto and co-supervisor Seyed Mohammad Javad Razavi for the help they gave me on the different challenges that occurred during this master thesis. Several hours of consulting were used when learning the necessary software, theory and numerical analyses used in this work. I would also like to thank Carl-Magnus Midtbø for the manufacturing of the mixed mode I/II/III loading device and for setting up the tensile testing machines. I would like to thank Øystein Hagemo and his colleagues, at the Realfagsbygget workshop, for manufacturing all of the specimens in this thesis. Finally, I would like to thank Andrey Krauklis and Abedin Gagani for teaching and letting me use their microscope for cracked specimen processing.

Abbreviations

FEA	Finite element analysis
LEFM	Linear elastic fracture mechanics
UTS	Ultimate tensile strength
ASED	Average strain energy density
MTS	Maximum tangential stress criterion
GMTS	Generalized maximum tangential stress criterion
PMMA	Polymethyl methacrylate
AFM	All fracture mode loading device
CTS	Compat tension shear specimen
CAD	Computer-aided design
CNC	Computer numerical control
MPC	Multipoint constraint
AECT	Asymmetric edge cracked triangular specimen
AECS	Asymmetric edge cracked semicircular specimen
SCB	Semi-circular bend specimen
SIF	Stress intensity factor
VPN	Virtual private network
NTNU	Norges teknisk-naturvitenskapelige universitet Norwegian university of science and technology
IPM	Institutt for produktutvikling og material Department for mechanical and industrial engineering

Contents

Preface i

Abstract iii

Sammendrag v

Acknowledgement vii

Abbreviations ix

1 Introduction 1
- 1.1 Background & Motivation . . . 1
- 1.2 Problem Description . . . 1
- 1.3 Scope of This Work . . . 1
  - 1.3.1 Objectives . . . 1
  - 1.3.2 Limitations . . . 2
- 1.4 Previous Work . . . 2
- 1.5 Thesis Structure . . . 2

2 Theory & Literature Review 3
- 2.1 Linear Elastic Fracture Mechanics . . . 3
- 2.2 Poly(Methyl Methacrylate), PMMA . . . 3
- 2.3 Stress Analysis of Cracks . . . 3
  - 2.3.1 Stress Intensity Factor . . . 4
- 2.4 Mixed Mode Loading . . . 5
- 2.5 The Elastic T Stress . . . 6
- 2.6 Fracture Criteria . . . 7
  - 2.6.1 Fracture Criteria Formulation . . . 7
  - 2.6.2 Maximum Tangential Stress Criterion, MTS . . . 12
  - 2.6.3 Generalized Maximum Tangential Stress Criterion, GMTS . . . 13
  - 2.6.4 Three Dimensional Criterion by Richard . . . 15
  - 2.6.5 Dimensionless Factors . . . 17
- 2.7 Existing Mixed Mode Loading Devices . . . 18

3 Modeling of Mixed Mode Loading Devices 19
- 3.1 AFM Loading Device . . . 19
  - 3.1.1 Modeling of AFM Specimen . . . 19
  - 3.1.2 Modeling of AFM Fixture . . . 19
  - 3.1.3 Assembly of AFM Loading Device . . . 20
- 3.2 Mixed Mode I/II/III Loading Device . . . 21
  - 3.2.1 Modeling of CTS Specimen . . . 21
  - 3.2.2 Modeling of C-Fixture . . . 21
  - 3.2.3 Modeling of J-Fixture . . . 22
  - 3.2.4 Forks . . . 23

3.2.5 Assembly of Mixed Mode I/II/III Loading Device 23

4 Manufacturing Method **25**
4.1 CTS Specimen 25
4.2 Mixed Mode I/II/III Loading Device 26

5 Numerical Analyses & Criteria Procedure **29**
5.1 Numerical Analysis Set-up for Loading Device 29
5.1.1 Properties 29
5.1.2 Interactions & Constraints 29
5.1.3 Partitioning & Crack Assignment 30
5.2 Verification of Fixtures 31
5.2.1 Fixture & Specimen Mesh 33
5.2.2 Total Mesh & Element Types 35
5.2.3 Load & Boundary Conditions 35
5.2.4 Loading Cases 36
5.3 Stress Intensity Factors & T-Stresses 37
5.4 Criteria Procedure 39
5.4.1 Mixed Mode I/II 39
5.4.2 Mixed Mode I/III 39
5.4.3 Mixed Mode II/III 41

6 Experimental Procedure **43**
6.1 PMMA Dog-bone Testing 43
6.2 Mixed Mode I/II/III Testing 46
6.2.1 Loading Device Setup 46
6.2.2 Mixed Mode Testing Cases 47
6.3 Specimen Crack Paths 50
6.3.1 In Plane Crack Path 50
6.3.2 Out of Plane Crack Path 53
6.3.3 Measured Crack Initiation Angles 56

7 Results & Discussion **59**
7.1 Geometry Factors 59
7.1.1 Geometry Factors for Mixed Mode I/II 59
7.1.2 Geometry Factors for Mixed Mode I/III 61
7.1.3 Geometry Factors for Mixed Mode I/II/III 62
7.1.4 Geometry Factors for Mixed Mode II/III 65
7.2 Mixed Mode I/II/III Fracture Loads 66
7.3 T-Stress 69
7.3.1 T-Stress for Mixed Mode I/II 69
7.3.2 T-Stress for Mixed Mode I/III 71
7.3.3 T-Stress for Mixed Mode I/II/III 72
7.3.4 T-Stress for Mixed Mode II/III 75
7.4 Fracture Criteria & Test Results 76

7.4.1 Mixed Mode I/II 76
7.4.2 Mixed Mode I/III 79
7.4.3 Mixed Mode II/III 81
7.4.4 Comparison of Measured and Theoretical Predictions of Fracture Angles 84
7.4.5 Three Dimensional Mixed Mode Criterion 85

8 Conclusion **87**

9 Further Work **88**

References **89**

Appendices **I**

A Technical Drawing of AFM Specimen **I**

B Technical Drawing of AFM Fixture **III**

C Technical Drawing of CTS Specimen **V**

D Technical Drawing of mixed mode I/II/III C-fixture **VII**

E Technical Drawing of mixed mode I/II/III J-fixture **IX**

F Table of KI Values **XI**

G Table of KII Values **XIII**

H Table of KIII Values **XV**

I Table of YI Values **XVII**

J Table of YII Values **XIX**

K Table of YIII Values **XXI**

L Table of T-Stress **XXIII**

M Table of Dimensionless T Values **XXV**

N Python Script For Mixed Mode I/II Crack Angle Plots **XXVII**

O Python Script For Mixed Mode I/II Fracture Limit Plots **XXXI**

P Python Script For Mixed Mode I/III Crack Angle Plots **XXXV**

Q Python Script For Mixed Mode I/III Fracture Limit Plots **XXXVII**

R Python Script For Three-Dimensional Richard Criterion XLI

1 Introduction

This section will cover a short overview of this thesis. The background and motivations are discussed, and the scope of this work is addressed.

1.1 Background & Motivation

Mixed mode loading often has a significant effect on fracture behavior in components. Cracks is in many cases the reason for failure or fracture of a component. When it comes to fracture mechanics, all of the mechanisms of fracture behavior is still not completely known. This especially applies to the three-dimensional loading cases of mixed mode I/II/III. Some loading devices exist for the two-dimensional cases of mixed mode I/II and I/III loading. However, few exist for the three-dimensional loading case of mixed mode I/II/III. The motivation behind this work is to contribute to the works on fracture mechanics on this topic, by analyzing a new mixed mode I/II/III loading device theoretically and experimentally.

1.2 Problem Description

Mixed mode I/II/III brittle fracture behavior of PMMA is studied experimentally and theoretically using CTS specimens containing pre-cracks. The specimens should be subjected to different mixed mode loading conditions, ranging from pure mode I to pure mode II and pure mode III. The main goal of this thesis is twofold. First, to conduct a complete set of experimental results on fracture of pre-cracked PMMA samples under various in-plane and out of plane loading conditions. These experimental tests should be conducted by using the new designed mixed mode I/II/III loading device. The second aim of this thesis is to predict the fracture limits of the tested samples under mixed mode I/II/III conditions using various fracture criteria. Maximum Tangential Stress, MTS, the Generalized Maximum Tangential Stress, GMTS, and the Richard criterion are the chosen fracture criteria in this thesis. The ability of different fracture criteria for predicting the fracture limit and crack initiation angles of the tested specimens will be evaluated as a final goal.

1.3 Scope of This Work

1.3.1 Objectives

This thesis consists of several objectives. The designed loading device should be manufactured at the IPM workshop. Material sheets of polymethyl methacrylate, PMMA, should be ordered. The received PMMA material should be manufactured into several pre-cracked CTS specimens. In addition to the CTS specimen, dog-bone samples should be manufactured for material data testing. When the manufacturing of the loading device and CTS specimens are completed, tensile tests until fracture should be conducted on all of the specimens. The in and out of plane crack initiation angles on all of the specimens should be measured and

fracture loads obtained. All of the experimental results should then be compared with the theoretical study and numerical analysis.

1.3.2 Limitations

In this thesis, three specimens were made for all of the twenty-five loading device combinations. For an improved empirical study, more specimens could have been tested for each of the loading cases. Only one specimen type, pre-cracked CTS, were tested in this thesis. One, out of two designed loading devices, was manufactured. These limitations are due to financial framework and limited time of this work. Another limitation of this study is the lack of prior mixed mode I/II/III experimental data, which makes comparison and verification of this work difficult.

1.4 Previous Work

This master thesis is a continuation of a specialization project from the autumn of 2017. The specialization project was written by the same author as this master thesis. The specialization project consisted of the designing and modeling of the mixed mode I/II/III loading devices, some theoretical study and the set-up of the numerical simulation model. The design of the loading devices and numerical analysis setup is also covered in this master thesis to give a better understanding of the work. The designed mixed mode loading devices are based on previous work. The first one was based on the AFM Loading device by Nils-Henrik Schirmeisen and Hans A. Richard. The second three-dimensional loading device is a modification and combination of the well-known arcan fixture and a new fixture by Ayatollahi and Saboori. This is further explained in section 2.7.

1.5 Thesis Structure

This thesis follows the scientific writing structure called IMRaD. IMRaD is an acronym for introduction, method, results, and discussion. Chapter 1 and 2 covers the introduction part. The method in this thesis consists of modeling, design, manufacturing, numerical analysis, criteria procedure and experimental procedure. The chapters covering the methods can be found in chapter 3, 4, 5 and 6. Results and discussion were covered in chapter 7. The thesis was rounded up with a conclusion and further work chapter. These were covered in chapters 8 and 9.

2 Theory & Literature Review

This chapter will cover a brief overview of some of the theoretical background used in this thesis. In addition to some basic theory, literature is reviewed. Some theory on finite element analysis and fracture criteria were also covered in chapter 5.

2.1 Linear Elastic Fracture Mechanics

Fracture mechanics concepts that only apply to materials that obey Hook's law, see equation 2.1, are called linear elastic fracture mechanics, LEFM. By using the concepts of linear elastic fracture mechanics, a linear elastic material behavior is assumed, see illustration to the right in figure 2.1. A common material behavior for metals is a linear stress-strain response, followed by a non-linear behavior, see illustration to the left in figure 2.1 [1].

$$\sigma = E \cdot \varepsilon \tag{2.1}$$

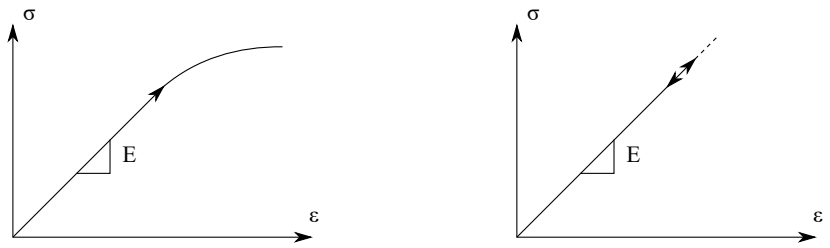

Figure 2.1: Left: Linear and non-Linear material behaviour, Right: Linear-elastic material behaviour.

2.2 Poly(Methyl Methacrylate), PMMA

The experiments done in this thesis uses specimens of the material Poly(Methyl Methacrylate), often called PMMA. PMMA is a polymer typically used for windows, lenses, clear shields and bone cement. The material is brittle at room temperature, relatively cheap and has transparent properties. The transparency helps when studying cracks and kinks in cracked specimens. PMMA has a typical linear elastic fracture behaviour. This can be seen to the right in figure 2.1 [1, 2].

2.3 Stress Analysis of Cracks

For isotropic linear elastic materials, subjected to a remote load, one can derive an expression for the stress in the body. By defining a polar coordinate system with an origin at the crack tip, the stress field in the cracked body can be given by equation 2.2 [1].

$$\sigma_{ij} = \left(\frac{k}{\sqrt{r}}\right) \cdot f_{ij}(\theta) + \sum_{m=0}^{\infty} A_m \cdot r^{\frac{m}{2}} \cdot g_{ij}^{m}(\theta) \tag{2.2}$$

σ_{ij} is the stress tensor, r and θ are geometrical properties (angle and distance to the stress body, see figure 2.3), k is a constant and f_{ij} is a dimensionless function of θ. For higher order terms, A_m is the amplitude and g_{ij}^{m} is a dimensionless function for the m-th term [1].

Any crack configurations contain the leading term $\frac{1}{\sqrt{r}}$, when r approaches zero, the term approaches infinity. Other terms approach zero or are finite [1].

2.3.1 Stress Intensity Factor

A crack can experience three different modes of loading. These can be explained as opening, shearing and tearing of a crack, see figure 2.2. The three modes are often called Mode I, opening, Mode II, shearing, and Mode III, tearing. A crack can undergo all of these three modes, alone or in a combination of two or three. Mode I, II and III produces the $\frac{1}{\sqrt{r}}$ singularity, but k and f is mode dependent, see equation 2.2 [1].

The constant k is replaced by the stress intensity factor, K. The relation between k and K is given by $K = k \cdot \sqrt{2\pi}$. Stress intensity factors are often denoted to K_I, K_{II} and K_{III}, which implies which mode load the crack is applied. Stress field at the crack tip for mode I can now be written as given in equation 2.3. For a singular stress field on the crack plane, the stress field can be written as equation 2.4. Here, the $\theta = 0$ which gives equal stresses in y and x-direction [1].

$$\lim_{x \to 0} \sigma_{ij}^{(I)} = \frac{K_I}{\sqrt{2\pi r}} \cdot f_{ij}^{(I)} \cdot (\theta) \tag{2.3}$$

$$\sigma_{xx} = \sigma_{yy} = \frac{K_I}{\sqrt{2\pi r}} \tag{2.4}$$

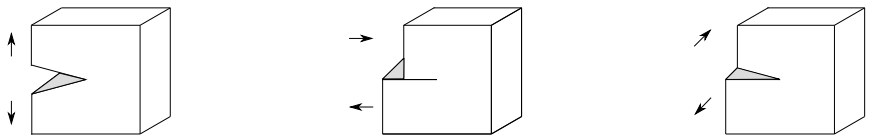

Figure 2.2: Fracture mode I, II and III

2.4 Mixed Mode Loading

Mixed mode fracture occurs when the fracture modes I, II and III occurs in a combination. These three modes can be explained as opening, shearing and tearing of a crack or a notch, see figure 2.2 [3]. The occurrence of a combination of only mode I and II is often called plane mixed mode or 2D mixed mode, and the combination of mode I, II and III are often called spatial mixed mode or 3D mixed mode. The crack tip's stress distribution is given by equation 2.5-2.10. For plane mixed mode problems, equation 2.5-2.7 are applied. The method is called near-field solution [4, 5].

$$\sigma_r = \frac{K_I}{4\sqrt{2\pi r}}\left\{5cos\left(\frac{\theta}{2}\right) - cos\left(\frac{3\theta}{2}\right)\right\} - \frac{K_{II}}{4\sqrt{2\pi r}}\left\{5sin\left(\frac{\theta}{2}\right) - 3sin\left(\frac{3\theta}{2}\right)\right\} \tag{2.5}$$

$$\sigma_\theta = \frac{K_I}{4\sqrt{2\pi r}}\left\{3cos\left(\frac{\theta}{2}\right) + cos\left(\frac{3\theta}{2}\right)\right\} - \frac{K_{II}}{4\sqrt{2\pi r}}\left\{3sin\left(\frac{\theta}{2}\right) + 3sin\left(\frac{3\theta}{2}\right)\right\} \tag{2.6}$$

$$\tau_{r\theta} = \frac{K_I}{4\sqrt{2\pi r}}\left\{sin\left(\frac{\theta}{2}\right) + sin\left(\frac{3\theta}{2}\right)\right\} + \frac{K_{II}}{4\sqrt{2\pi r}}\left\{cos\left(\frac{\theta}{2}\right) - 3cos\left(\frac{3\theta}{2}\right)\right\} \tag{2.7}$$

In the case of spatial mixed mode problems, additional three equations are added. As shown in equation 2.8-2.10. For plane strain σ_z is defined as shown in equation 2.10. However, for plane strain $\sigma_z = 0$ [4].

$$\tau_{rz} = \frac{K_{III}}{\sqrt{2\pi r}}sin\left(\frac{\theta}{2}\right) \tag{2.8}$$

$$\tau_{\phi z} = \frac{K_{III}}{\sqrt{2\pi r}}cos\left(\frac{\theta}{2}\right) \tag{2.9}$$

$$\sigma_z = \nu(\sigma_r + \sigma_\theta) = \frac{8\nu}{4\sqrt{2\pi r}}\left\{K_I cos\left(\frac{\theta}{2}\right) - K_{II}sin\left(\frac{\theta}{2}\right)\right\} \tag{2.10}$$

The equations are referring to r, ν, and z. These are co-ordinates in a cylindrical coordinate system originated at the crack tip. ν is the rotation about the z-axis and r is the x-direction, see the illustration to the right in figure 2.3 for all stress fields [4]. The illustration shows a kink. This is the propagation of a small crack, with another angle than the original crack [1].

2.5 The Elastic T Stress

The stress field at a crack tip, for isotropic linear elastic materials, is given by equation 2.2. This equation is given with m-th higher order terms. This is an infinite power series with the first term consists of a $\frac{1}{\sqrt{r}}$. The second term consists of r and so on [6]. Often, only the first, singular, term is used, and the higher orders are neglected. This leads to a single-parameter description of the stress field at the crack tip.

The third of the higher order terms vanishes at the crack tip, but the second term remains. This second term, which often is neglected, can have a considerable effect on stresses in the plastic zone, and the shape of the plastic zone [1]. Equation 2.11 covers the first two terms of Williams solution [6] for a crack in isotropic elastic materials.

$$\sigma_{ij} = \frac{K_I}{\sqrt{2\pi r}} \cdot f_{ij}(\theta) + \begin{bmatrix} T & 0 & 0 \\ 0 & 0 & 0 \\ 0 & 0 & vT \end{bmatrix} \tag{2.11}$$

The uniform stress in x-direction, see figure 2.3, is given by T. vT is the stress in z-direction in-plane strain. Biaxiality ratio, B, is an often used dimensionless factor, including T-stress and the stress intensity factor, see equation 2.12. For cracks exposed to mode I loading, the T-stress and K values scale with the amount of applied load.

$$B = \frac{T \cdot \sqrt{\pi a}}{K_I} \tag{2.12}$$

If remote normal stress is applied to an infinite thick plate, with a crack going through the thickness, the biaxiality ratio is equal to -1. T stress is given by equation 2.13 for common laboratory specimens.

$$T = \frac{B \cdot P}{A \cdot \sqrt{\pi a W}} \cdot f \cdot \left(\frac{a}{W}\right) \tag{2.13}$$

A specimen with negative T-stress lose constraint fast with deformation, and a specimen with positive t-stress generally leads to high constraints, under plastic conditions. The crack tip constraint of different geometries, can be indicated by the biaxiality ratio, B. A, W and a are dimensions for the chosen geometry.

Equation 2.12 or 2.13 can be used to obtain the t-stress for a given load. If the t-stress is calculated using equation 2.13 under a plastic condition, the t-stress estimation has no physical meaning. This is due to T-stress being an elastic parameter. Cases with plastic deformation lead to a higher amount of errors in T-stress, and it's inferred stress fields.

2.6 Fracture Criteria

Theoretical criteria were used for investigating fracture limits and to predict crack initiation angles. Numerous criteria exist for the loading case of mixed mode I/II. For the mixed mode cases of I/III, II/III and I/II/III, few fracture criteria exists [7]. Some of these are the extended maximum tangential stress criterion (Extended MTS) [8], the Pook criterion [9, 4], Richard criterion [4], criterion of Schöllmann [10], the maximum principal stress criterion [11, 10], the empirical elliptical criterion [12] and the extended generalized maximum tangential stress criterion (Extended GMTS) [7].

However, the existing fracture criteria for mixed mode I/II/III are not very sensitive to the effects of mode III, and some are not able to predict fracture direction [7]. This thesis will focus on the extended general GMTS criterion and the three-dimensional Richard criterion for the cases of general mixed mode I/II/III, mixed mode I/III and II/III.

As mentioned above, several criteria exist for the mixed mode case of I/II. This thesis will focus on the well known maximum tangential stress criterion (MTS) [13] and generalized maximum tangential stress criterion (GMTS) [14] for the in-plane mixed mode loading cases. The GMTS criterion is based on the MTS criterion. The MTS criterion takes basis in the equations for crack tip stress distribution, see equation 2.5-2.10. The GMTS criterion takes the higher order T-stress into consideration, see section 2.5 for further explanation of T-stress. Several experiments show that the GMTS criterion is in better agreement with test data than the MTS criterion [15, 16, 17, 18].

2.6.1 Fracture Criteria Formulation

In this subsection, the extended GMTS criterion is derived from the crack tip stress field equations. The same approach is used for the in-plane GMTS and MTS criteria. The only difference is that the terms that consist of T-stress are removed from the MTS formulation, and the terms including K_{III} is neglected for in the in-plane mixed mode I/II cases. This presented formulation of the extended GMTS criterion is adapted from the works of Ayatollahi [7].

The stress field under general mixed mode I/II/III loading are presented in equation 2.14-2.19. These equations consists of singular terms, see chapter 2.5, and non singular terms, see equation 2.5-2.10. They are valid for linear elastic homogeneous materials.

$$\sigma_{rr} = \frac{1}{\sqrt{2\pi r}}\left[\frac{K_I}{4}\left\{5cos\left(\frac{\theta}{2}\right) - cos\left(\frac{3\theta}{2}\right)\right\} + \frac{K_{II}}{4}\left\{-5sin\left(\frac{\theta}{2}\right) + 3sin\left(\frac{3\theta}{2}\right)\right\}\right] + T \cdot cos^2(\theta) + O \cdot (r^{\frac{1}{2}}) \tag{2.14}$$

$$\sigma_{\theta\theta} = \frac{1}{\sqrt{2\pi r}}\left[\frac{K_I}{4}\left\{3cos\left(\frac{\theta}{2}\right) + cos\left(\frac{3\theta}{2}\right)\right\} + \frac{K_{II}}{4}\left\{-3sin\left(\frac{\theta}{2}\right) - 3sin\left(\frac{3\theta}{2}\right)\right\}\right] + T \cdot sin^2(\theta) + O \cdot (r^{\frac{1}{2}}) \tag{2.15}$$

$$\sigma_{r\theta} = \frac{1}{\sqrt{2\pi r}}\left[\frac{K_I}{4}\left\{sin\left(\frac{\theta}{2}\right) + sin\left(\frac{3\theta}{2}\right)\right\} + \frac{K_{II}}{4}\left\{cos\left(\frac{\theta}{2}\right) + 3cos\left(\frac{3\theta}{2}\right)\right\}\right] - T \cdot sin(\theta)cos(\theta) + O \cdot (r^{\frac{1}{2}}) \tag{2.16}$$

The stress intensity factor for mode I, II and III are given by K_{I-III}. Poissons's ratio is given by v, and (r, θ, z) indicates directions in the cylindrical coordinates, see figure 2.3. T-stress is given by T and $O \cdot r^{\frac{1}{2}}$ represents the higher order terms. These higher often terms are often removed close to the crack tip.

$$\sigma_{\theta z} = \frac{K_{III}}{\sqrt{2\pi r}}cos\left(\frac{\theta}{2}\right) + O \cdot (r^{\frac{1}{2}}) \tag{2.17}$$

$$\sigma_{rz} = \frac{K_{III}}{\sqrt{2\pi r}}sin\left(\frac{\theta}{2}\right) + O \cdot (r^{\frac{1}{2}}) \tag{2.18}$$

$$\sigma_{zz} = \begin{cases} 0, & \text{Plane Stress} \\ v(\sigma_{\theta\theta} + \sigma_{rr}), & \text{Plane Strain} \end{cases} \tag{2.19}$$

As mentioned above, this formulation is derived using the same approach as for the MTS criterion [13]. This criterion is based on two hypotheses. They are given as [7]:

(i) Fracture initiates radially from the crack tip in the direction along which the tangential stress possesses its maximum value.

(ii) The onset of fracture occurs when the tangential stress at a critical radial distance from the crack tip, r_c, and along the above direction reaches a critical value of σ_c.

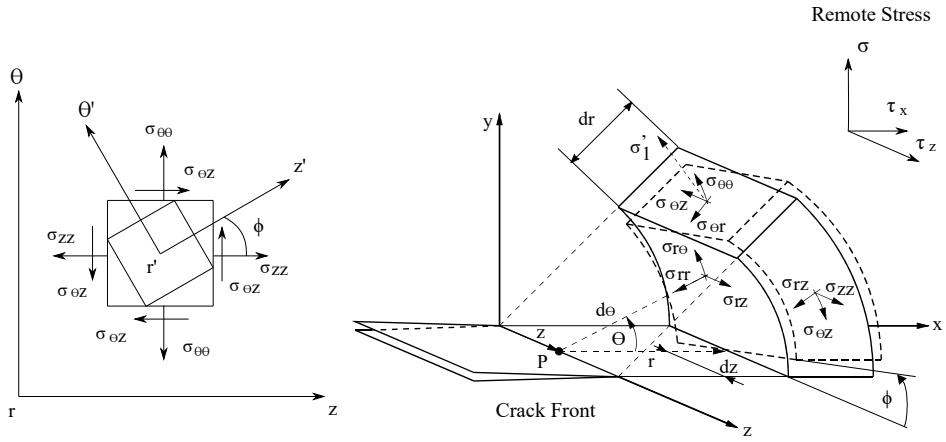

Figure 2.3: Left: Stress State in θ-Z plane [19], Right: Cylindrical co-ordinate system and stress comonents at crack front. [4]

Figure 2.3 shows the cylindrical coordinate system used in the equations above. The kinking angle is given by θ and the twisting angle is given by ϕ. One assumption is made to the extended GMTS criterion. This assumption is that the stress state, in the θ-z plane equal to an element rotated by an angle ϕ around the coordinate axis r. This is to make the extended GMTS criterion able to predict out of plane fracture angle, ϕ, in addition to in-plane fracture angle, θ. The rotation around the co-ordinate system r is illustrated to the left in figure 2.3. The stresses given in equation 2.14-2.19 are combined to make a stress tensor. The stress tensor is given in equation 2.20 [7].

$$S = \begin{bmatrix} \sigma_{rr} & \sigma_{r\theta} & \sigma_{rz} \\ \sigma_{r\theta} & \sigma_{\theta\theta} & \sigma_{\theta z} \\ \sigma_{rz} & \sigma_{\theta z} & \sigma_{zz} \end{bmatrix} \tag{2.20}$$

Mode II loading leads to kinking of the crack, and mode III loading results in a twisting of the crack. For the loading cases of mixed mode I/II/III, a combination of twisting and kinking occurs. This combination results in a more curved form of crack propagation. Typical crack propagation for pure mode I, pure mode II, pure mode III and mixed mode I/II/III is illustrated in figure 2.4.

Transforming the coordinate system of (r, θ, z) to (r', θ', z'), gives us the transformed stress tensor S', see to the left in figure 2.3. This can be calculated using the equation 2.21.

$$S' = QSQ^T \tag{2.21}$$

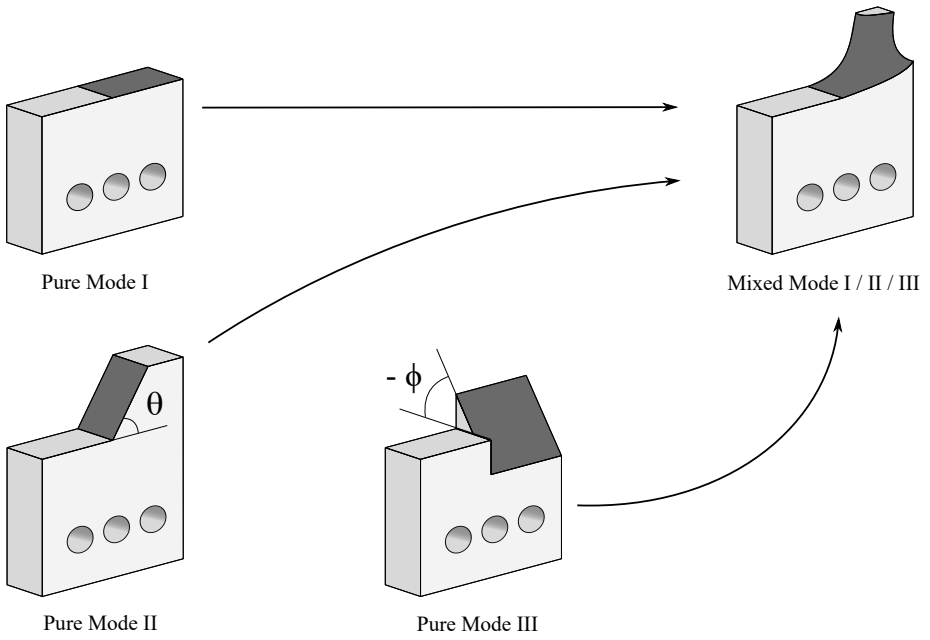

Figure 2.4: Crack growth for different fracture modes.

Where Q, in equation 2.21, is the transformation matrix, and Q^T is the transposed transformation matrix. Q is given in equation 2.22

$$Q = \begin{bmatrix} 1 & 0 & 0 \\ 0 & cos(\phi) & -sin(\phi) \\ 0 & sin(\phi) & cos(\phi) \end{bmatrix} \tag{2.22}$$

The transformed stress tensor is given in equation 2.23.

$$S' = \begin{bmatrix} \sigma_{rr} & \sigma_{r\theta'} & \sigma_{rz'} \\ \sigma_{r\theta'} & \sigma_{\theta'\theta'} & \sigma_{\theta'z'} \\ \sigma_{rz'} & \sigma_{\theta z} & \sigma_{z'z'} \end{bmatrix} \tag{2.23}$$

The tangential stress, including T-stress, is given in equation 2.24. This equation can be used as the basis for both GMTS and MTS criterion, plane stress, plane strain and the loading cases of mixed mode I/II, I/III and II/III.

$$\sigma_{\theta'\theta'}(\theta,\phi) = \frac{1}{\sqrt{2\pi r}}\left(cos^2\frac{\theta}{2}\left[K_I cos\frac{\theta}{2} - 3K_{II}sin\frac{\theta}{2} + 2T\sqrt{2\pi r}(1-cos\theta)\right]cos^2\phi \right.$$
$$\left. -K_{III}cos\frac{\theta}{2}sin(2\phi) + 2v\left[K_I cos\frac{\theta}{2} - K_{II}sin\frac{\theta}{2} + \frac{T\sqrt{2\pi r}}{2}\right]sin^2\phi \right) \tag{2.24}$$

For the plane stress condition, $\sigma_{zz} = 0$, the last term in equation 2.24 is neglected by setting v equal to zero. The plane stress case is given in equation 2.25.

$$\sigma_{\theta'\theta'}(\theta,\phi) = \frac{1}{\sqrt{2\pi r}}\left(cos^2\frac{\theta}{2}\left[K_I cos\frac{\theta}{2} - 3K_{II}sin\frac{\theta}{2} + 2T\sqrt{2\pi r}(1-cos\theta)\right]cos^2\phi - K_{III}cos\frac{\theta}{2}sin(2\phi)\right) \tag{2.25}$$

As showed in equation 2.12, the T-stress can be normalized. In the cases of stress intensity factors for mode II and III in addition to K_I, K_{eff} are often introduced [7]. K_{eff} is called the effective stress intensity factor and is given in equation 2.26

$$K_{eff} = \sqrt{K_I^2 + K_{II}^2 + K_{III}^2} \tag{2.26}$$

K_I is simply replaced by K_{eff} in equation 2.12 whichs forms equation 2.27

$$B = \frac{T \cdot \sqrt{\pi a}}{K_{eff}} \tag{2.27}$$

Equation 2.24 can be changed by replacing $T\sqrt{2\pi r}$ with $B \cdot K_{eff}\sqrt{2r/a}$, as seen in equation 2.28

$$\sigma_{\theta'\theta'}(\theta,\phi) = \frac{1}{\sqrt{2\pi r}}\left(cos^2\frac{\theta}{2}\left[K_I cos\frac{\theta}{2} - 3K_{II}sin\frac{\theta}{2} + 2B\cdot K_{eff}\sqrt{\frac{2r}{a}}(1-cos\theta)\right]cos^2\phi - K_{III}cos\frac{\theta}{2}sin(2\phi) + 2v\left[K_I cos\frac{\theta}{2} - K_{II}sin\frac{\theta}{2} + \frac{B\cdot K_{eff}\sqrt{r/a}}{\sqrt{2}}\right]sin^2\phi\right) \tag{2.28}$$

The two main hypothesis of the MTS criterion, and using partial derivative to find extreme values of two variable functions, leads to a mathematical description of the extended GMTS criterion. The first hypothesis is shown in equation 2.29 [7].

$$\frac{\partial\sigma_{\theta'\theta'}}{\partial\theta} = 0, \frac{\partial\sigma_{\theta'\theta'}}{\partial\phi} = 0, \frac{\partial^2\sigma_{\theta'\theta'}}{\partial\theta^2} < 0, \frac{\partial^2\sigma_{\theta'\theta'}}{\partial\theta^2}\frac{\partial^2\sigma_{\theta'\theta'}}{\partial\phi^2} - \left[\frac{\partial}{\partial\phi}\frac{\partial\sigma_{\theta'\theta'}}{\partial\theta}\right]^2 > 0 \tag{2.29}$$

The second hypothesis for the MTS criterion is given in equation 2.30. K_{IC} is the pure mode I fracture toughness, and σ_c is the critical tangential stress. These two were obtained for this thesis's choice of material in section 6.

$$\sigma_{\theta'\theta'} = \sigma_c = \frac{K_{IC}}{\sqrt{2\pi r_c}} \tag{2.30}$$

2.6.2 Maximum Tangential Stress Criterion, MTS

As mentioned above, a well-known fracture criterion is the maximum tangential stress criterion, MTS. This criterion is valid in the case of mixed mode I/II loading, and the T-stress is not considered. By neglecting the terms consisting of T, K_{III} and ϕ from equation 2.24, the general tangential stress can be expressed as in equation 2.31 [7].

$$\sigma_{\theta'\theta'} = \frac{1}{\sqrt{2\pi r}}\left(cos^2\frac{\theta}{2}\left[K_I cos\frac{\theta}{2} - 3K_{II}sin\frac{\theta}{2}\right]\right) \tag{2.31}$$

Combining equation 2.31 and the first hypothesis of the MTS criterion, equation 2.29, gives an implicit expression for the in plane fracture initiation angle, θ_f, see equation 2.32. The equation is partial derivative, and trigonometric identities are used to simplify the expression [13, 4].

$$K_I sin\theta_f + K_{II}(3cos\theta_f - 1) = 0 \tag{2.32}$$

By combining equation 2.31 with the second hypothesis of Erdogan and Sih, equation 2.30, an expression for the fracture limit surface is formed, see equation 2.33

$$K_{IC} = cos\frac{\theta_f}{2}\left[K_I \cdot cos^2\frac{\theta_f}{2} - \frac{3}{2}K_{II}sin\theta_f\right] \tag{2.33}$$

An usual presentation of the MTS criterion is through e fracture limit curve and a mixity parameter-initiation angle curve, e.g. [7, 3, 20, 4]. The mixity paramter, M^e_{12}, is given by equation 2.34.

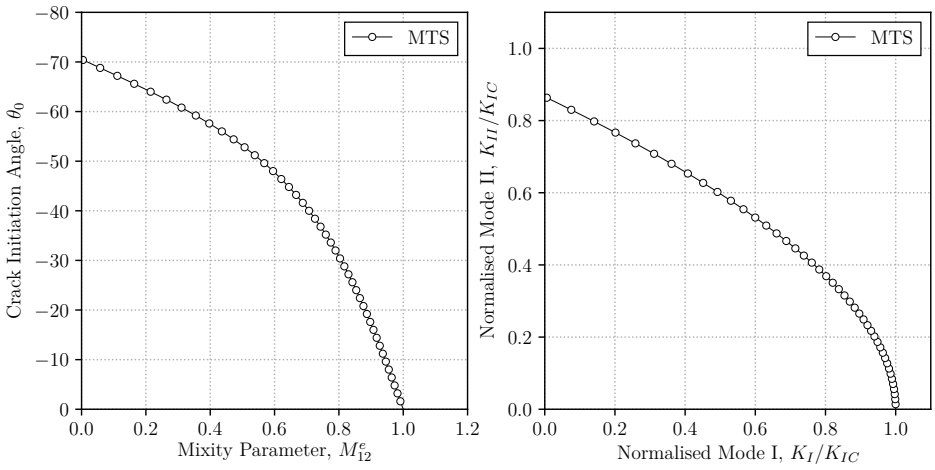

Figure 2.5: Left: Mixity Paramter vs Crack initiation angle Plot Right: Fracture limit plot, normalised Mode I vs Mode II

$$M_{12}^{e} = \frac{2}{\pi} tan^{-1}\left(\frac{K_1}{K_{II}}\right) \tag{2.34}$$

The notation of 12 indicates mode I and II. Figure 2.5 shows two plots. The plot to the left represent a curve of the relationship between the mixity parameter and the initiation fracture angle. The plot to the right in figure 2.5 represents the fracture limit curve for mode I and II for the MTS criterion.

The fracture limit plot indicates where the crack becomes unstable. If the stress intensity factor exceeds the fracture toughness, the crack becomes unstable [4]. According to this criterion, the in-plane crack initiation angle, θ_f, for pure mode II is $-70°$ and $0°$ for pure mode I, see figure 2.5.

2.6.3 Generalized Maximum Tangential Stress Criterion, GMTS

As for the MTS criterion, equation 2.24 can be used as the basis to derive the general form of tangential stress, for the GMTS, mixed mode I/II criterion, see equation 2.35.

$$\sigma_{\theta'\theta'} = \frac{1}{\sqrt{2\pi r}}\left(cos^2\frac{\theta}{2}\left[K_I cos\frac{\theta}{2} - 3K_{II}sin\frac{\theta}{2} + 2T\sqrt{2\pi r}(1-cos\theta)\right]\right) \tag{2.35}$$

Combining equation 2.29 and the first MTS hypothesis, 2.35, gives an implicit equation for the crack initation angle, including the consideration of T-stress, equation 2.36.

$$K_I sin\theta_f + K_{II}(3cos\theta_f - 1) - \frac{16T}{3}\sqrt{2\pi r_c}\cdot cos\theta_f \cdot sin\frac{\theta_f}{2} = 0 \tag{2.36}$$

When combining equation 2.35 with the second MTS hypothesis, equation 2.30, an expression for the fracture limit surface, including T-stress is formed, see equation 2.37 [7].

$$K_{IC} = cos\frac{\theta_f}{2}\left[K_I \cdot cos^2\frac{\theta_f}{2} - \frac{3}{2}K_{II}sin\theta_f\right] - T\sqrt{2\pi r_c}\cdot sin^2\theta_f \tag{2.37}$$

The effects of T-stress on the crack initiation angle and fracture limit can be studied by replacing T and r_c with $B\alpha_r$ [14, 7]. T is replaced by the biaxiality ratio, B, as shown in equation 2.27. The relation $\alpha_r = \sqrt{2r_c/a}$ is used to replace r_c. The plot in figure 2.6 shows the effect of negative T-stress in the generalized maximum tangential stress criterion. The MTS criterion is also plotted in the same figure for comparison. Note that the MTS criterion is equal to $B\alpha_r = 0$. As shown in figure 2.6, a negative T-stress leads to a higher value of normalized mode II, K_{II}/K_{IC} [14].

These plots show a constant $B\alpha_r$, for different crack initiation angles. In real mixed mode loading cases, the T-stress, which will affect the $B\alpha_r$, will vary for different loading cases and initiation angles. Figure 2.7 shows a plot of crack initiation angle versus mixity parameter, equation 2.34. A negative $T - stress$, therefore negative $B\alpha_r$, leads to a lower crack initiation angle, θ_f, in a negative direction. Positive T-stress leads to a higher, in a negative direction, crack initiation angle [14].

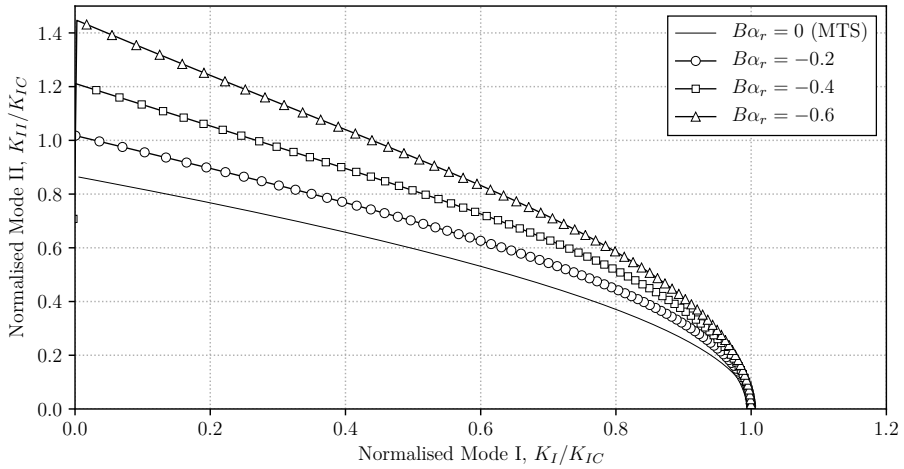

Figure 2.6: Fracture limit plot for different values of negative $B\alpha_r$ [14].

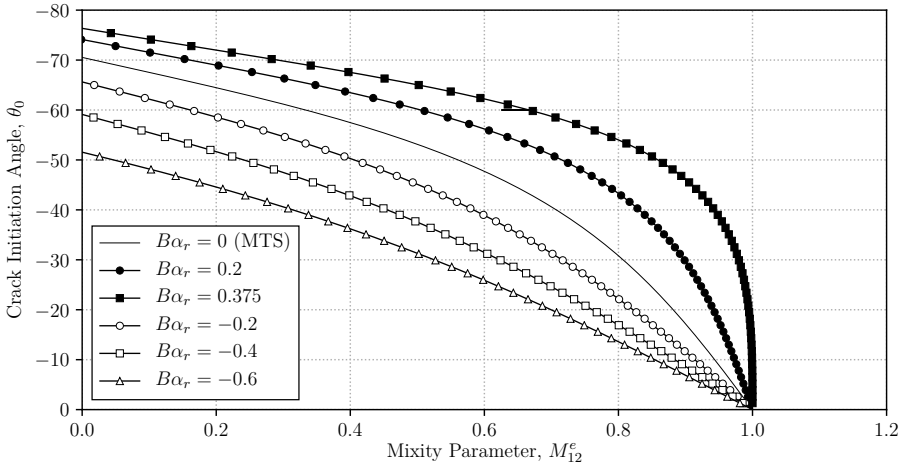

Figure 2.7: Crack initation angle vs mixity paramter plot for different values of negative and positive $B\alpha_r$ [14].

2.6.4 Three Dimensional Criterion by Richard

As mentioned above, few criteria exist for spatial, three dimensional, mixed mode problems. This thesis will cover the three-dimensional criterion of Richard [4, 21, 3], in addition to the extended GMTS criterion derived above. This criterion is a superposition of the three fracture modes. The stress intensity factors K_I, K_{II} and K_{III} are all considered in this criterion.

For deriving the spatial criterion, Richards two dimensional fracture criterion is expanded to three dimensions. Richards in plane fracture criterion consists of two hypothesis. The equation for fracture limit is given in equation 2.38 [4].

$$K_{IC} \geq \frac{K_I}{2} + \frac{1}{2}\sqrt{K_I^2 + 4(\alpha_1 K_{II})^2} \tag{2.38}$$

It is shown that by setting the parameter α_1 equal to 1.155, the fracture limit curve has a good agreement with the MTS criterion. The equation for in-plane crack initiation angle is shown in equation 2.39 [4].

$$\theta_f = \mp \left[155.5^\circ \frac{|K_{II}|}{|K_I| + |K_{II}|} - 83.4^\circ \left(\frac{|K_{II}|}{|K_I| + |K_{II}|} \right)^2 \right] \tag{2.39}$$

When extended to three modes, the equation for in plane fracture angle, θ_f, is expressed as in equation 2.40. $\theta_f < 0^\circ$ for $K_{II} > 0$ and $\theta_f > 0^\circ$ for $K_{II} < 0$.

$$\theta_f = \mp \left[A \frac{|K_{II}|}{K_I + |K_{II}| + |K_{III}|} + B \left(\frac{|K_{II}|}{K_I + |K_{II}| + |K_{III}|} \right)^2 \right] \tag{2.40}$$

The out of plane, twisting, angle, ϕ_f, is expressed in equation 2.41. $\phi_f < 0^\circ$ for $K_{III} > 0$ and $\phi_f > 0^\circ$ for $K_{III} < 0$.

$$\phi_f = \mp \left[C \frac{|K_{III}|}{K_I + |K_{II}| + |K_{III}|} + D \left(\frac{|K_{III}|}{K_I + |K_{II}| + |K_{III}|} \right)^2 \right] \tag{2.41}$$

The equations for in plane, and out of plane angles were found to be in good agreement with the criterion of Schöllmann with the parameters $A = 140^\circ$, $B = -70^\circ$, $C = 78^\circ$ and $D = -33^\circ$ [10, 4].

The equation for fracture limit for Richards three dimensional fracture criterion is given in equatiopn 2.42.

$$K_{IC} = \frac{K_I}{2} + \frac{1}{2}\sqrt{K_I^2 + 4(\alpha_1 K_{II})^2 + 4(\alpha_2 K_{II})^2} \tag{2.42}$$

In equation 2.42, $\alpha_1 = K_{IC}/K_{IIC}$ and $\alpha_2 = K_{IC}/K_{IIIC}$, where K_{IC}, K_{IIC} and K_{IIIC} are the fracture toughness for pure mode I, II and III.

By replacing the paramter α_1 with 1.155 and α_2 with 1.0, the fracture limit equation 2.42 fits well with the more complex criterion of Schöllmann [4]. Figure 2.8 shows and illustration of the three dimensional fracture limit curves, generated from equation 2.42.

The presented three-dimensional plots show the fracture limit for mixed mode I/II, I/III and II/III loading on the two-dimensional curves. In addition, a three-dimensional fracture limit surface is plotted, combining the three two dimensional mixed mode loading cases. This three-dimensional fracture limit surface represents the mixed mode I/II/III loading cases, see illustration to the left in figure 2.8.

To the right in illustration 2.8, a representation of equation 2.42 is shown. It is shown that the relation between stress intensity factors K_I and K_{II} is in a good agreement with the MTS criterion, see figure 2.5. With a K_{II}/K_{IC} value of 0.87, and K_I/K_{IC} value of 1.0.

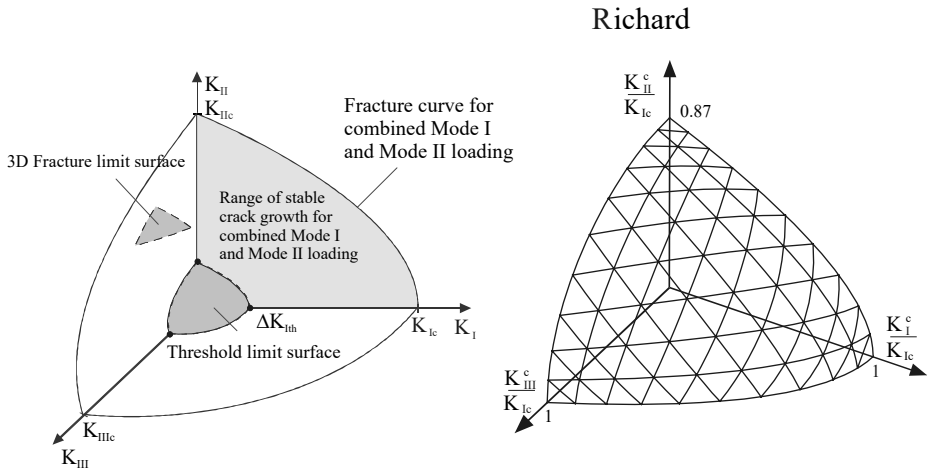

Figure 2.8: Left: Illustration of Three dimensional fracture limit curves, Right: 3D Criterion of H.A. Richard [4]

2.6.5 Dimensionless Factors

Ayatollahi et al. [20] suggested a solution method to calculate the onset of brittle fracture, by implementing dimensionless factors to the GMTS criterion. In this work the stress intensity factors, K_I, K_{II} and the T-stress, T, were replaced with the dimensionless factors Y_I, Y_{II} and T^*. The GMTS equation for crack initiation angle, see equation 2.36, can be rewritten as equation 2.43.

$$Y_I sin\theta_f + Y_{II}(3cos\theta_f - 1) - \frac{16T^*}{3}\sqrt{\frac{2r_c}{a}} \cdot cos\theta_f \cdot sin\frac{\theta_f}{2} = 0 \tag{2.43}$$

The second equation of the GMTS criterion, see equation 2.37, can be derived by K_{If} to form the equation for plotting the fracture limit curve, see figure 2.6. This is shown in equation 2.44.

$$\frac{K_{IC}}{K_{If}} = cos\frac{\theta_f}{2}\left[cos^2\frac{\theta_f}{2} - \frac{3}{2}\frac{K_{IIf}}{K_{If}}sin\theta_f\right] - \frac{T_f}{K_{If}}\sqrt{2\pi r_c} \cdot sin^2\theta_f \tag{2.44}$$

K_{If}, K_{IIf} and T_f are stress intensity factors and T-stress at the fracture load in each mixed mode loading case. By rewriting equation 2.44 with dimensionless factors, it can be expressed as equation 2.45 [20].

$$\frac{K_{IC}}{K_{If}} = cos\frac{\theta_f}{2}\left[cos^2\frac{\theta_f}{2} - \frac{3}{2}\frac{Y_{II}}{Y_I}sin\theta_f\right] - \frac{T^*}{Y_I}\sqrt{\frac{2r_c}{a}} \cdot sin^2\theta_f \tag{2.45}$$

The same procedure is followed for the K_{IIf}/K_{IC} relation and can be seen in equation 2.46.

$$\frac{K_{IC}}{K_{IIf}} = cos\frac{\theta_f}{2}\left[\frac{Y_I}{Y_{II}}cos^2\frac{\theta_f}{2} - \frac{3}{2}sin\theta_f\right] - \frac{T^*}{Y_{II}}\sqrt{\frac{2r_c}{a}} \cdot sin^2\theta_f \tag{2.46}$$

This method can be used for plotting the GMTS curves when the fracture load, and therefore K_{If} and K_{IIf}, is unknown. The dimensionless geometry factors, Y_I, Y_{II} and Y_{III}, can be calculated by using the relation in equation 2.47 with K_I, K_{II} and K_{III} [2].

$$K = Y\sigma\sqrt{\pi a} \tag{2.47}$$

This thesis use the relation in equation 2.48 to calculate the non-dimensional T-stress, T^*.

$$T = \sigma \cdot T^* \tag{2.48}$$

2.7 Existing Mixed Mode Loading Devices

The second modeled loading device is a combination of the well-known arcan loading device and a new fixture by Ayatollahi and Saboori [22]. The arcan fixture covers several degrees of mode I/II combinations. The arcan loading device is illustrated to the right in figure 2.9 [3].

The new fixture by Ayatollahi and Saboori [22], is a fixture for fracture tests under mixed mode I/III loading. This fixture is illustrated in the middle in figure 2.9.

In this project, mixed mode loading devices will be designed and simulated. The first loading device to be modeled was the all fracture mode (AFM) loading device. This loading device is based on the works of Schirmeisen and Richard [23]. This loading device is illustrated to the left in figure 2.9.

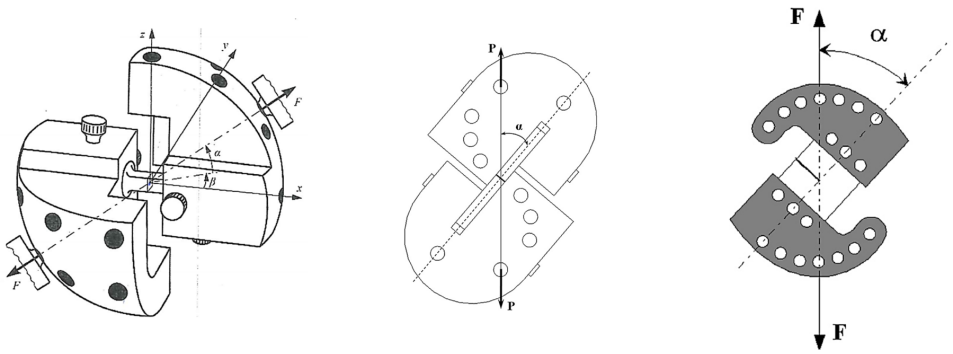

Figure 2.9: Left: AFM loading device [23], Middle: New mixed mode I/III fixture [22], Right: Arcan fixture for mixed mode I/II [3].

3 Modeling of Mixed Mode Loading Devices

This chapter covers the modeling and design method of the two mentioned loading devices. The first presented loading device is based on Richard's work, and the second is a combination of the work by Ayatollahi and the well-known arcan fixture, see chapter 2.7.

3.1 AFM Loading Device

In this work, fabrication of a mixed mode loading device was needed. Among the different mixed mode loading devices, an AFM (All fracture mode) fixture was chosen, see section 2.7. For a correct and accurate fabrication, a CAD model and detailed machine drawings were made and delivered to the IPM workshop. The software used for modeling was Siemens NX. See appendix A and B for complete technical drawings.

3.1.1 Modeling of AFM Specimen

For designing and applying dimensions an article covering the AFM specimen were used [5]. The specimen has the width, $w = 27mm$, thickness, $t = 0.45w$ and crack length, $a = 0.5w$. The length of the specimen is $150.5mm$, and the diameter of the cylindrical ends are $35mm$. As illustrated in figure 3.1, four holes are used to fix the specimen to the fixture with the help of four pins. The holes for the pins have a diameter of $10mm$. The ends have a 1 mm chamfer, for easier assembly of the specimen to the fixtures.

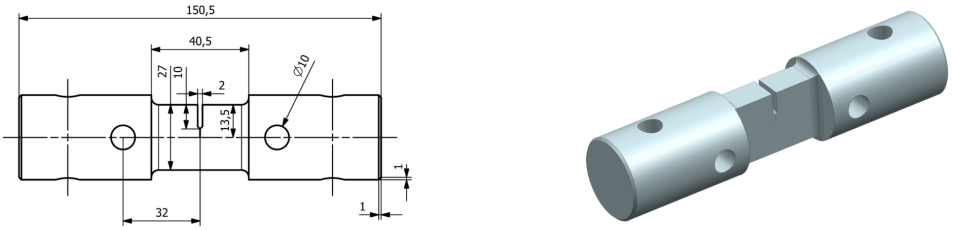

Figure 3.1: Caption of AFM specimen, CAD model and technical drawing

3.1.2 Modeling of AFM Fixture

As opposed to the specimen, there were no dimensions or technical drawings for the AFM fixture. However, in the article used for designing the specimen [5] a photograph of the assembled fixture and specimen was found. This photograph was used to get an approximate relationship between the length of the specimen and the two fixtures. The AFM fixture consists of two identical parts, which fix the specimen in both ends. As illustrated in figure 3.2, four holes are surrounding the hole for the specimen. They have the diameter of $10mm$ and have the purpose

of connecting the specimen and fixture with pins. The reason for four holes in one end, instead of two as for the specimen, is symmetry and easier fabrication. With four holes, the two fixtures are identical, and the holes do not have to be mirrored. The back of the fixture has a spherical shape with thirteen threaded holes. The holes are placed in an order so that any combination of Mode I to Mode II and III can be generated in steps of 30°.

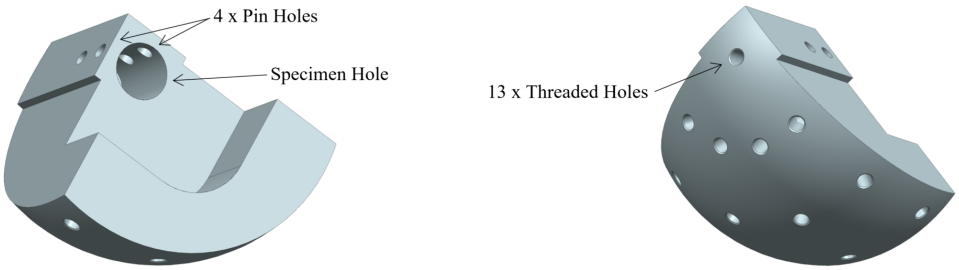

Figure 3.2: Caption of AFM Fixture, CAD model

3.1.3 Assembly of AFM Loading Device

The assembly consists of two fixtures and one specimen. The fixtures are mirrored to create symmetrical properties, see figure 3.3. A uni-axial testing device can be fixed to one of the threaded holes in the fixture, and at the opposing hole on the second fixture. Different threaded holes will enable different combinations of mixed mode loading. The threaded holes were fabricated in a way that the center line of the holes, and the load line of action, always passes through the center of the specimen [3]. This is illustrated to the right in figure 3.3, where lines from the threaded holes are crossing at the center of the specimen crack tip.

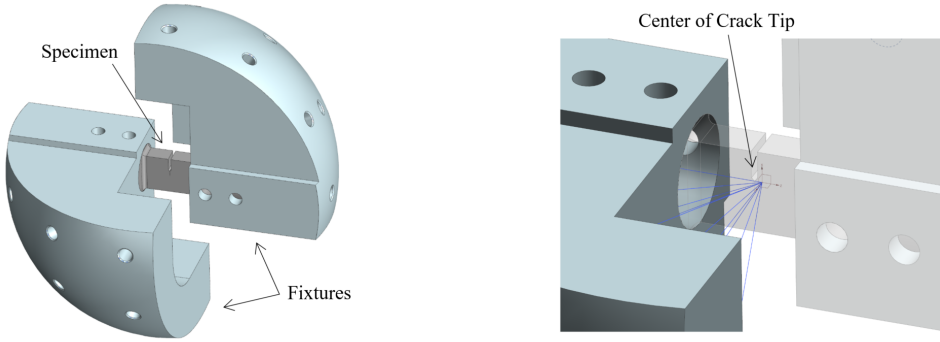

Figure 3.3: Left: Assembly of AFM Fixture and Specimen, Right: Sketches crossing at the center of specimen crack tip

3.2 Mixed Mode I/II/III Loading Device

Because of the somewhat complicated fabrication of the AFM loading device, another mixed mode loading device was modeled. This loading device is a modification and combination of the two-dimensional arcan fixture, and the mixed mode I/III fixture by Ayatollahi and Saboori [22]. See chapter 2.7. Modeling of the loading device was done in Siemens NX. Technical drawings were made from the CAD-model and delivered to IPM workshop for fabrication. Complete technical drawings can be studied in appendix C, D and E.

3.2.1 Modeling of CTS Specimen

The CTS specimen has six holes to allow a pinned connection to the fixture. It's width is, $w = 37.5mm$, thickness, $t = 10mm$ and crack length, $a = 18.8mm$. The length of the specimen is $60mm$, and it has six holes, with a diameter of $6mm$, for the pinned connections, see figure 3.4. The presented CTS specimen is based on the specimen used for mixed mode I/II testing, with the Arcan fixture, by Richard and Sander, see figure 2.9 [24].

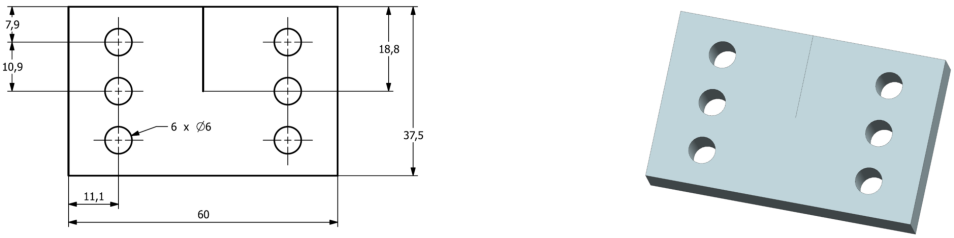

Figure 3.4: Caption of CTS specimen, CAD model and technical drawing

3.2.2 Modeling of C-Fixture

The specimen is fixed to a fixture referred to as the c-fixture, because of its shape. As illustrated in figure 3.5, there are three holes to allow pinned connection to the specimen. In addition to the specimen holes, five holes are covering the rounded edge of the fixture. These holes allow connection to the second fixture. They are modeled in a circular pattern in steps of 22.5°, at a radius of $45mm$ from the specimen center (crack tip). In the case of a two dimensional CTS loading device, the load is applied directly to these holes. In that case, the fixture allows pure mode I, pure mode II and a mixed mode loading combinations in steps of 22.5° between fracture mode I and II. In this work, the fixture is connected to a second fixture to allow third-dimensional mixed mode loading.

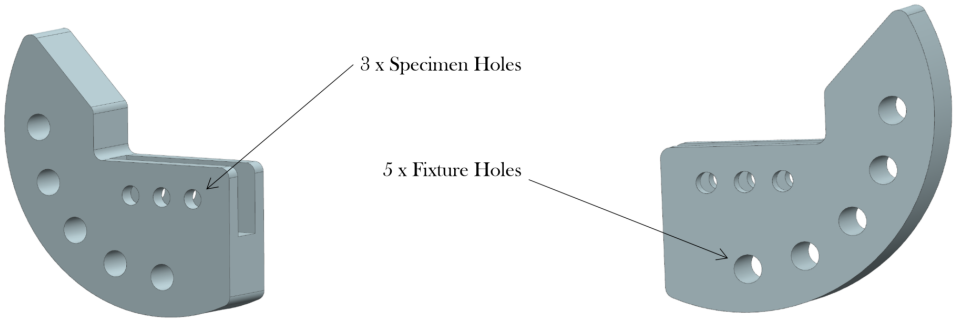

Figure 3.5: Illustration of modeled C-Fixture

3.2.3 Modeling of J-Fixture

The c-fixture is connected to a second fixture. This second fixture is referred to as the j-fixture, because of its shape. As shown in figure 3.6, the j-fixture has a hole across its body to allow pinned connection to the c-fixture. The j-fixture also has five holes, covering the edge, in a circular pattern. These holes are also modeled in steps of 22.5° from the specimens crack tip center. During physical experiments, the load is applied through these holes. The combination of mode III, to the mixed mode loading combination, is determined by which of these holes the load is applied to.

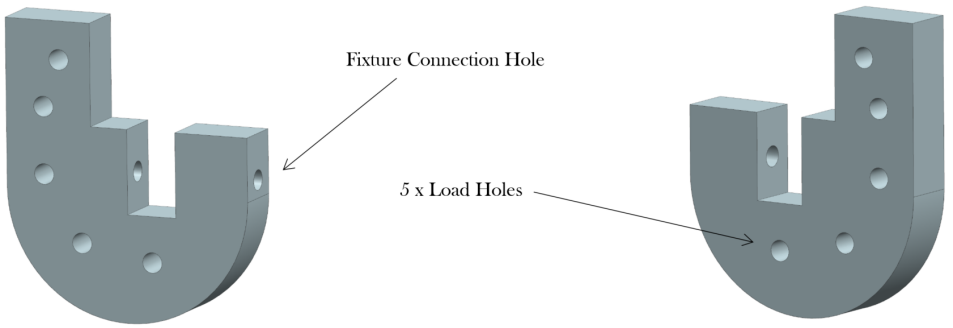

Figure 3.6: Illustration of modeled J-Fixture

3.2.4 Forks

To translate the force from the tensile testing machine, to the loading device, two forks were designed, see figure 3.7. They were designed with a gap, to insert the j-fixture, and is connected to the fixture using pins. The solid end has a thickness of twelve mm, and is designed to fit the grips of the tensile testing machine. The testing machine grips are basic clamps, which uses hydraulic force for clamping.

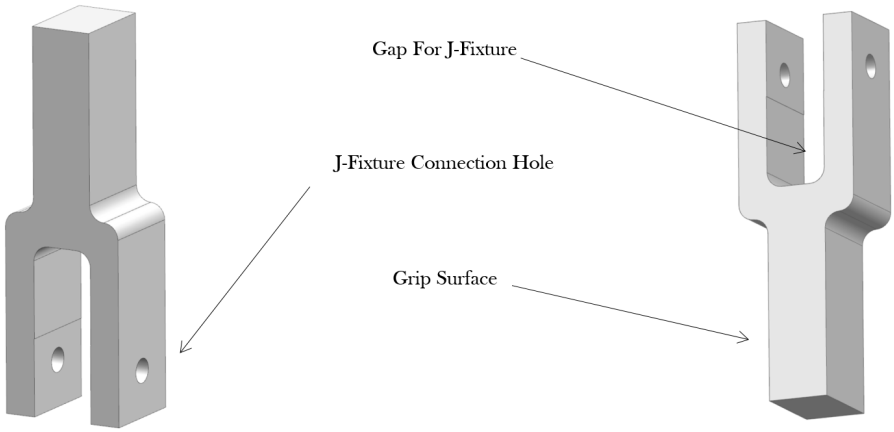

Figure 3.7: Illustration of Modelled Forks

3.2.5 Assembly of Mixed Mode I/II/III Loading Device

The assembled loading device consists of two j-fixtures, two c-fixtures, and one specimen, see figure 3.8. All the holes on the j- and c-fixture were designed in a way, so all center lines crossed the center of the specimen crack tip.

When the specimen is assembled, pinned connections go through the specimen fixture, the specimen, and the c-fixture. The desired combination of mode I and II is selected by connecting the j-fixture to different holes in the c-fixture. The same concept applies for the j-fixture, different combinations of mode III loading is determined by which hole the load, from the uniaxial testing machine, is applied.

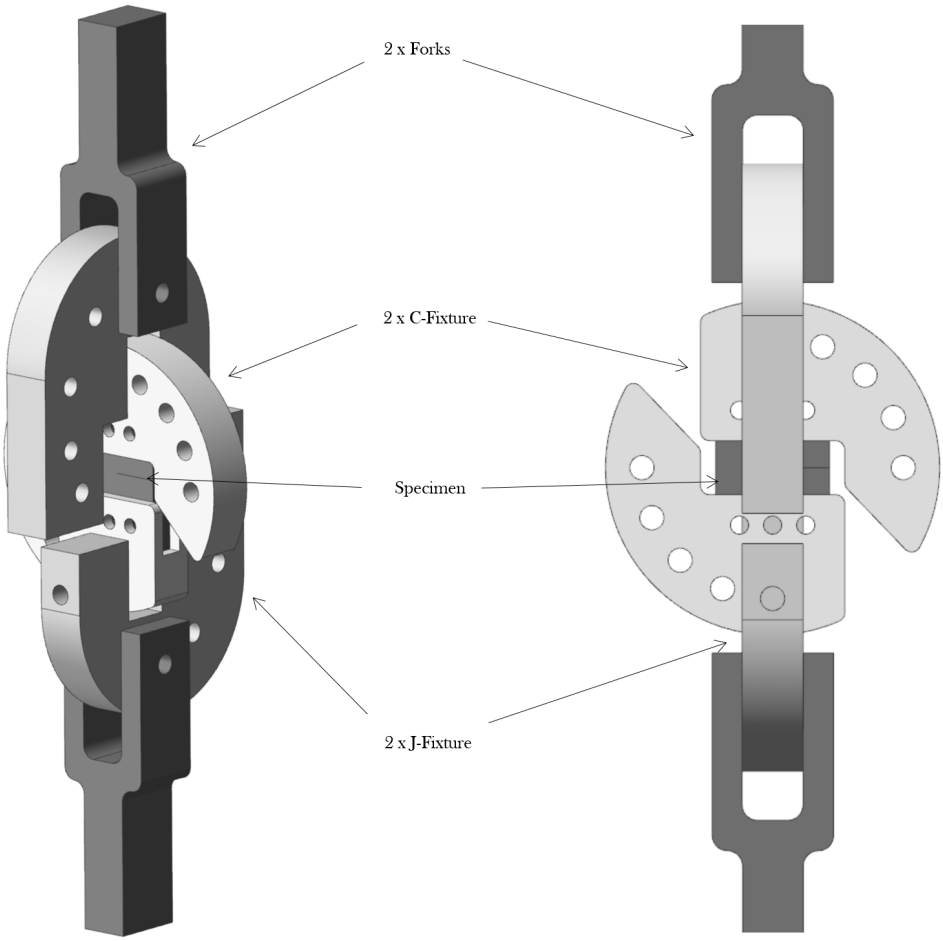

Figure 3.8: Illustration of assembled Mixed Mode I/II/III Loading Device

4 Manufacturing Method

This chapter will cover the fabrication process of the presented loading device, and specimens. Technical drawings, used for manufacturing, are covered in appendices C, D and E.

4.1 CTS Specimen

As mentioned above, the chosen material for the cracked specimens was PMMA, see chapter 2.2. A large plate of this material was ordered and cut into smaller pieces before delivering it to the 'Realfabsbygget' workshop, for manufacturing of the specimens. The PMMA plate can be seen to the left in figure 4.4.

The dimensions of the cracked specimen can be studied in appendix C. As illustrated in the technical drawing, the crack length, a, is set to 18.75 *mm*. The main issue with the fabrication was the making of the crack.

The thinnest available blade had a thickness of 0.5 *mm*. However, the desired thickness of the crack was 0.2 *mm*. This was solved by using the 0.5 *mm* saw for 18.5 *mm* of the crack length and cutting the remaining 0.25 *mm* crack length with a razor blade. The manufactured specimen is shown to the right in figure 4.4.

The razorblade cutting process is illustrated in figure 4.1. In this figure, a scaled up image of the crack tip is presented. In the middle of the figure, the crack tip after manufacturing is shown. The crack tip had a squared front, with a width of 0.5 *mm*, after the 0.5 *mm* saw. To the right in figure 4.1, an illustration of the crack tip, after the razor blade cutting, is shown. This resulted in a sharper crack tip.

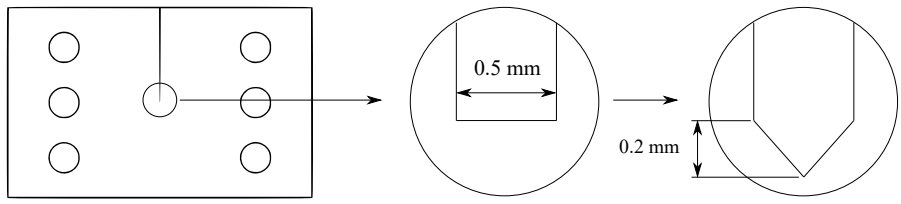

Figure 4.1: Left: Cracked specimen, Middle: Machined crack, Right: Crack tip after the razor-blade cutting process

4.2 Mixed Mode I/II/III Loading Device

After the mixed mode I/II/III loading device was modeled, as explained in chapter 3, the drawings, and step-files were delivered to the IPM workshop for fabrication. The fabrication method used for these fixtures were CNC (computer numerical control) milling.

Figure 4.2 presents the completed c-fixtures. Both parts were found to be precisely and identical. This was measured and controlled with a caliper as measuring tool. The symmetry of the c-fixtures was important for correct force distribution, from the tensile testing machine to the crack tip. Six small pins were made for fastening the CTS specimen to the c-fixtures. These were cut from a solid steel rod. Edges of the pins were graded, for a smoother penetration in the c-fixture. Figure 4.3 shows the manufactured j-fixtures. The complete components were found to be in a good agreement with the designed CAD models. In addition to the initial design, a small hole was drilled for the pinhole for c-fixture connection. This was done to obtain a smoother pin penetration, and to avoid a vacuum. Figure 4.5 shows this small hole, on the j-fixture surface.

Figure 4.5 shows the complete assembled loading device, with the manufactured forks to the right. The forks were used to transform the force from the tensile testing machine to the loading device and specimen. As seen in the figure, six pins were used to fasten the specimen to the c-fixtures. Two additional pins were used to fasten the j-fixture to the c-fixture. Bolts and nuts were used to fasten the forks to the j-fixtures. This was due to the heavy weight of the j-fixtures. Most of the weight was held by the bolts, instead of adding more out of plane force to the specimen than tended.

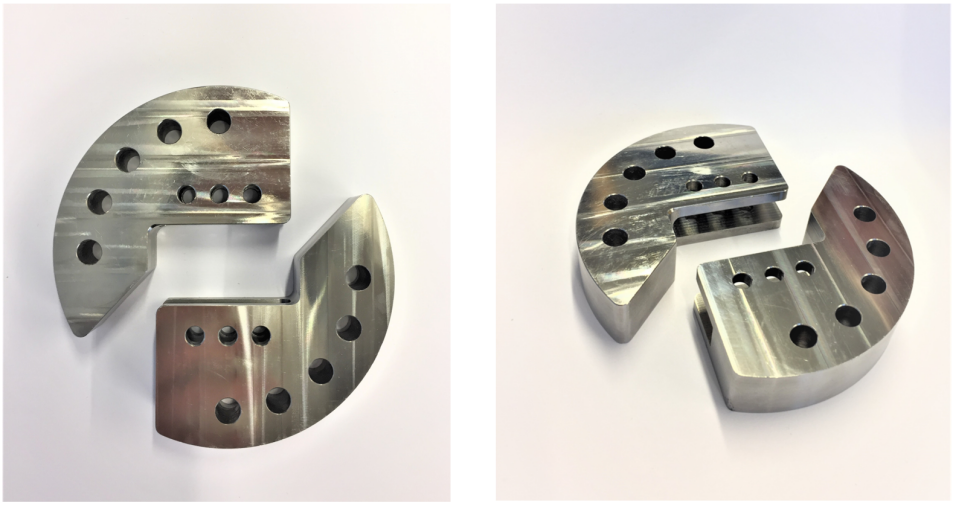

Figure 4.2: Manufactured c-fixtures.

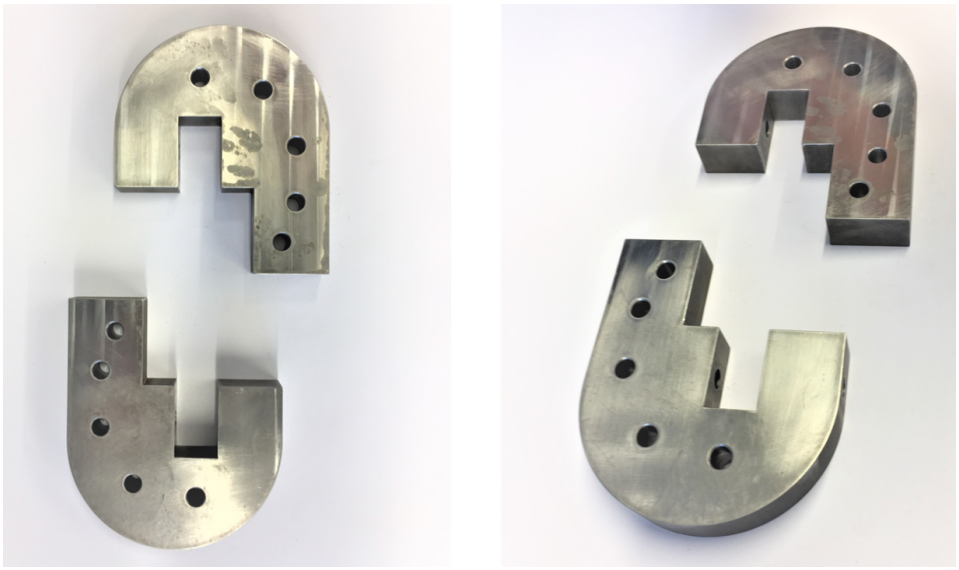

Figure 4.3: Manufactured j-fixtures.

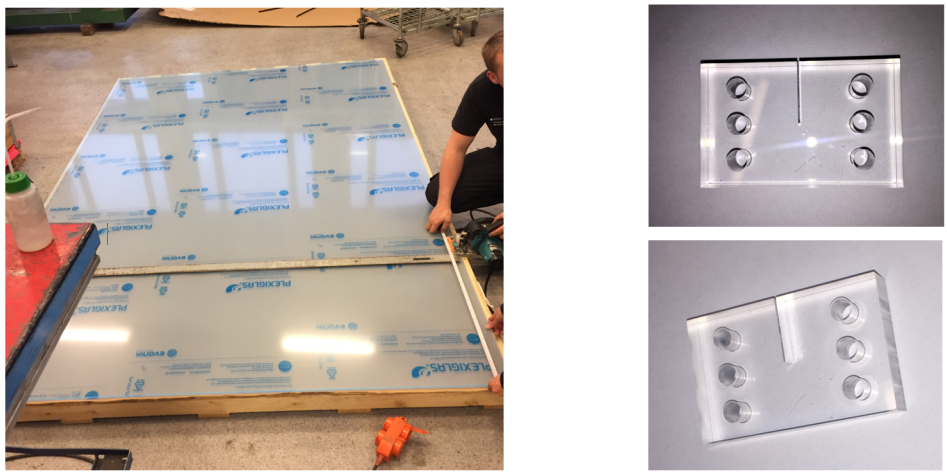

Figure 4.4: Left: Ordered PMMA plate, Right: Manufactured mixed Mode CTS specimens.

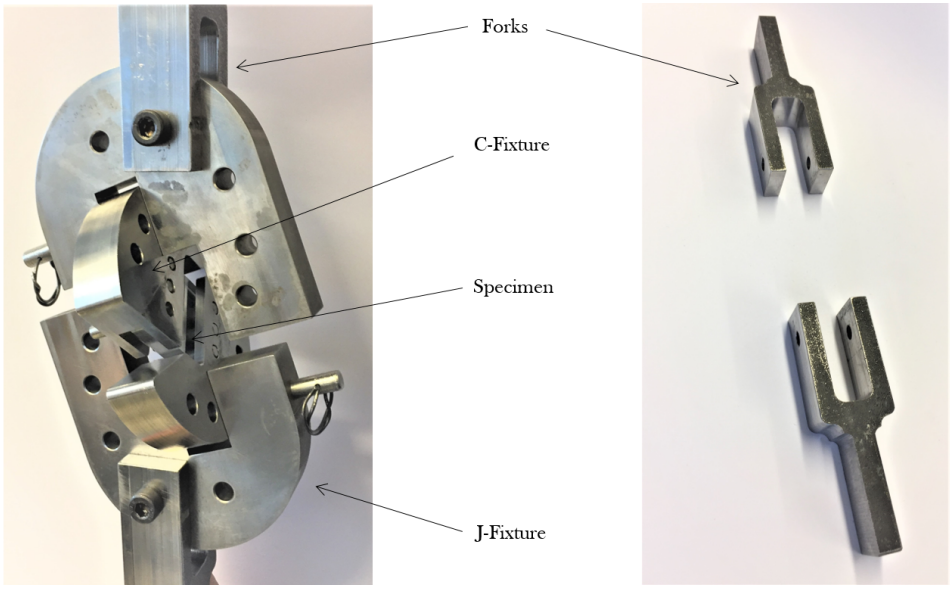

Figure 4.5: Left: Manufactured assembly, Right:Manufactured forks.

5 Numerical Analyses & Criteria Procedure

This chapter will cover a numerical analysis of the designed loading devices and specimens, numerical outputs from the analysis and some fracture criteria procedures. After the design and modeling of the loading device, all of the parts were saved as step-files and imported to the simulation software, Abaqus.

5.1 Numerical Analysis Set-up for Loading Device

5.1.1 Properties

The step-file of the loading device was imported to Abaqus and assembled. Two different materials were assigned to the specimen and the fixtures. The specimen was assigned the material polymethyl methacrylate, PMMA. This is also the material used for the physical specimens. PMMA has transparent properties, which makes visual tracking of crack initiation angles easier.

The material was assigned Young's modulus of 2900 MPa and a Poisson's ratio of 0.35 [25, 26]. The fixtures were manufactured from steel, which is stiffer than the specimen material. This led to the assumption that deformation would only occur in the specimen, and not in the fixture. See chapter 5.2. For the fixtures, steel was applied. The steel material was assigned Young's modulus of 193 GPa and a Poisson's ratio of 0.25 [27].

5.1.2 Interactions & Constraints

As mentioned in the modeling chapter, pins were used to connect the specimen to the c-fixture, and the c-fixture to the j-fixture. To simplify the model, pins were not imported. Instead, these connections were simulated using constraints and interactions in Abaqus. This is illustrated to the left in figure 5.1. To simulate pins, multiple point constraints, MPC, were used. They establish a relation between degrees of freedom in nodes [28].

In this case, a reference point, at the center of pinholes, were constrained to the inner surface of the hole. This is illustrated to the right in figure 5.1. This constraint was applied to all pinned surfaces between the specimen and c-fixtures, eighteen in total. Between the mentioned MPC constraints, a connector section was made. The type for this connector section was a beam. This was applied by choosing two reference point, with attached MPC constraint. This was done for each of the six specimen holes. In this way, MPC constraints were connected in sets of three. This lead to a total of six beam connections. Because of the assumption of no deformation in the fixtures, a different type of constraint was chosen to simulate these pins. For the two pins connecting the two c-fixtures to j-fixtures, a rigid pin constraint was used to simplify to FEA model. Verification of this assumption was conducted in chapter 5.2.

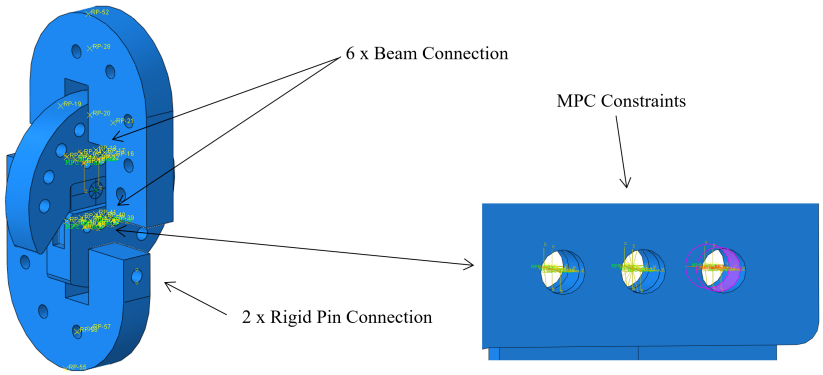

Figure 5.1: Overview of different Interactions and Constraints used in the loading device model set-up

5.1.3 Partitioning & Crack Assignment

To be able to apply correct mesh, and crack properties to the specimen, it was partitioned into smaller parts. Because this is a three-dimensional model, the face was first partitioned using the sketch method in Abaqus. The partitioning of the face was then used for partitioning the cell, using the extrude/sweep edges method.

The specimen was partitioned into four squares, and one additional circle, see figure 5.2. The circle has an origin in the specimen center. The circle has a radius of 5 *mm*. The circle was divided into eight parts, see illustration to the right in figure 5.2. This circle was added at the crack tip, to provide a finer mesh in this area. This finer mesh was necessary for the stress intensity factor simulations.

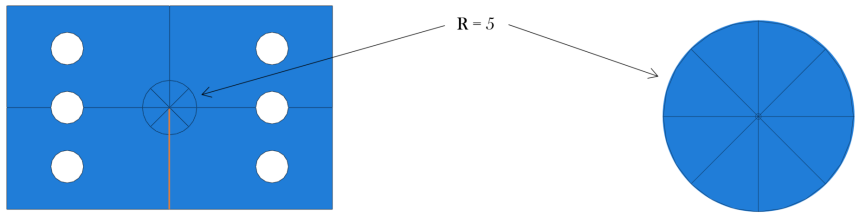

Figure 5.2: Illustration of the Specimen Partitioning Process and Crack assignment

For assigning the crack, the tool assign seam was used. Two of the partition lines were chosen, illustrated with an orange line in figure 5.2. After the seam was assigned, a crack was created. The chosen type was contour integral, to be able to obtain K values. Crack extension direction was applied by using q vectors. For the singularity options, the midside node of elements was changed from half the length to one-quarter of the length. After assigning the crack, a new history output was made. To obtain stress intensity factors, the domain 'crack' was selected. A number of ten contours were applied, and the type was set to stress intensity factors, maximum tangential stress. T-stresses were obtained in addition to K-values. This was done with the same procedure, by applying T-stress as a new history output. A number of ten contours was also applied in this case.

5.2 Verification of Fixtures

Previous in this chapter, it was assumed that no stresses and deformation of importance would appear in the c- and j-fixture. The assumption was based on the fact that the material of the fixtures, steel, was stiffer than the material properties of the specimen, PMMA. This was verified by studying the local stresses in these fixtures when the model was set-up for simulation. As a safety factor, the load 2000 N was applied during this verification. Figure 5.3 illustrates the first stress study of the fixtures. Pure mode I was set up and simulated. In the visualization, a display group was made, and the specimen was hidden. This allowed an isolated study of stresses in the fixtures, and neglect the stresses in the specimen. As shown in figure 5.3 the maximum occurring stress in both fixtures was 21.62 MPa. This stress was found in the c-fixture, in the area around the pinned connection with the specimen. For the j-fixture, the maximum stress was found at the end of its pinhole. This is illustrated in the figure with a section view along the y-z plane.

Fixture stresses were studied for all loading cases. Figure 5.4 illustrates stresses for loading case $\alpha = 90°$-$\beta = 90°$ and $\alpha = 45°$-$\beta = 45°$. These were the loading cases with highest obtained stresses in the fixtures. For the $\alpha = 90°$-$\beta = 90°$ case, the highest stress was 97.9 MPa. This stress concentration was found around the pin holes for specimen fixture. For the $\alpha = 45°$-$\beta = 45°$ case, the highest stress was 70.8 MPa. This maximum stress concentration was found around the loading holes on the j-fixture.

The highest obtained stress during all loading cases was found to be 97.9 MPa, which is below the yield stress of the chosen steel material. This led to the conclusion that deformation would occur in the specimen, rather than in the fixtures. After the fixture stress study, all simulations were set up for the simulation case. The applied load was set to 1000 N. The FEA model for each simulation was studied to verify that the model behaved as intended. Figure 5.5, illustrates the deformation of the specimen for pure mode I, II and III. The visualization of deformation is scaled fifty times.

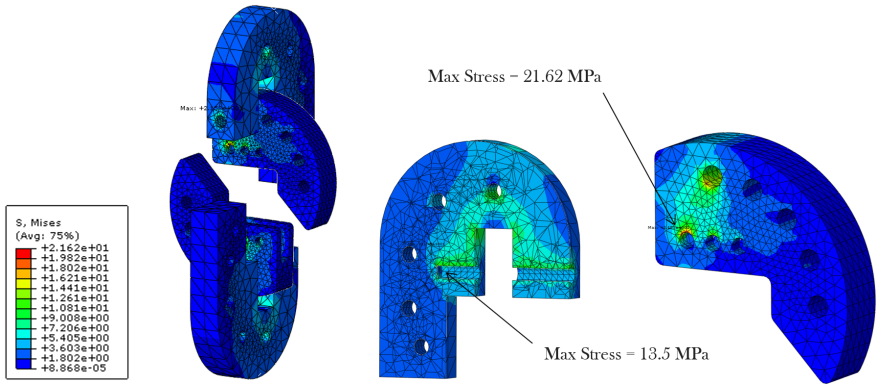

Figure 5.3: Von Mises stresses in fixtures during Pure mode I, Middle: Max von Mises stress in J-fixture, Right: Max von Mises stress in C-fixture

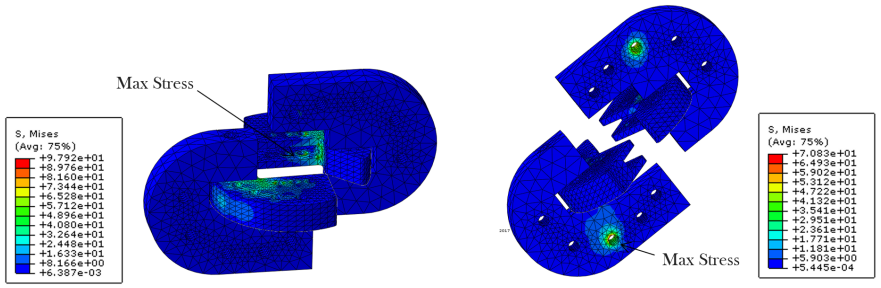

Figure 5.4: Left: Fixture stresses for loading case $\alpha = 90°$ & $\beta = 90°$, Right: Fixture stresses for loading case $\alpha = 45°$ & $\beta = 45°$

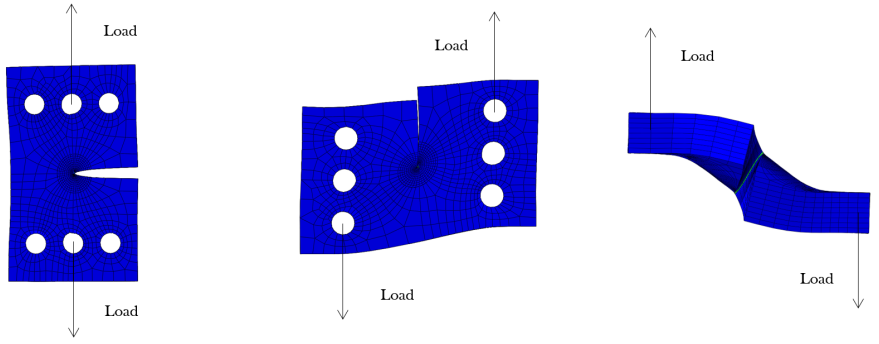

Figure 5.5: Illustration of deformed specimen. Left: Pure Mode I, Middle: Pure Mode II, Right: Pure Mode III

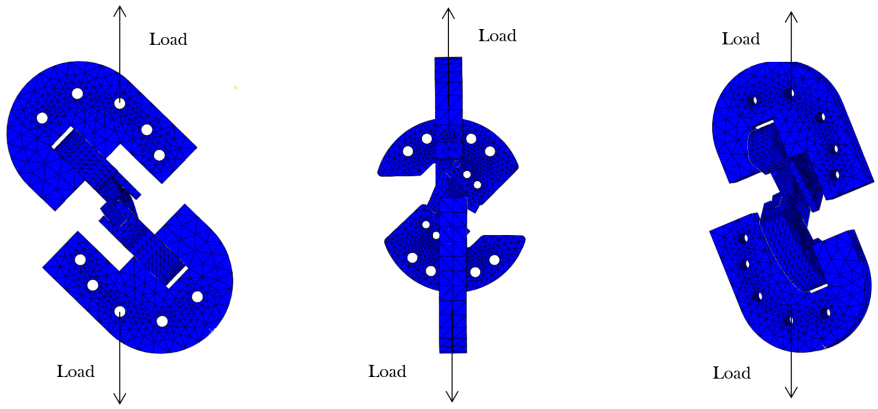

Figure 5.6: Illustration of deformed loading device. Left: $\alpha = 45°$ *&* $\beta = 45°$*, Middle:* $\alpha = 45°$ *&* $\beta = 0°$*, Right:* $\alpha = 67.5°$ *&* $\beta = 25°$

Figure 5.6 illustrates the deformed FEA models for three different loading cases. They were studied to see if the constraints and conditions behaved as intended. They were also used to look for unwanted surface penetrations. All of the twenty-five loading device combinations were set-up and simulated, and studied for expected behavior.

5.2.1 Fixture & Specimen Mesh

After the verification of the fixtures and specimens, a finer mesh was applied. This finer mesh led to computer heavy and time-consuming simulations, which was conducted on a workstation owned by NTNU. This workstation was accessed by using a VPN, virtual private network. For the four fixtures, element shapes were set to Tet. The j-fixtures were assigned four elements to its thickness. The c-fixture were assigned five elements to its thickness. This is illustrated in figure 5.7. As mentioned earlier, the material for the fixtures has a much higher stiffness than the specimen. Because of this, it was assumed that no considerable stresses would occur in the fixtures. See chapter 5.2 for validation.

Two different element shapes were assigned to the specimen. For the four-square partitions and the $R = 5$ circle, a hex-dominated element shape was selected. For the rest of the specimen, the element shape hex was selected. The technique for meshing was sweep, with the algorithm type medial axis. The function local seeds were used to assign more elements in areas were a finer mesh was desired. Eight elements were chosen for the specimen thickness. For the circle around the crack tip, a finer mesh was desired. A circular mesh, with element sizing from large to small, was created. With elements getting smaller as they get closer to the center of the circle, see figure 5.7. Ten elements were assigned on each of the four lines in the r5 circle. A quadratic geometric order and family 3D stress were chosen for all elements. After the meshing of the specimen, it had a total of 10 840 elements.

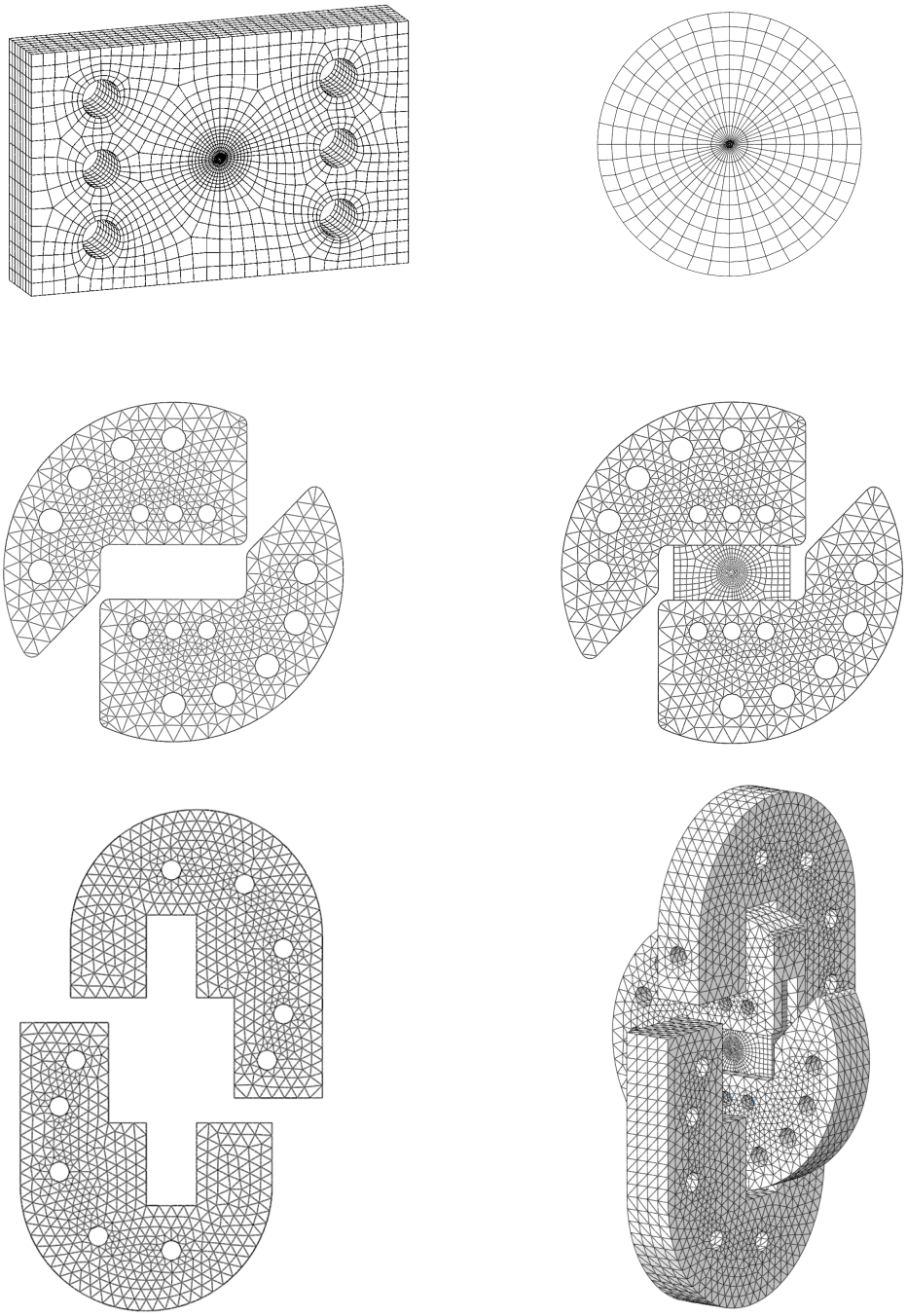

Figure 5.7: Top: Specimen mesh, Middle: C-Fixture mesh, Bottom left: J-fixture mesh, Bottom right: Assembly mesh

5.2.2 Total Mesh & Element Types

Table 1 shows the element type, number of elements and number of nodes for the two fixtures and the specimen. As mentioned earlier, the meshing of the specimen was the main focus of this loading device. The element type used in the specimen was quadratic hexahedral C3D20R. C3D20R-elements are a quadratic, 20-node brick. This element is illustrated in figure 5.8. Compared to linear elements, quadratic elements have midside nodes. 20-node brick elements use quadratic interpolation and are often called quadratic elements or second-order elements, [28].

Table 1: Element type, number of elements & nodes for Fixtures & Specimen

Component	Element Type	Number of Elements	Number of Nodes
Specimen	Quadratic Hexahedral, C3D20R	10 840	50 226
C-Fixtures	Quadratic Tetrahedral, C3D10	2 x 16 528	2 x 25 405
J-Fixtures	Quadratic Tetrahedral, C3D10	2 x 9 324	2 x 15 295

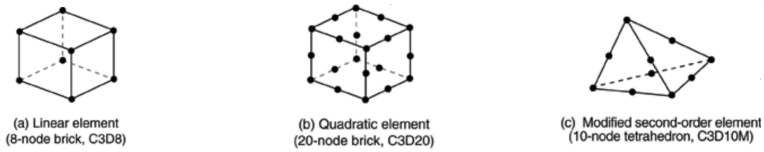

Figure 5.8: Illustration of different element types used in Abaqus [28]

The element type used in the fixtures was quadratic tetrahedral C3D10. See figure 5.8 for illustration. This element has a pyramid shape, and contain ten nodes. C3D10 also has midside nodes, and they use a modified second-order interpolation. They are often called modified second-order elements, [28].

5.2.3 Load & Boundary Conditions

To apply loads, coupling constraints were added for all the holes on the j-fixture. A center reference point was made and set as the couplings master control point, and the inner surface of the hole was set as the slave surface. The boundary condition was set to the opposite hole of the load. The type encastre was chosen, and the region was set to the inner surface of the hole. This boundary condition stops rotation about all axes and translation in all directions (U1=U2=U3=UR1=UR2=UR3=0).

Another boundary condition was also assigned to the model. This condition was applied to the reference point, which load and MPC constraint were assigned to.

The boundary condition type was set to displacement/rotation. For this boundary condition, translation and rotation around every axis were locked except translation in the z-direction (U1=U2=UR1=UR2 =UR3=0). This is the same direction the load was applied to.

5.2.4 Loading Cases

To be able to simulate all combinations of fracture mode one, two and three, different loading cases had to be applied. From no one, this report will refer to these combinations with degrees of α and β. α will be used for rotation of the c-fixture, mode I/II, and β will be used for rotation of the j-fixture, mode III. This is illustrated in figure 5.9.

Table 2: Overview of α and β degree combinations for all loading cases

Modes	Alpha Rotation	Beta Rotation	Number
I/II	$\alpha = 0°, 22.5°, 45°, 67.5°, 90°$	$\beta = 0°$	5
I/III	$\alpha = 0°$	$\beta = 22.5°, 45°, 67.5°, 90°$	4
I/II/III	$\alpha = 22.5°$	$\beta = 22.5°, 45°, 67.5°, 90°$	4
I/II/III	$\alpha = 45°$	$\beta = 22.5°, 45°, 67.5°, 90°$	4
I/II/III	$\alpha = 67.5°$	$\beta = 22.5°, 45°, 67.5°, 90°$	4
II/III	$\alpha = 90°$	$\beta = 22.5°, 45°, 67.5°, 90°$	4

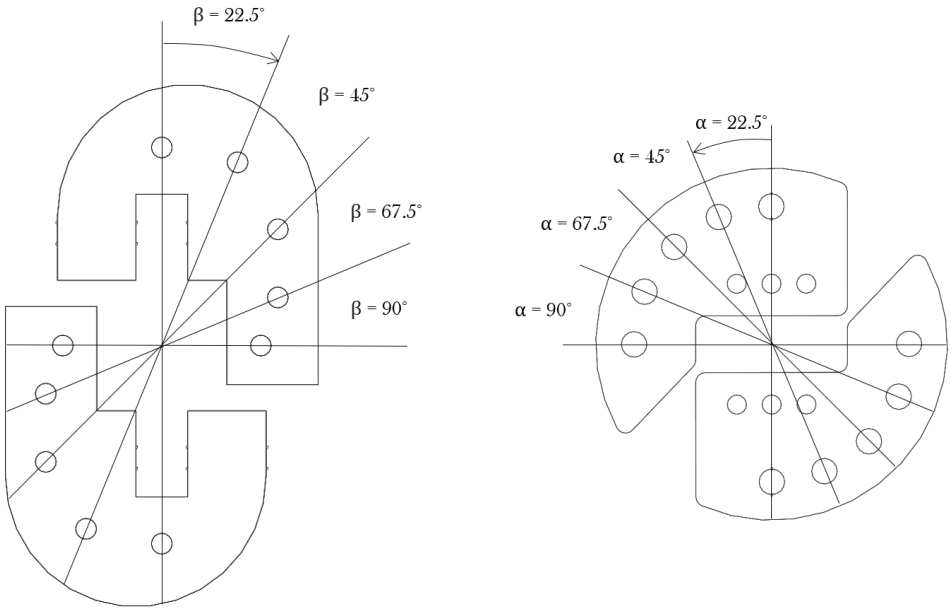

Figure 5.9: Illustration of degrees for different loading cases

When both fixtures is fixed in $\alpha = 0°$ and $\beta = 0°$, pure mode one is obtained. To obtain a pure fracture mode two, the c-fixture is set to $\alpha = 90°$ and j-fixture is set to $\beta = 0°$. For obtaining pure mode I/III, the c-fixture is set to $\alpha = 0°$ and j-fixture is set to $\beta = 90°$.

To obtain results for all combinations, 25 different simulations were set-up. This was done to obtain all available combinations of fracture modes I/II/III, for this loading device. The different loading cases were set-up by applying load and boundary conditions, as explained in section 5.2.3, to the desired degrees of β. A pinned constraint, from the j-fixture through the c-fixture, was applied to the desired degree of α. Table 2 gives an overview of all 25 different combinations of α and β. All of these combinations are simulated and analyzed later on in this project thesis.

5.3 Stress Intensity Factors & T-Stresses

For each loading case, the stress intensity factors were obtained. As mentioned, a load of 1000 N was applied, and the history outputs stress intensity factor was chosen. The stress intensity factors were obtained using contour integral, with the number of ten contours, this is explained in chapter 5.1.3. This history output provides stress intensity factor estimates for all three modes, K_I, K_{II} and K_{III}, for each node on the crack thickness. As mentioned earlier, the thickness in this study was set to eight elements. See chapter 5.2.1. The element type for the specimen was set to quadratic hexahedral, C3D20R, explained in chapter 5.2.2. As covered, this element type has midside and corner nodes. This results in a total of 17 nodes along the crack thickness.

To obtain the desired K-values, a text-file had to be opened. The text-file is created in the same directory as the FEA model and the file-name ends with `.DAT`. The K factor estimates are at the bottom of this text-file.

Figure 5.10 is a caption of the `DAT` file for the results from load case $\alpha = 0°$ and $\beta = 0°$. The relevant stress intensity factors are the ones of the tenth contour. These are located at the bottom right in figure 5.10. At the left in this row, one can see the order of K values. The figure also highlights the number 216. This is the node number. In this case, node number 216 is the first node on the crack thickness. Node number two is called 217 and so on. As shown in the figure, the k values are $K_I = 22.18, K_{II} = -1.94e-02$ and $K_{III} = -7.21e-03$ for the first node in the crack thickness, for this loading case.

These three stress intensity factors (K values), for the tenth contour, was obtained for every 17 nodes, for each 25 of the loading cases. K values was was sorted into K_I, K_{II} and K_{III} in tables, see appendix F, G and H. All of the twenty-five simulations, loading device combinations, resulted in 1275 stress intensity factors.

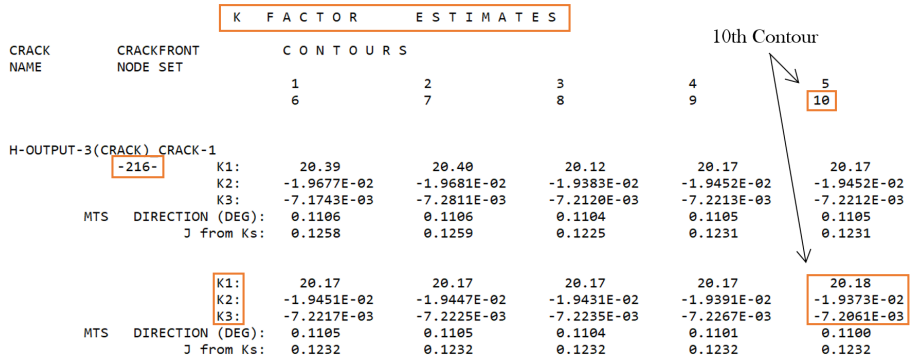

Figure 5.10: Caption of K factor Estimates from DAT-File

From these, the same amount of geometry factors were calculated, by applying the relation in equation 2.47. The stress, σ, in equation 2.47 was calculated by inserting the applied load of 1000 N and the area of the specimen cross section, $37.5mm \cdot 10mm$. The geometry factors along the thickness were plotted in the following figures, 7.1, 7.2, 7.3, 7.4 and 7.5. All of the results are covered in chapter 7 and the appendices I, J and K.

To obtain the t-stress, the history output type was set to t-stress. As for the stress intensity factors, this history output also creates a `DAT` file. A caption from this `DAT` file is shown in figure 5.11. The t-stress estimate, for the 10th contour, for each of the 17 nodes along the specimen thickness are shown in appendix L. The obtained t-stresses are presented and discussed in chapter 7. Figure 5.11 shows four nodes, for the loading case of $\alpha = 0°$ and $\beta = 0°$. The dimensionless t-stress, T^*, was obtained by applying the relation in equation 2.48, see chapter 2.6.5. All of the dimensionless t-stresses are shown in appendix M, and presented in chapter 7.

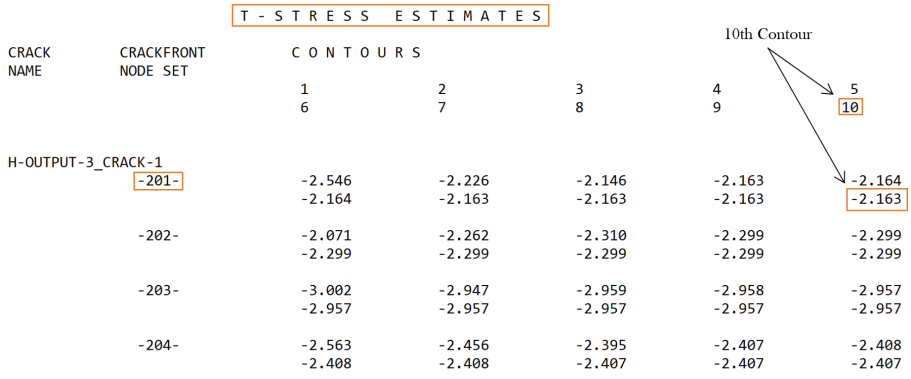

Figure 5.11: Caption of T-Stress Estimates from DAT-File

5.4 Criteria Procedure

This subsection will cover some of the fracture criteria procedure and solution methods used in this thesis. After the numerical results were calculated, values could be used in the different fracture criteria. Some of the simpler criteria could be written and solved implicit, and others had to be derived and written as explicit functions.

5.4.1 Mixed Mode I/II

The criteria predictions for mixed mode I/II was straightforward solutions. For the MTS criterion, equation 2.32 were used to predict θ for each loading device position. θ values were put into plots with M^e_{12}. The estimated θ values were then put into equation 2.33 to plot the fracture limit curves. The same procedure were used for GMTS, see equation 2.36 and 2.37, and for dimensionless factors, see chapter 2.6.5. In the works of Smith et al. [14] a solution method, for plotting the MTS and GMTS criterion for mixed mode I/II cases, were proposed. Equations were derived as functions of one parameter, θ. This solution method was used for plotting the mixed mode I/II curve in figure 2.5. This was solution method for GMTS were not used in this thesis, as it assumes constant T values. The step by step solution above was therefore conducted instead.

5.4.2 Mixed Mode I/III

MTS

For the loading cases of mixed mode I/III, the criteria MTS, GMTS, and Richard were used for predictions. In the works of Liu et al. [19], the MTS criterion for mixed mode I/III were derived. The out of plane crack initiation angle was given as equation 5.1, and the fracture limit relation were given as expressed in equation 5.2.

$$\phi_f = \frac{1}{2} \cdot tan^{-1}\left[\frac{2K_{III}}{(2v-1)K_I}\right] \tag{5.1}$$

$$\frac{K_I}{K_{IC}} \cdot cos^2\phi_f - \frac{K_{III}}{K_{IC}} \cdot sin2\phi_f + \frac{2vK_I}{K_{IC}} sin^2\phi_f = 1 \tag{5.2}$$

In addition to the mixity parameters of mode I/II, Aytollahi et. al [7] presented relations for mixity parameters of mode I/III and II/III as well, these can be studied in equation 5.3 and 5.11.

$$M^e_{13} = \frac{2}{\pi} tan^{-1}\left(\frac{K_I}{K_{III}}\right) \tag{5.3}$$

By placing the relation from equation in equation 5.3 an equation for I/III mixity parameter as a function of ϕ were made, see equation 5.4. This equation was used when plotting the curve for the M^e_{13} in steps of ϕ, see chapter 7. The `python` script used for plotting this relation can be studied in appendix P.

$$M_{13}^{e} = \frac{2}{\pi} tan^{-1}\left(\frac{2}{tan(2\phi)(2v-1)}\right) \tag{5.4}$$

The relation in equation 5.4.2 was also used in equation 5.2. Two equations were derived, K_I/K_{IC} as a function of ϕ and v, given in equation 5.5, and K_{III}/K_{IC} as a function of ϕ and v, given in equation 5.6. The python script covering the fracture limit plots of mixed mode I/III can be studied in appendix Q.

$$\frac{K_I}{K_{IC}} = \frac{1}{cos^2(\phi) - \frac{tan(2\phi)\cdot(2v-1)\cdot sin(2\phi)}{2} + 2v \cdot sin^2(\phi)} \tag{5.5}$$

$$\frac{K_{III}}{K_{IC}} = \frac{1}{\frac{2cos^2(\phi)}{tan(2\phi)(2v-1)} + \frac{4v\cdot sin^2(\phi)}{tan(2\phi)\cdot(2v-1)} - sin(2\phi)} \tag{5.6}$$

GMTS

For the plotting of the GMTS criterion for mixed mode I/III loading, a step by step solution was performed. This was due to the complex equations, and a function with one changing parameter was not easily derived. Therefore, equation 2.24 were derived by replacing $K_{II} = 0$ and $\theta = 0$. The derived equation is given in 5.7.

$$\sigma_{\theta\theta} = \frac{1}{\sqrt{2\pi r_c}}\left(K_I \cdot cos^2(\phi) - K_{III} \cdot sin(2\phi) + 2v\left[K_I + \frac{T\sqrt{2\pi r_c}}{2}\right] sin^2(\phi)\right) \tag{5.7}$$

By applying the first hypothesis of GMTS, equation 2.29, an equation for crack initiation angle, ϕ_f, were found, see equation 5.8. This relation was used to calculate ϕ. The equation was solved implicitly in excel, by inserting K_I, K_{III} and T values obtained from Abaqus. These equations were also solved by applying the dimensionless factors Y_I, Y_{III} and T^*, see chapter 2.6.5.

$$-K_I cos(\phi) sin(\phi) - K_{III} \cdot cos(2\phi) + 2v\left[K_I + T\sqrt{2\pi r_c} \cdot \frac{1}{2}\right] cos(\phi) sin(\phi) = 0 \tag{5.8}$$

When ϕ were found for each of the mixed mode I/III loading device combinations, the obtained values were placed in equation 5.9 and 5.10. When the K_{IC}/K_I and K_{IC}/K_{III} were obtained for each loading combinations, they were inverted to and plotted as fracture limit plots, K_I/K_{IC} - K_{III}/K_{IC}. The plots can be studied in chapter 7 and the python scripts can be found in appendix Q.

$$\frac{K_{IC}}{K_I} = cos^2(\phi) - \frac{K_{III}}{KI} \cdot sin(2\phi) + 2v\left[1 + \frac{T\sqrt{2\pi r_c}}{2K_I}\right] \cdot sin^2(\phi) \tag{5.9}$$

$$\frac{K_{IC}}{K_{III}} = \frac{K_I}{K_{III}} \cdot cos^2(\phi) - sin(2\phi) + 2v\left[\frac{K_I}{K_{III}} + \frac{T\sqrt{2\pi r_c}}{2K_{III}}\right] \cdot sin^2(\phi) \tag{5.10}$$

5.4.3 Mixed Mode II/III

For the mixed mode cases of II/III, two crack initiation angles were present, θ and ϕ. In these mixed mode situations, the Richard criterion was used for prediction. This was due to the low obtained T values, this is discussed in chapter 7. Equations 2.40 and 2.41 were used to predict the in and out of plane crack initiation angles for each loading device position. These were plotted with the mixity parameter, M_{23}^{e}, see equation 5.11. All plots were presented in chapter 7.

$$M_{23}^{e} = \frac{2}{\pi} tan^{-1}\left(\frac{K_{II}}{K_{III}}\right) \tag{5.11}$$

6 Experimental Procedure

This chapter consists of the testing of this thesis. The material used for all of the tests were PMMA. Dog-bone tests were conducted to gather and verify material properties. These were followed by mixed mode tests, with the designed loading device.

6.1 PMMA Dog-bone Testing

In addition to the 90 CTS samples, four dog-bones samples were manufactured. They were manufactured from the same PMMA plate as the CTS specimens. Two of the samples were cut out in a transverse direction on the PMMA plate, and the other two in a longitudinal direction. Figure 6.1 shows photographs of the four manufactured dog-bone samples. These dog-bone specimens were also manufactured at Realfagsbygget.

The dog-bone specimens have the length of 69 mm, the outer width of 12.5 mm and a thickness of 3 mm. Two curves with a radius of R30 can be found on each side of the specimen, with a minimum width of 5 mm. These measurements and features are illustrated to the left in figure 6.1.

A MTS tensile testing machine was used for the dog-bone tests. To be able to obtain the precise inputs for the tensile test, and to calculate a stress-strain curve, a caliper was used. Despite precise fabrication methods of the specimen, some variations in the measurements may occur. The caliper was used to measure four different values, the specimen width at the center of the specimen, the length of the curved area and the thickness for three positions along the curved area of the specimen. All of these values are presented in tabular 3. An illustration of the location of the measurements are found beneath this tabular, see figure 6.2.

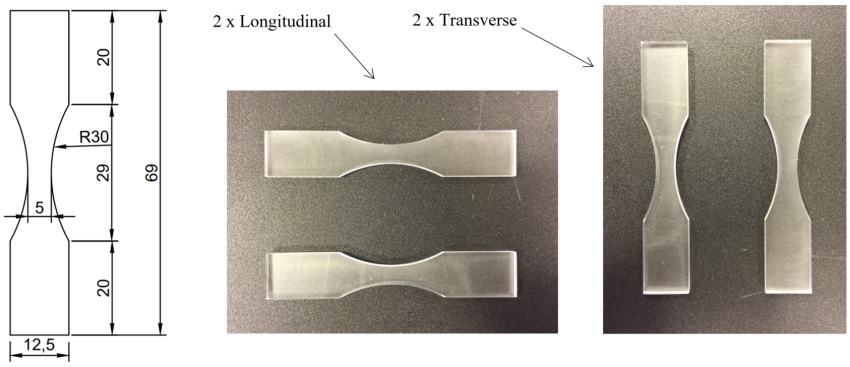

Figure 6.1: Left: Dogbone measurements, Middle and Right: Two longitudinal and transverse dog-bone specimens.

Table 3: Specific measurements of all four dog-bone specimens

Specimen Type & Number	Width	t1	t2	t3	Length
Longitudinal 1	5.04	3.01	2.98	3.00	29.17
Longitudinal 2	5.02	3.00	2.98	3.01	28.84
Transverse 1	5.02	2.99	2.98	2.99	29.06
Transverse 2	5.02	2.99	2.98	3.00	28.98

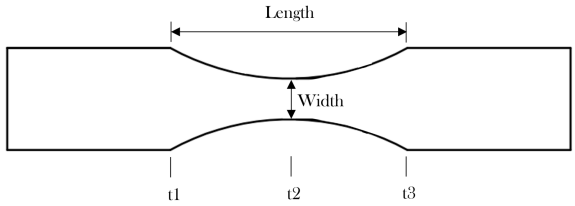

Figure 6.2: Illustration of t1, t2, t3, width and length measurements of the dog-bone specimen.

After the caliper measuring, the tensile tests were initiated. The dog-bone specimens were mounted to the tensile testing machine with clamps. This is illustrated to the left in figure 6.3. After the mounting, the test was initiated. The load is applied until fracture occurs. A closeup of the fractured specimen is illustrated to the right in figure 6.3.

After fracture occurs, the test is stopped, and the text file is saved to a chosen directory. The outputs of the test were time, elongation and load. These outputs were used to create a stress-strain curve. Engineering stress and engineering strain were calculated.

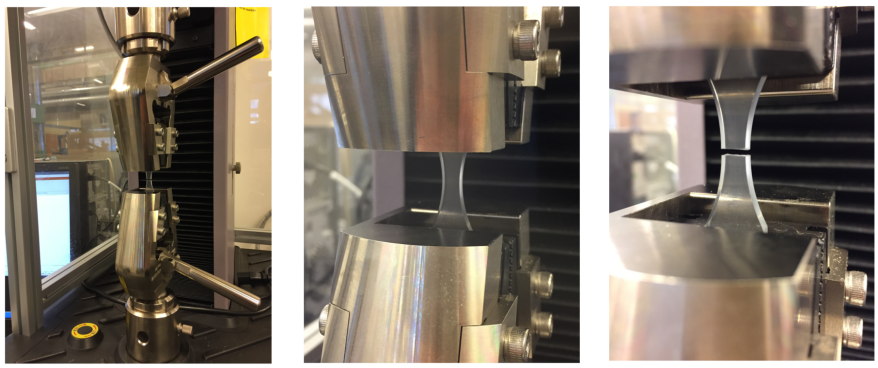

Figure 6.3: Left: Tensile test overview, Middle: Specimen closeup before fracture, Right: Specimen closeup after fracture.

The engineering strain was calculated by dividing the elongation by the original length, see table 3. The engineering stress was calculated by dividing the applied load by the cross-section. The cross section is calculated by multiplying the width by the thickness, t3, see table 3 [2].

The calculated engineering stress and strain are presented in figure 6.4. Each of the four plots consists of 9300 points. Small variations of were found. The maximum stress for the longitudinal specimen number one was 66.63 MPa, 65.47 MPa for longitudinal number two, 65.69 MPa for transverse number one and 66.39 MPa for transverse specimen number two. The average of these values were used as the tensile strength, ϵ_t, through this thesis. Average tensile strength was calculated to be 66.05 MPa. The stress-strain curves for each PMMA sample all have a brittle form, which can be expected from this polymer at room temperature. By comparing the plots in figure 6.4, almost no variation was found between the longitudinal and transverse specimens. This shows an isotropic material behavior. An isotropic behavior was expected for this material, see chapter 2.2.

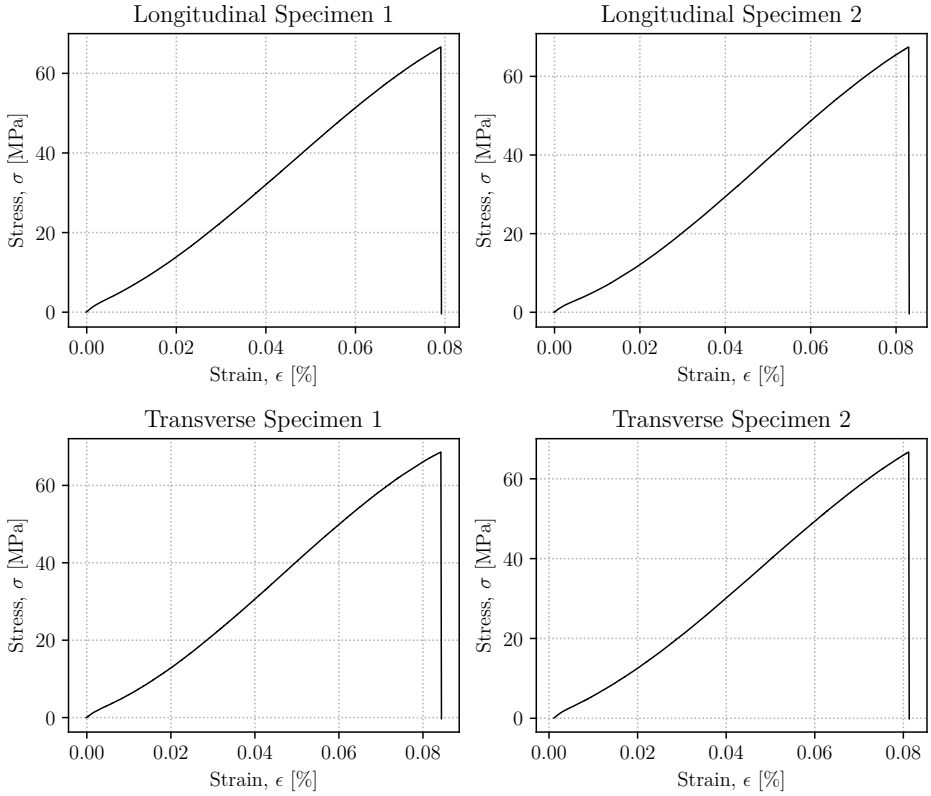

Figure 6.4: Four Stress-Strain plots for each of the four PMMA dogbones.

6.2 Mixed Mode I/II/III Testing

6.2.1 Loading Device Setup

For the mixed mode I/II/III testing, a MTS tensile testing machine was used. A testing machine, with a higher capacity than the dog-bone specimen tests, was used. Mainly because of hydraulic controlled grips. This was needed to get a good and steady grip, to be able to install the forks rigidly and perpendicularly. The perpendicular installation of the forks was important to ensure desired testing results, and to be able to obtain results for pure fracture modes. In addition to a perpendicular installation, it was important to align the two forks with respect to each other. After proper installation, the forks did not have to be moved or changed during all of the mixed mode tests. The finished installed forks is shown in the photography to the left in figure 6.5.

After the installation of the forks, the j-fixtures could be mounted. Instead of pins, bolts were used for assembling the j-fixtures to the forks. This was due to the weight of the j-fixture, and to prevent this weight to add more torsion, mode III, to the loading case than desired. The j-fixtures was installed in the desired angle, and the bolts were fastened with nuts.

A j-fixture installation with the angle of $\beta = 45°$ is shown in middle of figure 6.5. When the j-fixtures were installed in the correct position, the c-fixture and specimen could be installed. The specimen was assembled to the c-fixture before both were mounted to the j-fixtures. The specimen was installed to the c-fixture with the help of six pins, as explained in chapter 4. The c-fixtures and specimen were then fastened to the j-fixture with the help of two pins. This is shown in the photography to the right in figure 6.5. A c-fixture installation with the angle $\alpha = 0°$ is shown in figure 6.5.

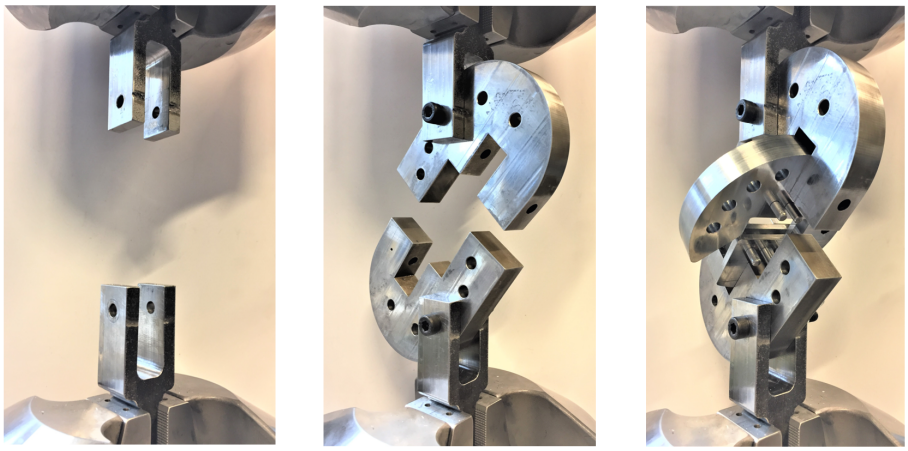

Figure 6.5: Left: Fork Setup, Middle: J-Fixture Setup, Right: C-Fixture and specimen setup

6.2.2 Mixed Mode Testing Cases

Each of the twenty five loading cases, see table 2, were set up as explained in chapter 6.2.1 and figure 6.5. Because of the bolted connection between the forks and j-fixtures, all of the combinations for each j-fixture were conducted before changing the β angle. Three specimens were tested in each combination, which gave a total of 75 initial fracture tests. A few more samples were used for retesting. Figure 6.6 to 6.10 shows three out of five c-fixture loading case for each of the five j-fixture loading cases. Each of the figures shows e sideways view of the j-fixture position to the left, followed by three isometric views of three different c-fixture positions, $\alpha = 0°$, $\alpha = 45°$ and $\alpha = 90°$.

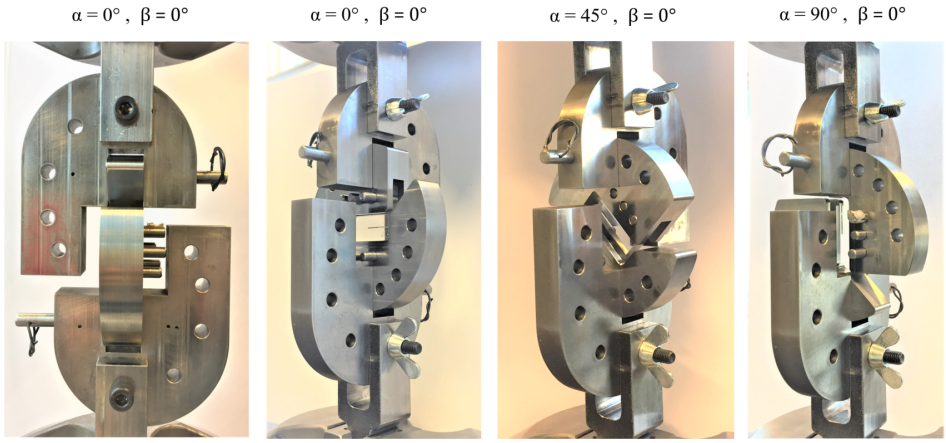

Figure 6.6: Three out of five loading cases for J-fixture angle $\beta = 0°$.

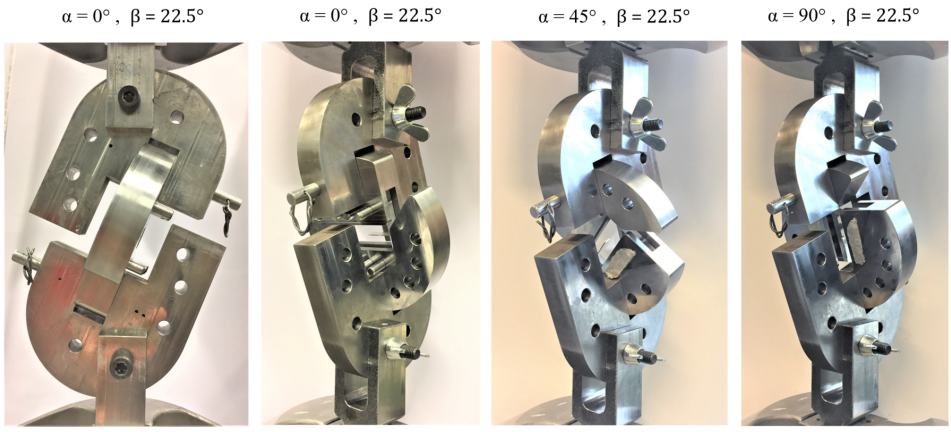

Figure 6.7: Three out of five loading cases for J-fixture angle $\beta = 22.5°$.

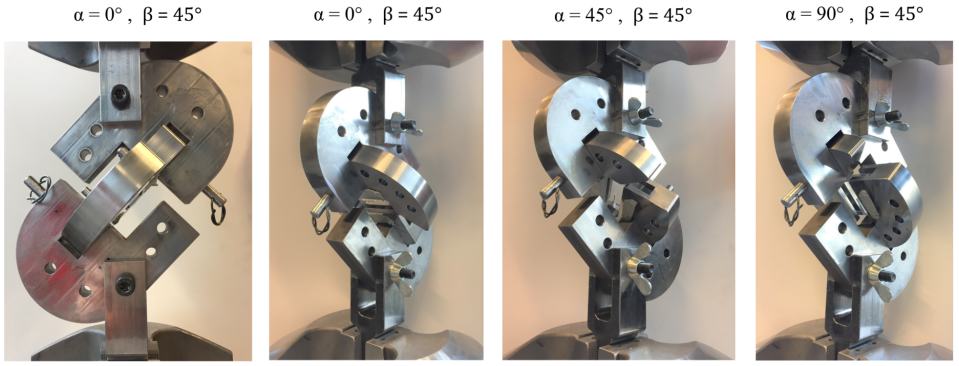

Figure 6.8: Three out of five loading cases for J-fixture angle $\beta = 45°$.

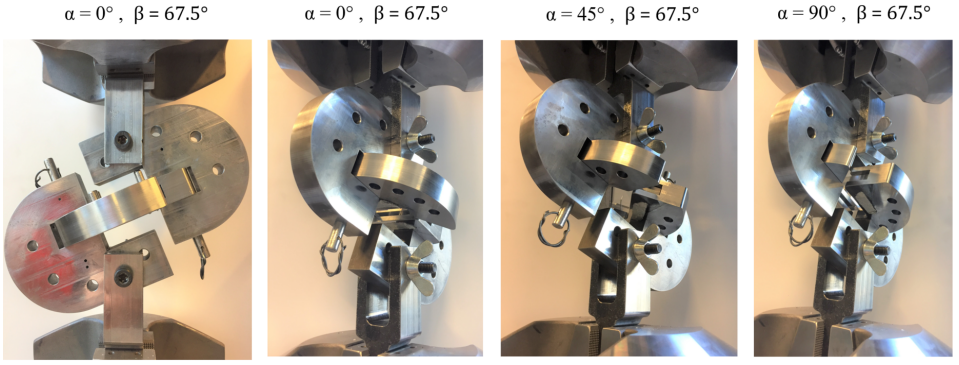

Figure 6.9: Three out of five loading cases for J-fixture angle $\beta = 67.5°$.

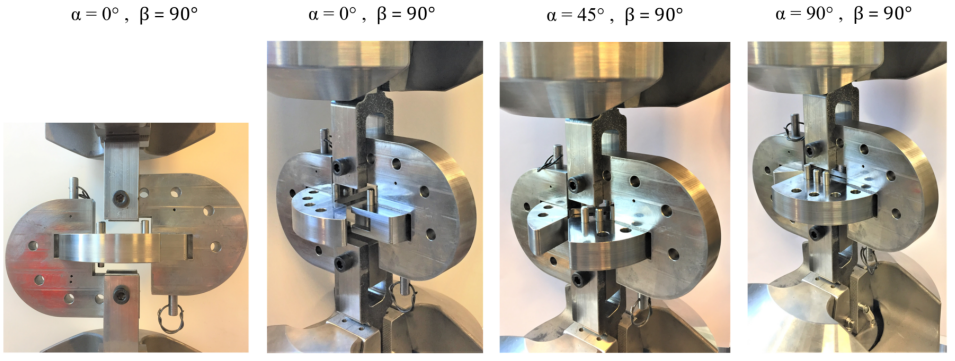

Figure 6.10: Loading positions for J-fixture angle $\beta = 90°$, Pure Mode III.

Figure 6.11 shows the load-displacement plots for three of the twenty-five mixed mode loading cases. The plots show the loading cases of pure mode I, pure mode II and pure mode III for the mixed mode CTS specimen installed in the loading device. Each plot consists of about fifteen thousand points. The plots were constructed from the text files generated from the MTS tensile testing machine. `Python` scripts were used for plotting and management of the large amounts of data. The fracture load for all of the twenty-five mixed mode loading combinations can be found in chapter 7. The load-displacement plots have a brittle form, as expected for the chosen material, PMMA, see figure 6.4. A slightly curved relation between load and displacement can be seen at the beginning of each loading case, see figure 6.11. This can be due to adjustments between the moving parts and pins in the loading device.

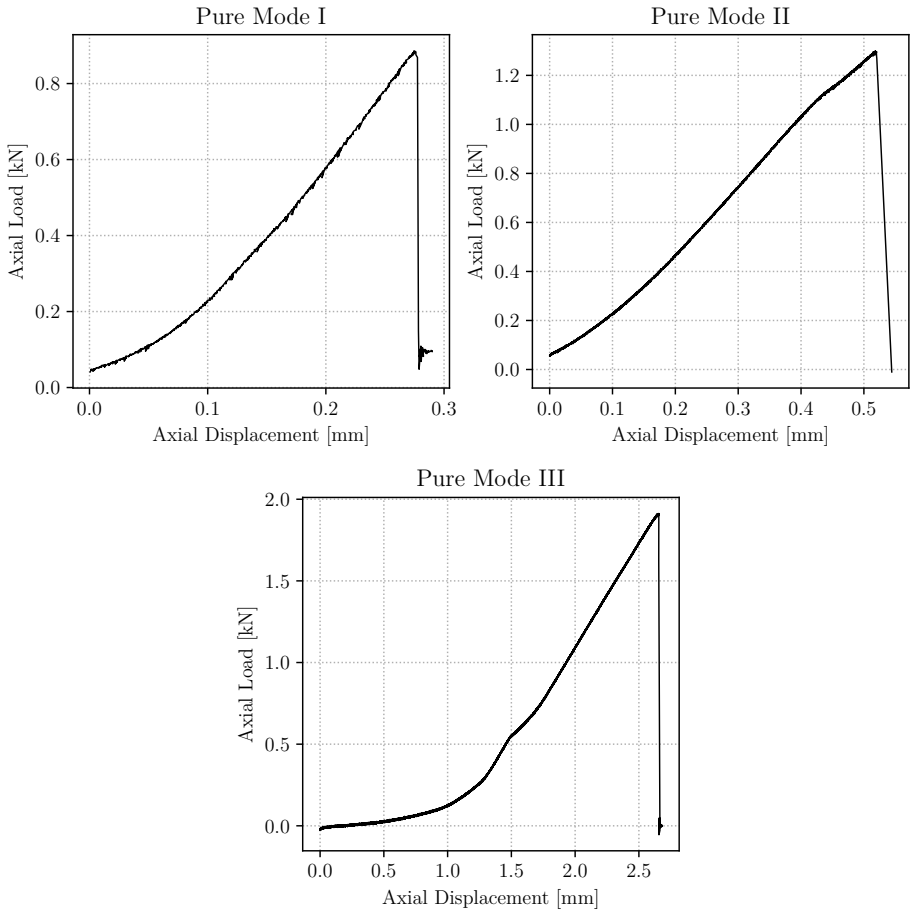

Figure 6.11: Load-Displacement curves for the loading case of Pure Mode I, Pure Mode II and Pure Mode III.

6.3 Specimen Crack Paths

After three specimens had been tested for each of the twenty-five loading cases, the fractured specimens were studied. Crack paths and kinking angles were easily studied, due to the transparency properties of PMMA. In this section, both the in-plane crack angle, θ, and the out of plane crack angle, ϕ were studied.

6.3.1 In Plane Crack Path

Figure 6.12 shows a photography of five fractured specimen. Each of the specimens represents one loading case, for each of the five combinations for j-fixture angle $\beta = 0°$. Only one out of three specimens for each loading case is presented, due to similar features.

From right to left in figure 6.12, the loading case is changed by increasing the c-fixture angle of 22.5°. It was shown that for each increment of the c-fixture angle, the kinking angle also increases.

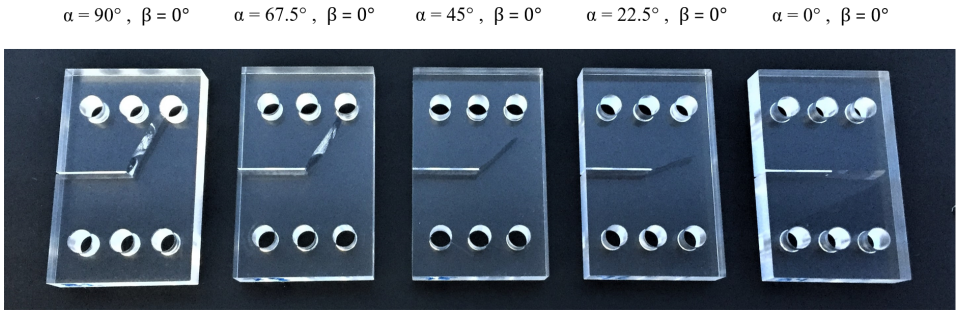

Figure 6.12: Specimen in plane crack paths for all C-fixture combinations, of J-fixture position $\beta = 0°$.

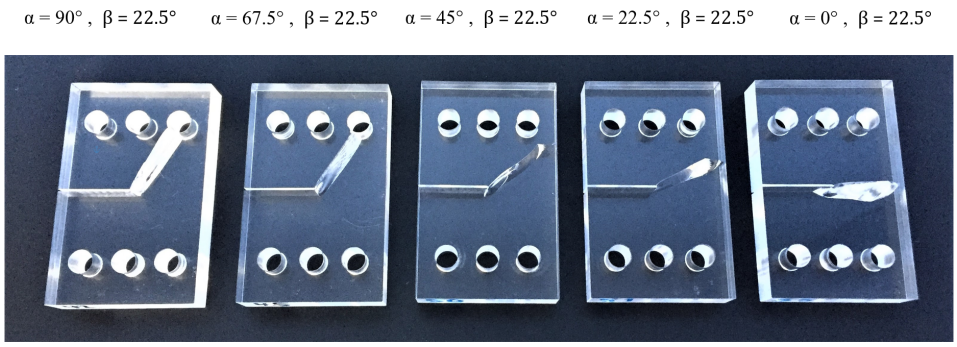

Figure 6.13: Specimen in plane crack paths for all C-fixture combinations, of J-fixture position $\beta = 22.5°$.

α = 90° , β = 45° α = 67.5° , β = 45° α = 45° , β = 45° α = 22.5° , β = 45° α = 0° , β = 45°

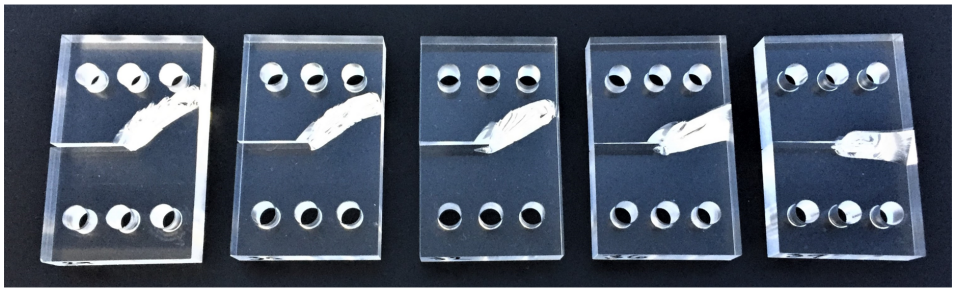

Figure 6.14: Specimen in plane crack paths for all C-fixture combinations, of J-fixture position $\beta = 45°$.

α = 90° , β = 67.5° α = 67.5° , β = 67.5° α = 45° , β = 67.5° α = 22.5° , β = 67.5° α = 0° , β = 67.5°

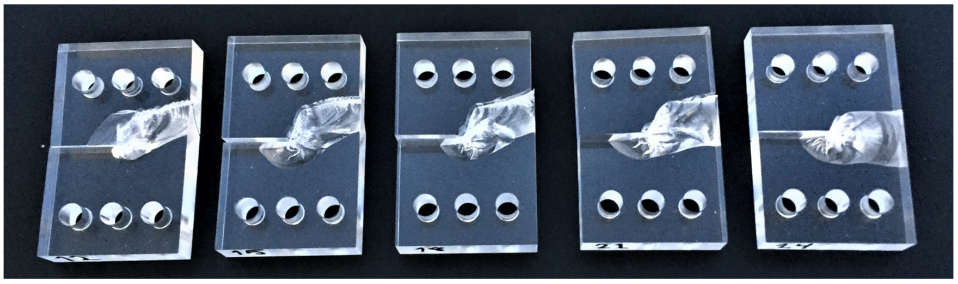

Figure 6.15: Specimen in plane crack paths for all C-fixture combinations, of J-fixture position $\beta = 67.5°$.

α = 90° , β = 90° α = 67.5° , β = 90° α = 45° , β = 90° α = 22.5° , β = 90° α = 0° , β = 90°

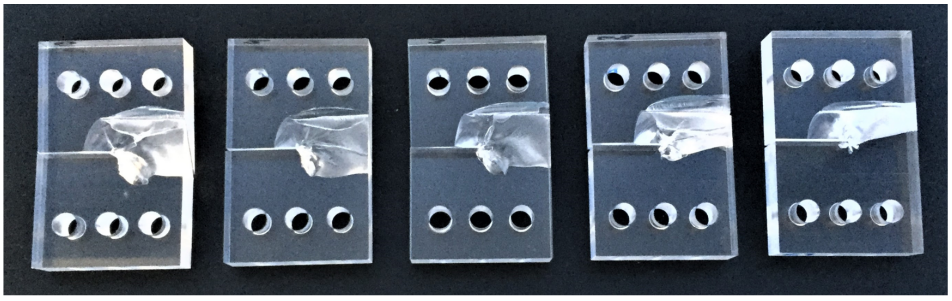

Figure 6.16: Specimen in plane crack paths for all C-fixture combinations, of J-fixture position $\beta = 90°$, Pure Mode III.

To the right in figure 6.12, a pure mode I fracture case is shown, as expected from the loading case $alpha = 0°, \beta = 0°$, see table 2. This is a straight and plane crack, with no in-plane or out of plane angle. To the left in figure 6.12, the cracked specimen of a pure mode II case can be seen. A large in-plane crack angle can be seen. The crack stops when it enters one of the six pin holes.

Figure 6.13 shows five specimens for five c-fixture combinations, of the j-fixture position $\beta = 0°$. The increasing in-plane crack angle for each position of α, were found to be almost similar to the case of $\alpha = 0°$, figure 6.12. However, the β position of 22.5° gives a twisting, out of plane angle, to the kink as well. The out of plane angle is further discussed in chapter 6.3.2.

The next presented loading case is all five c-fixture combinations of, the j-fixture position $\beta = 45°$, see figure 6.14. Compared to the two previous presented β positions, $\beta = 0°$ and $\beta = 22.5°$, the in-plane crack angle is not increasing in the same extent for each c-fixture position. A slightly more curved kink is also observed, where the cracks are straight for $\beta = 0°$ and $\beta = 22.5°$. The β position of 45° gives larger out of plane angel of the kink, than for the case of $\beta = 22.5°$. The out of plane angle is further discussed in chapter 6.3.2.

For the case of $\beta = 67.5°$ and $\beta = 90°$, the in plane angle did not change much with the different combinations of c-fixture, see figure 6.15 and 6.16. Altough there is a visual change in the out of plane angle, which is further discussed in chapter 6.3.2. The testing of the j-fixture case $\beta = 90°$, led to some of the specimens breaking into three pieces or more. This loading case led to some inequalities in the fracture pattern. However the fracture loads, see chapter 7.2, shows consistent test results. All of the exact measure angles can be studied in chapter 6.3.3.

6.3.2 Out of Plane Crack Path

All of the out of plane angles, for $\beta = 0°$, can be studied in figure 6.17. The two specimens to the left in the figure gives a bad representation of the out of plane angle. This is because of the crack arrest in the pin holes, see figure 6.12 and 6.13. The crack arrest in the pin hole also applies for the two specimens to the left in figure 6.18. The out of plane angles for all fractured specimens can be studied in figure 6.17-6.21. A good overview of the increasing of out of plane angle can be given by studying the $\alpha = 45°$ specimen for all β positions, see center specimen in figure 6.17-6.21. The out of plane angle for $\alpha = 45°/\beta = 0°$ can be seen as flat and the out of plane angle of $\alpha = 45°/\beta = 90°$ can be seen as sharp. Note that all of the loading positions in figure 6.21 were pure mode III. An isometric projection and overview of all fractured specimens can also be studied in figure 6.22.

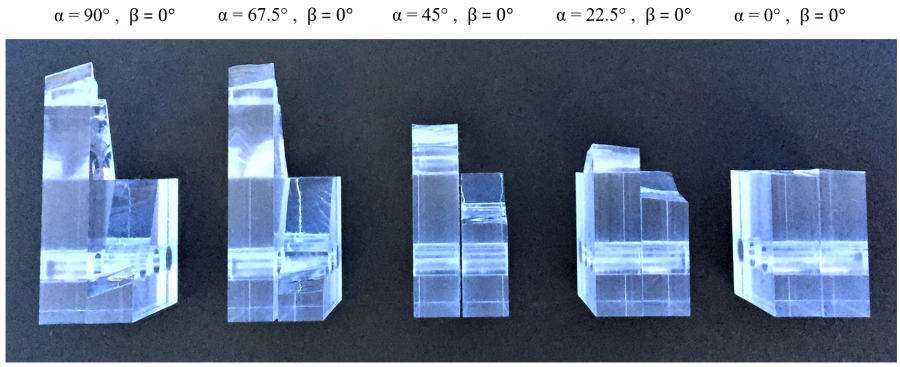

Figure 6.17: Specimen out of plane crack paths for all C-fixture combinations, of J-fixture position $\beta = 0°$.

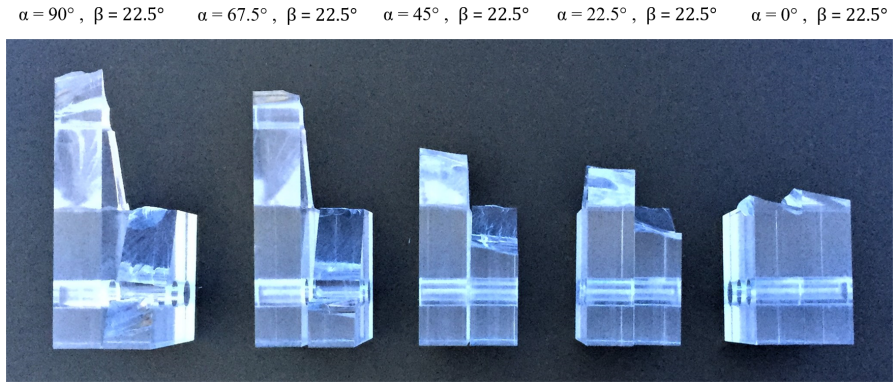

Figure 6.18: Specimen out of plane crack paths for all C-fixture combinations, of J-fixture position $\beta = 22.5°$.

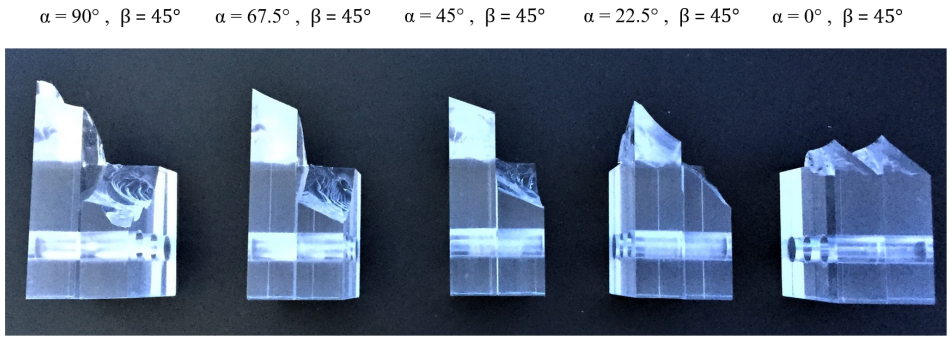

Figure 6.19: Specimen out of plane crack paths for all C-fixture combinations, of J-fixture position $\beta = 45°$.

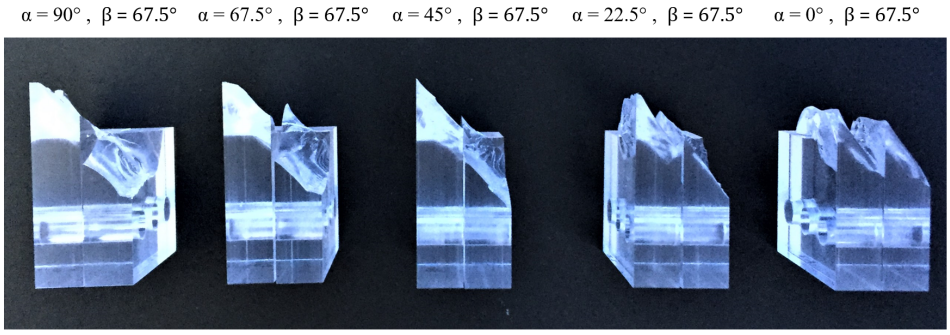

Figure 6.20: Specimen out of plane crack paths for all C-fixture combinations, of J-fixture position $\beta = 67.5°$.

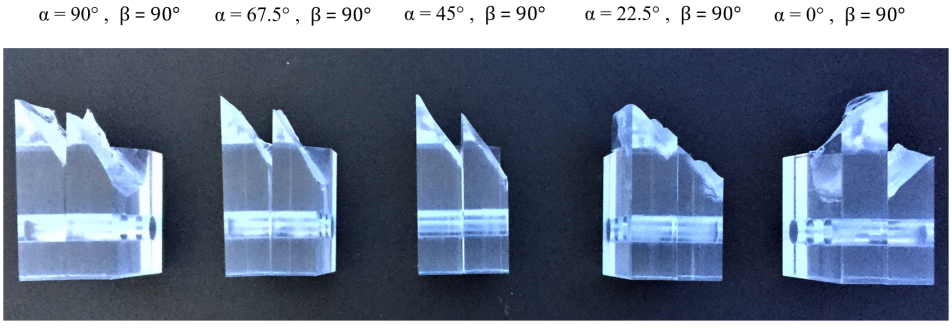

Figure 6.21: Specimen out of plane crack paths for all C-fixture combinations, of J-fixture position $\beta = 90°$, Pure Mode III.

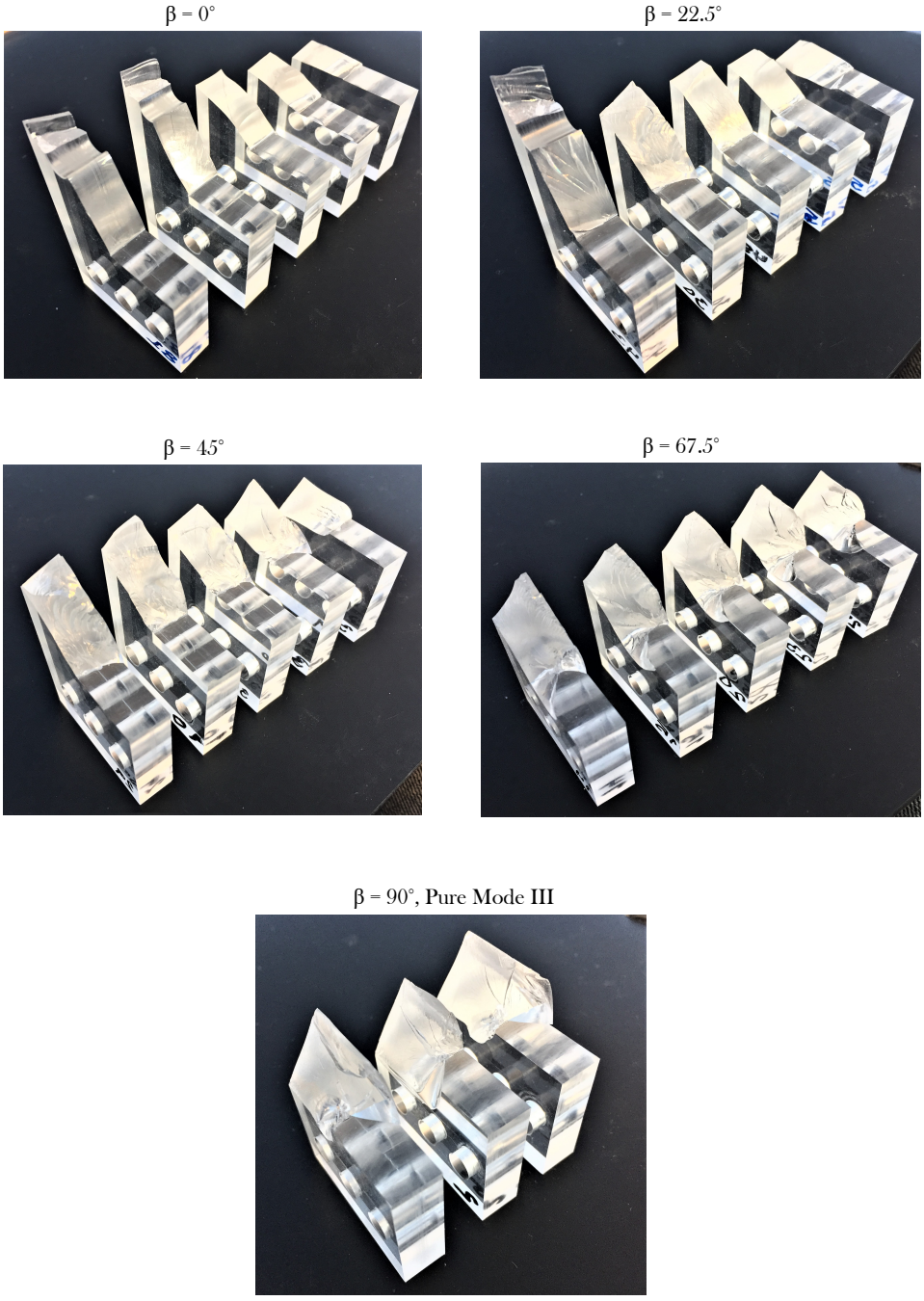

Figure 6.22: Isotropic projection photographs of all of the fractured specimens, with $\alpha = 0°$ to the right and $\alpha = 90°$ to the left.

6.3.3 Measured Crack Initiation Angles

All of the out of plane and in-plane angles were measured by using a microscope. Some of the microscope photographs can be studied in figure 6.23. Angles were measured by placing two straight lines manually, to fit the crack, and measuring the angle between these drawn lines. This was done with high accuracy, but some deviations from reality may still occur. With a higher amount of out of plane angles, the in-plane angles were found more difficult to measure. This can be seen in the loading case of $\alpha = 90°/\beta = 45°$ in figure 6.23. These may lead to some deviations from the actual angles. The out of plane angle for the specimens with crack arrest in the pinhole were also found difficult to measure precisely. All of the measured specimen angles can be studied in table 4. The sign of the angles was set to negative because of the practice in previous work and fracture criteria [29, 7, 16].

Table 4: Overview of all microscope measured in plane, and out of plane crack initiation angles.

Modes	Alpha & Beta Rotation	In Plane, θ_f	Out of Plane, ϕ_f
I	$\alpha = 0°$, $\beta = 0°$	$0°$	$0°$
I/II	$\alpha = 22.5°$, $\beta = 0°$	$-21.29°$	$0°$
I/II	$\alpha = 45.0°$, $\beta = 0°$	$-35.15°$	$0°$
I/II	$\alpha = 67.5°$, $\beta = 0°$	$-55.71°$	$0°$
II	$\alpha = 90.0°$, $\beta = 0°$	$-68.19°$	$0°$
I/III	$\alpha = 0°$, $\beta = 22.5°$	$0°$	$-19.23°$
I/III	$\alpha = 0°$, $\beta = 45.0°$	$0°$	$-37.08°$
I/III	$\alpha = 0°$, $\beta = 67.5°$	$0°$	$-46.71°$
II/III	$\alpha = 90°$, $\beta = 22.5°$	$-53.80°$	$-10.41°$
II/III	$\alpha = 90°$, $\beta = 45.0°$	$-40.35°$	$-19.26°$
II/III	$\alpha = 90°$, $\beta = 67.5°$	$-37.53°$	$-40.05°$
I/II/III	$\alpha = 22.5°$, $\beta = 22.5°$	$-33.83°$	$-8°$
I/II/III	$\alpha = 22.5°$, $\beta = 45.0°$	$-18.04°$	$-36.61°$
I/II/III	$\alpha = 22.5°$, $\beta = 67.5°$	$-15.42°$	$-48.96°$
I/II/III	$\alpha = 45.0°$, $\beta = 22.5°$	$-45.99°$	$-9.36°$
I/II/III	$\alpha = 45.0°$, $\beta = 45.0°$	$-25.03°$	$-18.47°$
I/II/III	$\alpha = 45.0°$, $\beta = 67.5°$	$-17.52°$	$-44.39°$
I/II/III	$\alpha = 67.5°$, $\beta = 22.5°$	$-67.13°$	$-25.34°$
I/II/III	$\alpha = 67.5°$, $\beta = 45.0°$	$-32.91°$	$-13.67°$
I/II/III	$\alpha = 67.5°$, $\beta = 67.5°$	$-20.99°$	$-38.25°$
III	$\alpha = 0°$, $\beta = 90°$	$0°$	$-42.02°$
III	$\alpha = 22.5°$, $\beta = 90°$	$0°$	$-42.37°$
III	$\alpha = 45.0°$, $\beta = 90°$	$0°$	$-53.19°$
III	$\alpha = 90.0°$, $\beta = 90°$	$0°$	$-54.43°$
III	$\alpha = 67.5°$, $\beta = 90°$	$0°$	$-53.04°$

α = 90°, β = 22.5°

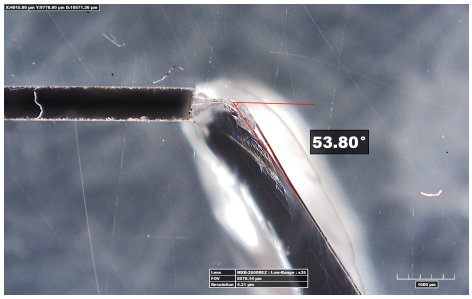

α = 22.5°, β = 0°

α = 22.5°, β = 22.5°

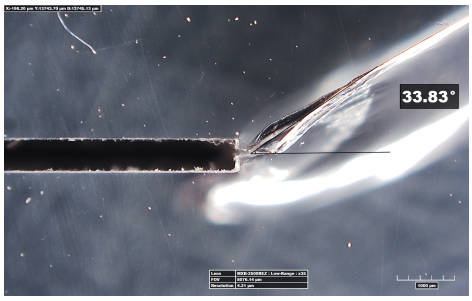

α = 45°, β = 22.5°

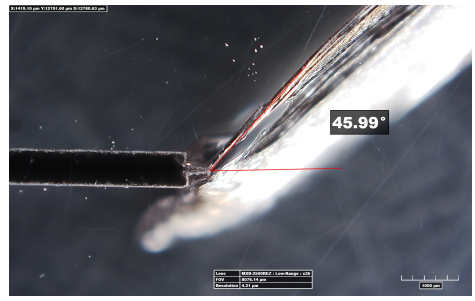

α = 67.5°, β = 22.5°

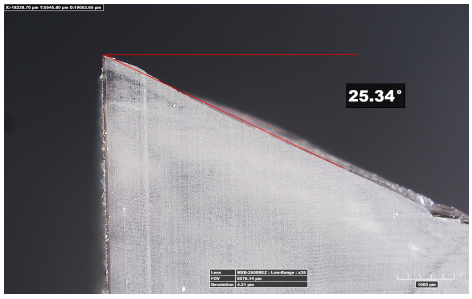

α = 0°, β = 45°

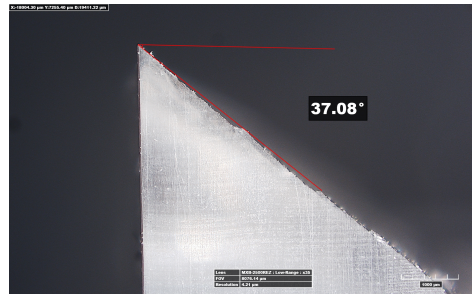

α = 90°, β = 67.5°

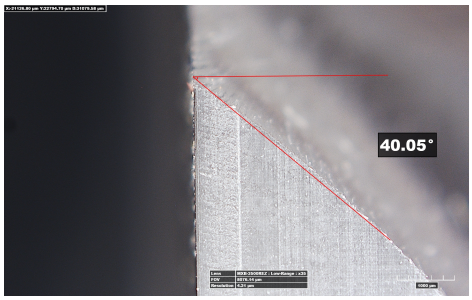

α = 45°, β = 90°

Figure 6.23: Microscope photograpies and measurements of out of plane, and in plane crack initiation angles.

7 Results & Discussion

This chapter will cover the results and discussion for all 25 loading device combinations, see table 2. Theoretical and experimental data were gathered and compared. The numerical analyses set-up and criteria procedure for these results were covered in chapter 5. The experimental procedure was covered in chapter 6.

7.1 Geometry Factors

7.1.1 Geometry Factors for Mixed Mode I/II

As mentioned, all Y-values used for the plots can be studied in the appendices. How to obtain the Y-values were covered in chapter 2.6.5. All Y-values for this subsection, geometry factors for Mode I/II, can be found in appendix I, J and K. Each appendix contains Y values for each mode, I, II and III, for all twenty-five fixture combinations. The appendix tables show the geometry factors for each 17 nodes, along the specimen thickness. The reason for 17 nodes along the thickness, is given by the mesh properties. Eight elements were assigned for the specimen thickness, and quadratic elements were applied, this is explained in section 5.2.1 and 5.2.2. The plots in figure 7.1 show the specimen thickness along their horizontal axis. Instead of 17 nodes, the thickness is given in mm. The length between each node is 0.625 mm. The vertical axis, in the mentioned plots, shows the geometry factors given dimensionless.

The loading case $\alpha = 0°/\beta = 0°$ shows symmetric Y-values along the specimen thickness. This is a pure mode I loading case, and the plot shows Y_{II} and Y_{III} values almost equal to zero. This indicates that the simulated model behaves as intended for a pure mode I loading case. The maximum Y_I for this case is 1.1. This maximum value can be located at the center nodes of the specimen. All the plots in figure 7.1, except for pure mode II ,$\alpha = 0°$, $\beta = 90°$, have similar Y_I behaviour. A symmetric form with maximum values at the specimen center nodes, and lowest values at the specimen surface nodes, $z/t = 0$ and $z/t = 10$.

As the loading cases approaches towards pure mode II, the Y_{II} values increases. This can be studied in figure 7.1 plots, for cases $\alpha = 22.5°/\beta = 0°$, $\alpha = 45°/\beta = 0°$, $\alpha = 67.5°/\beta = 0°$ and $\alpha = 90°/\beta = 0°$. The highest Y_{II} values were obtained for pure mode II. These were found to be 1.4, see appendix J. Unlike the Y_I plots, the Y_{II} plots show maximum values at the specimen surfaces, and lowest values at the center nodes. The Y_{II} plots were still found to be symmetric.

When approaching pure mode II, the mode I/II analysis also resulted in higher Y_{III} values, which indicates a relation between Y_{II} and Y_{III}. As shown in the plots in figure 7.1, the Y_{III} values have a descending form. The maximum Y_{III} value is found for pure mode II, and was found to be 0.7. The maximum Y_{III} values were found at the surface ,$z/t = 0$. Opposite minimum values were found at the opposite specimen surface, $z/t = 10$.

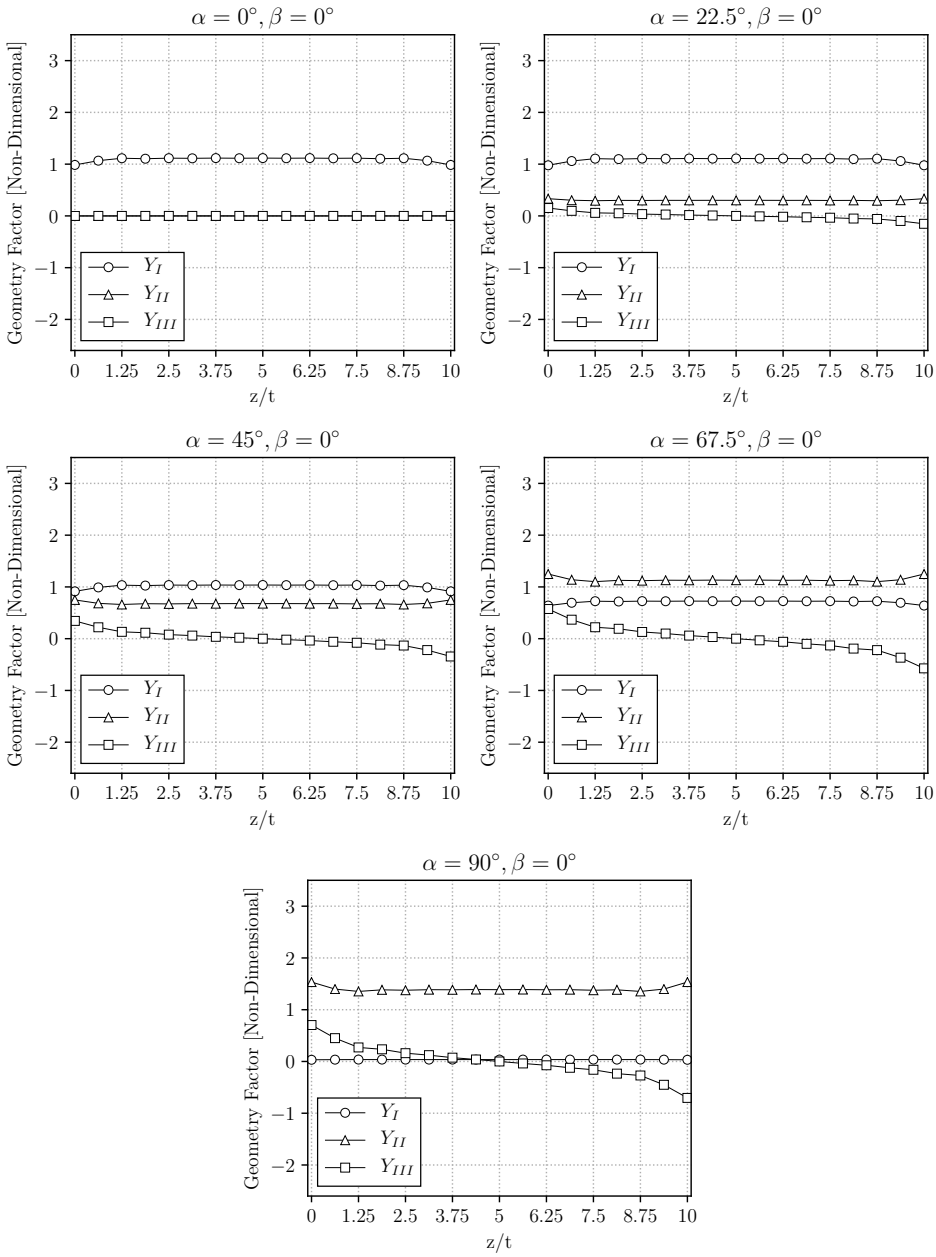

Figure 7.1: Plot of Geometry Factors along specimen thickness for Mixed Mode I/II.

7.1.2 Geometry Factors for Mixed Mode I/III

The mixed mode I/III loading cases can be studied in figure 7.2. All of these plots shows symmetry for Y_I and Y_{III} values, and a descending plot for Y_{II} values. As the loading cases approach towards pure mode I, the Y_I values increases and Y_{III} values decreases. Both Y_I and Y_{III} plots have higher values at the specimen center. However, the Y_{III} plots show a clear top at the thickness 5 mm, were the Y_I plots are flatter.

As expected, the Y_I values for pure mode III were close to zero. This case also shows maximum Y_{III} values. The plot for pure mode III, $\alpha = 0°/\beta = 90°$, also indicates a relation between Y_{II} and Y_{III}.

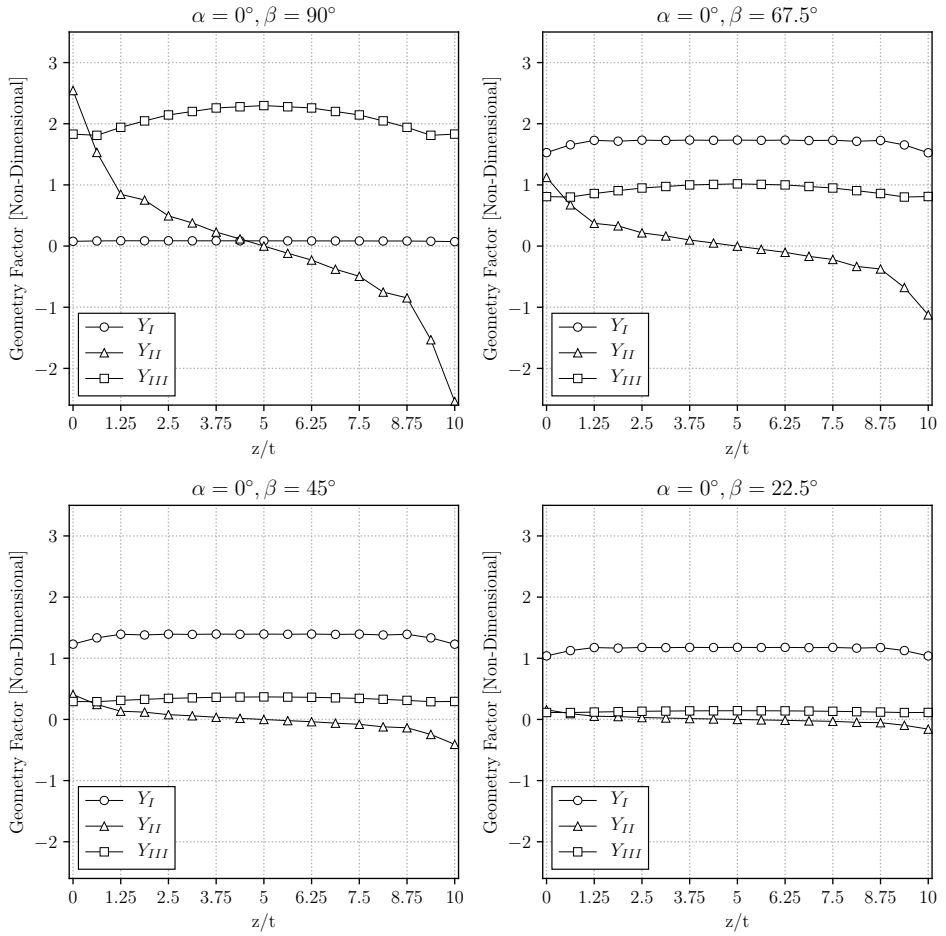

Figure 7.2: Plot of Geometry Factors along specimen thickness for Mixed Mode I/III.

7.1.3 Geometry Factors for Mixed Mode I/II/III

Figures 7.3 and 7.4 shows the twelve plots for all mixed mode I/II/III cases, as presented in table 2. All loading cases in figure 7.4 shows a descending plot for Y_{II} values. Y_{III} values are also descending for every loading case except $\alpha = 22.5°/\beta = 90°$ and $\alpha = 45°/\beta = 90°$. For these cases, Y_I values have a symmetric plot, with maximum values for the nodes inside the specimen. The two Y_I plots for cases $\alpha = 22.5°/\beta = 90°$ and $\alpha = 45°/\beta = 90°$ are almost flat, with values close to zero.

The last six loading cases for mixed mode I/II/III are shown in figure 7.4. These show a descending Y_{II} plot for all loading cases. They also show descending Y_{III} values for every loading case except $\alpha = 67.5°/\beta = 90°$, which shows a peak value at the specimen center , $z/t = 5$. For these six loading cases, the Y_I values have a symmetrical form, with maximum values for the center nodes.

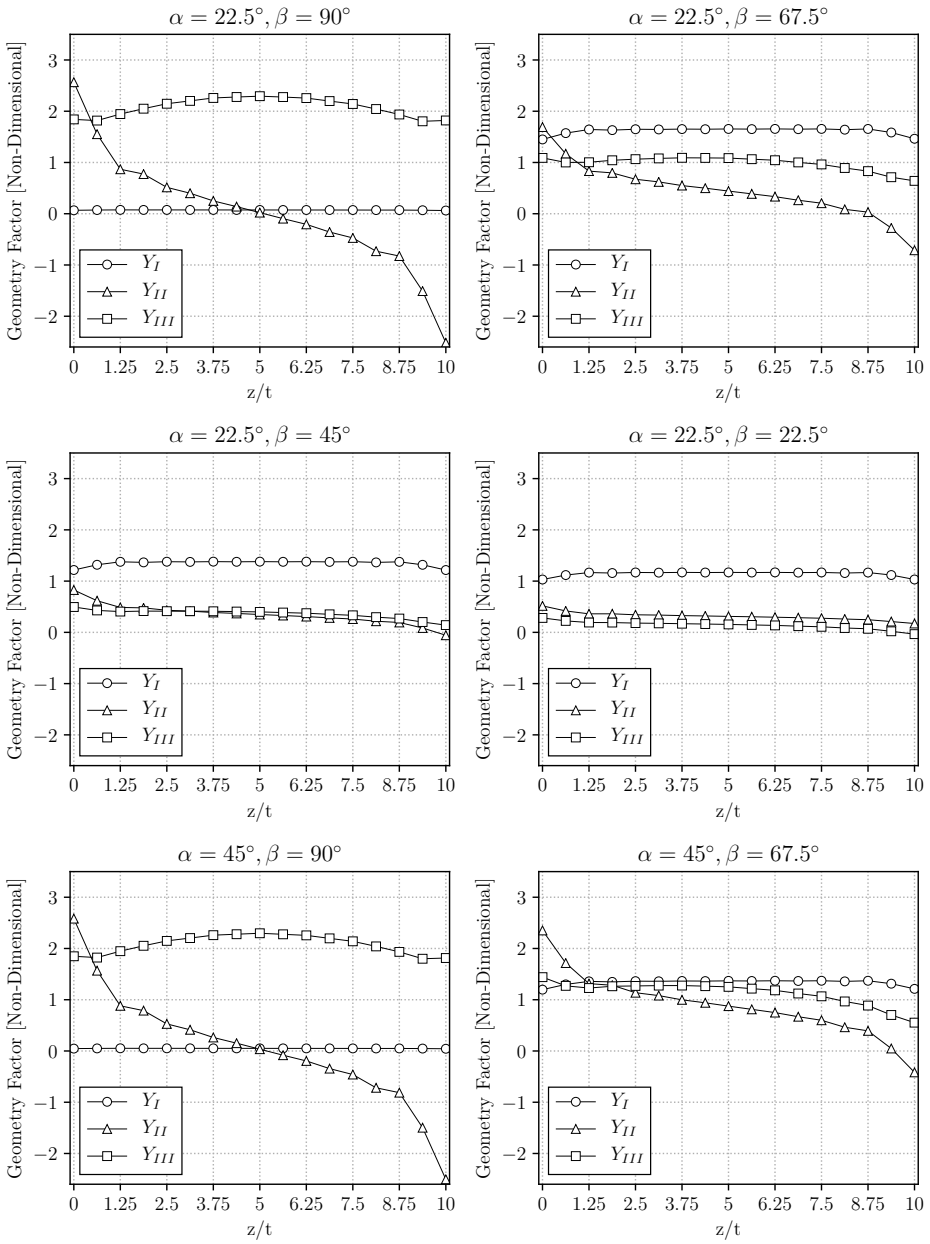

Figure 7.3: Plot of Geometry Factors along specimen thickness for Mixed Mode I/II/III.

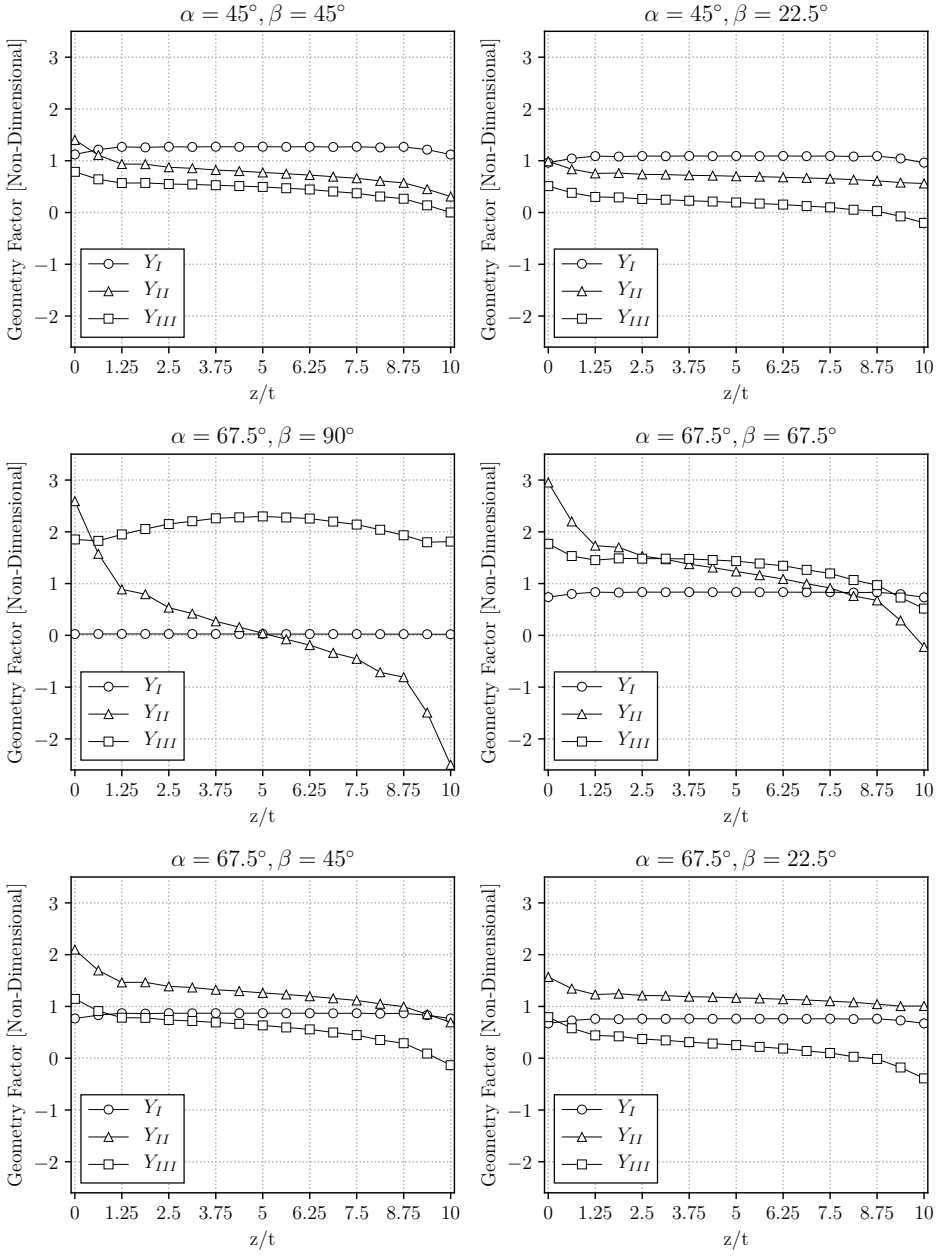

Figure 7.4: Continued - Plot of Geometry Factors along specimen thickness for Mixed Mode I/II/III.

7.1.4 Geometry Factors for Mixed Mode II/III

Figure 7.5 shows Y value plots for the four mixed mode II/III loading cases. They show descending Y_{II} and Y_{III} values for all loading cases except $\alpha = 90°/\beta = 90°$. Y_I values are close to zero for all four mixed mode II/III loading cases. The loading case $\alpha = 90°/\beta = 90°$, in figure 7.5, is almost identical to the loading case $\alpha = 0°/\beta = 90°$ in figure 7.2. They are both pure mode III loading cases.

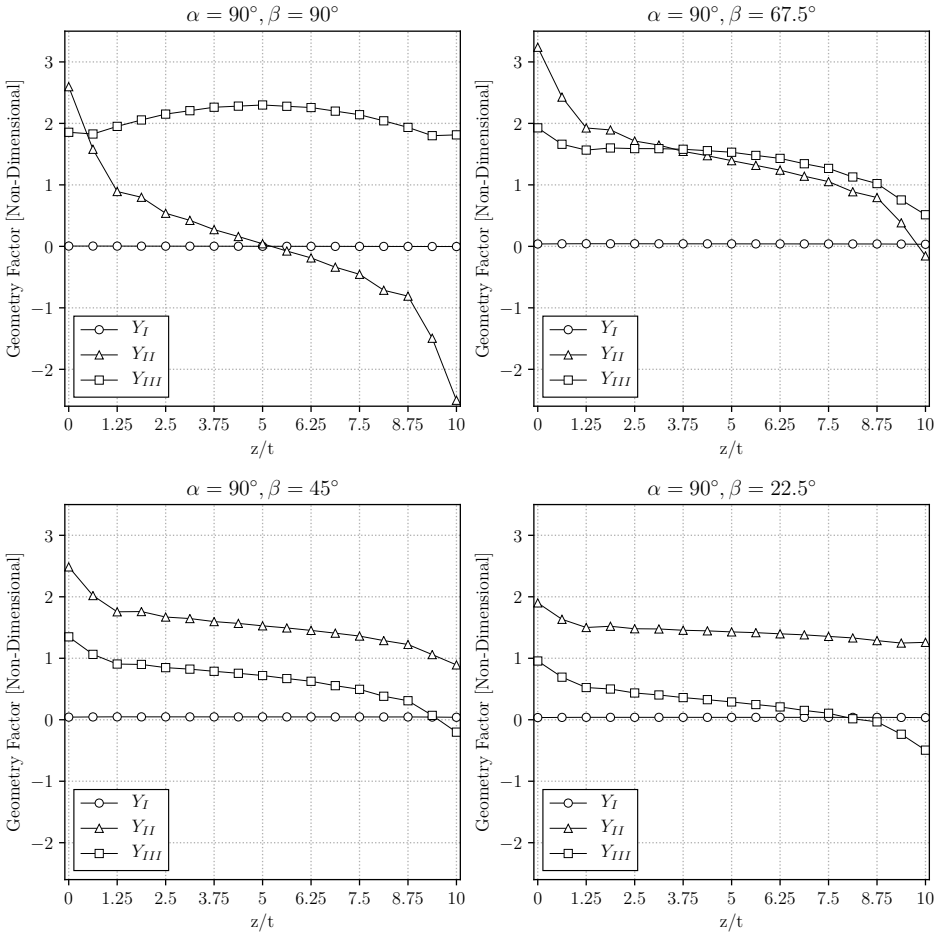

Figure 7.5: Plot of Geometry Factors along specimen thickness for Mixed Mode II/III.

7.2 Mixed Mode I/II/III Fracture Loads

The fracture loads for each of the mixed mode I/II/III combinations can be studied in figure 7.6. As mentioned earlier, three tensile tests were conducted for each of the twenty-five loading device combinations. Figure 7.6 shows five different plots. Each plot presents the five c-fixture combinations, α, for each j-fixture, β, combination.

To the top left in figure 7.6, fracture loads for $\beta = 0°$ can be studied. For the loading case of pure mode I, $\alpha = 0°/\beta = 0°$, the three fracture loads were 886.36 N, 713.14 N and 791.02 N. For each fracture load, the critical values of stress intensity factors, K_{If}, K_{IIf} and K_{IIIf}, were calculated. These were determined by using the relation in equation 2.47. In this case, the stresses, σ, were calculated by applying the fracture loads. The geometry factors, Y, for each loading case can be found in appendices I, J and K. For the three mentioned fracture loads, in the case of pure mode one, the critical stress intensity factors, K_{If}, were 20.26 MPa$\sqrt{mm}$, 16.30 MPa$\sqrt{mm}$ and 18.08 MPa$\sqrt{mm}$. These gave an average K_{If} of 18.22 MPa$\sqrt{mm}$. This average K_{If}, for pure mode one, was used as the fracture toughness, K_{IC}, in this thesis. By applying the relation in equation 2.47, each of the K_{If}, K_{IIf} and K_{IIIf} were calculated, for all three specimens for each of the twenty-five loading cases. This led to a number of 225 critical stress intensity factors. The average K_f's for each loading case can be studied in table 5.

The plots in figure 7.6 shows an increasing fracture load for $\alpha = 0°$ cases, for each steps of β. The average fracture load was 796.84 N for pure mode I, $\alpha = 0°/\beta = 0°$, and 2180.06 N for pure mode III, $\alpha = 0°/\beta = 90°$, see table 5. For each of the β positions, a slight descending fracture load can be seen from $\alpha = 0°$ to $\alpha = 45°$. From $\alpha = 45°$ to $\alpha = 90°$ the fracture load increases, resulting in a higher fracture load for $\alpha = 90°$ than for the cases of $\alpha = 0°$.

As mentioned, 75 initial tensile tests were conducted with the mixed mode loading device. The remaining samples were used for retesting some of the loading device combinations. The fracture tests for the j-fixture position of $\beta = 90°$ resulted in high fracture loads. These fracture loads also had a relatively large spread in test data, see the plot in figure 7.6. Note that the fracture loads for $\beta = 90°$ have a flatter curve for the different α positions, than for the other β cases. Even though the α angle is changing, the loading case is still considered as pure mode III. The $\beta = 90°$ case were some of the first conducted tensile tests. A large spread of data may be due to some set-up adjustments at the beginning of the conducted experiments. When considering which loading case to retest, the spread in fracture loads was studied. One sample was used for retesting the case of $\alpha = 45°/\beta = 67.5°$ and the rest were used for all $\beta = 90°$ combinations. Apart from the loading case of $\beta = 90°$ and $\alpha = 45°/\beta = 67.5°$, the tests results in figure 7.6 show consistency in fracture loads for each mixed mode loading situation.

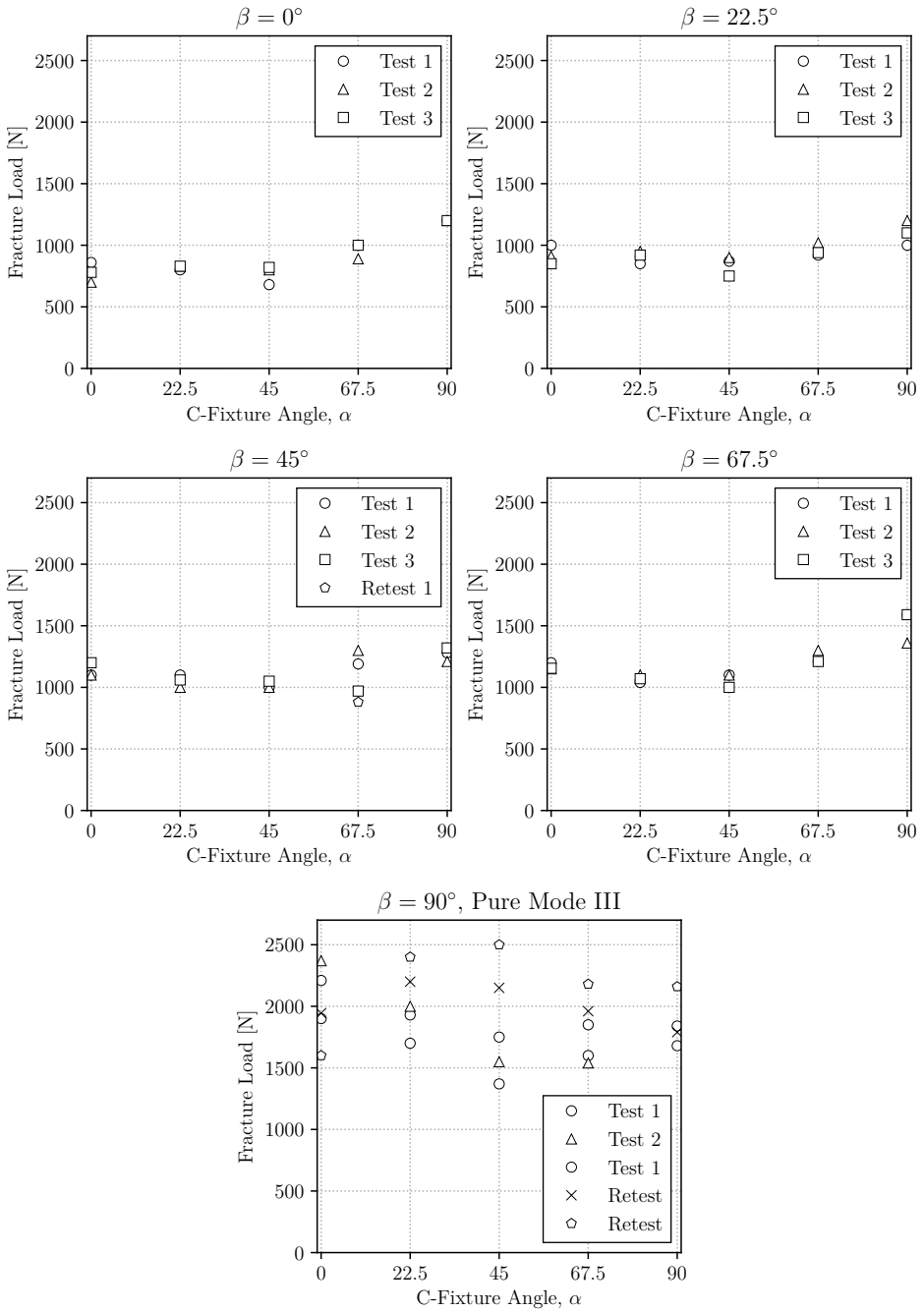

Figure 7.6: Fracture load plots, covering fracture tests for all loading device combinations.

Table 5: Average fracture loads and critical stress intensity factors for all mixed mode loading cases.

Fracture Modes -	Fixture Positions -	Avg. Load [N]	Avg. K_{If} [MPa $\sqrt{mm}$]	Avg. K_{IIf} [MPa $\sqrt{mm}$]	Avg. K_{IIIf} [MPa $\sqrt{mm}$]
I	$\alpha = 0°$, $\beta = 0°$	796.84	18.22	0	0
I/II	$\alpha = 22.5°$, $\beta = 0°$	833.04	20.09	5.124	0
I/II	$\alpha = 45.0°$, $\beta = 0°$	779.72	16.55	10.81	0
I/II	$\alpha = 67.5°$, $\beta = 0°$	976.76	14.52	22.58	0
II	$\alpha = 90.0°$, $\beta = 0°$	1295.36	0	36.77	0
I/III	$\alpha = 0°$, $\beta = 22.5°$	928.20	22.39	0	2.706
I/III	$\alpha = 0°$, $\beta = 45.0°$	1285.92	36.73	0	9.697
I/III	$\alpha = 0°$, $\beta = 67.5°$	1174.41	41.65	0	24.44
II/III	$\alpha = 90.0°$, $\beta = 22.5°$	1189.88	0	34.79	7.052
II/III	$\alpha = 90.0°$, $\beta = 45.0°$	1277.91	0	39.95	18.81
II/III	$\alpha = 90.0°$, $\beta = 67.5°$	1519.20	0	43.33	47.60
I/II/III	$\alpha = 22.5°$, $\beta = 22.5°$	928.51	22.24	5.921	2.944
I/II/III	$\alpha = 22.5°$, $\beta = 45.0°$	1090.25	30.79	7.676	8.911
I/II/III	$\alpha = 22.5°$, $\beta = 67.5°$	1075.41	36.41	9.733	23.89
I/II/III	$\alpha = 45.0°$, $\beta = 22.5°$	877.24	19.62	12.57	3.477
I/II/III	$\alpha = 45.0°$, $\beta = 45.0°$	1025.04	26.67	16.22	10.37
I/II/III	$\alpha = 45.0°$, $\beta = 67.5°$	1070.44	29.98	19.17	27.41
I/II/III	$\alpha = 67.5°$, $\beta = 22.5°$	972.37	15.19	23.19	5.034
I/II/III	$\alpha = 67.5°$, $\beta = 45.0°$	1116.06	19.89	28.81	14.49
I/II/III	$\alpha = 67.5°$, $\beta = 67.5°$	1254.95	21.47	31.69	36.84
III	$\alpha = 0°$, $\beta = 90.0°$	2180.06	0	0	102.5
III	$\alpha = 22.5°$, $\beta = 90.0°$	2227.38	0	0.981	104.6
III	$\alpha = 45.0°$, $\beta = 90.0°$	2025.65	0	1.444	95.23
III	$\alpha = 67.5°$, $\beta = 90.0°$	2007.01	0	1.687	94.37
III	$\alpha = 90.0°$, $\beta = 90.0°$	1920.47	0	1.659	90.38

As mentioned above, table 5 shows all the average values of the calculated critical stress intensity factors. These values are necessary for the criteria used in this thesis, see chapter 2.6. The values are divided by the fracture toughness, K_{IC}, and used for plotting and comparison with the fracture limit curves, for different criteria. The values of $K_{If} = 18.22$ MPa$\sqrt{mm}$ was used as the fracture toughness, K_{IC}, in this thesis. Out of all the tested pure mode III cases, the $\alpha = 0°/\beta = 90°$ case was used as the pure mode III case in later comparisons. The three highest loads of this pure mode III loading case were used for plotting of test results in chapter 7.4. For the fracture modes of I/II, the table shows a descending K_{If} from pure mode I to pure mode II. An increasing K_{IIf} can be seen from pure mode I to pure mode II. Trends like this were studied and compared with the geometry factors in chapter 7.1 to control the results. As seen in table 5, some critical stress intensity factors were set to zero. This is due to low geometry factors in these mixed mode situations. An example of this is for the loading case of pure mode II, where Y_I was 0.036 and Y_{III} was 0.00, see appendices I, J and K.

7.3 T-Stress

As for the geometry factors, the T-stress for all the loading device combinations were estimated using Abaqus. The procedure to obtain these values were explained in chapter 5. The T-stresses along the specimen thickness were studied. All of these values, along the seventeen nodes, can be found in appendix L. The T-stresses were necessary for the GMTS criterion. This fracture criterion is an extension of the MTS criterion, with an additional term including T-stress, see chapter 2.

After all of the T-stresses were obtained, the dimensionless T-stresses were calculated by applying the relation in equation 2.48. The dimensionless T-stress is given the symbol T^* in this thesis. See chapter 2.6.5 to study how the dimensionless factors can be used in the fracture criteria. All of the calculated T^*-stresses can be found in appendix M. All of the T-stress estimates were of negative values, and therefore the dimensionless T^*-stresses were negative.

7.3.1 T-Stress for Mixed Mode I/II

Figure 7.7 shows five plots. Each of the plots presents the T^*-stresses along the specimen thickness, for mixed mode I/II loading cases. The $\alpha = 0°/\beta = 0°$ presents the pure mode I case, and $\alpha = 90°/\beta = 0°$ is the T^*-stress plot for pure mode II. The plots for the cases of $\alpha = 0°$, $\alpha = 22.5°$, $\alpha = 45°$ and $\alpha = 67.5°$ in figure 7.7 all have similar patterns. The two highest T^* values were found at the third node from each surface. The two lowest values were found at the surface nodes. All of the plots in figure 7.7 were found to be symmetrical about the specimen center, $z/t = 5$.

For each increasing step of $\alpha = 22.5°$, the T^*-stress decreases. At the surface node, $z/t = 0$, the T^* value was -0.81 for $\alpha = 0°/\beta = 0°$ and -0.51 for $\alpha = 67.5°/\beta = 0°$. For the case of pure mode II, the T^* values were found to be almost zero for each node. The overall decreasing T^* values, from pure mode I to pure mode II, also affected the highest values at the nodes $z/t = 1.25$ and $z/t = 8.75$. The difference between these two peaking values, and the rest of the loading cases T^* values, decreases for each increasing step of $\alpha = 22.5°$. A visualization of this effect is clear in the $\alpha = 67.5°/\beta = 0°$ plot, see figure 7.7.

The T^* values for mixed mode I/II show decreasing values from pure mode I to pure mode II. The works of Ayatollahi [20] shows increasing T^* values from pure mode I to II. In this work, a SCB specimen was used. The SCB specimen is circular with different angles on the pre-cracks. The different specimens make it hard to compare the results of Ayatollahi with the work in this thesis. However, his work shows a negative T^* value close to -1, for pure mode I, which is close to the obtained value in this thesis. Ayatollahi obtained a positive T^*-stress value of 3, for pure mode II.

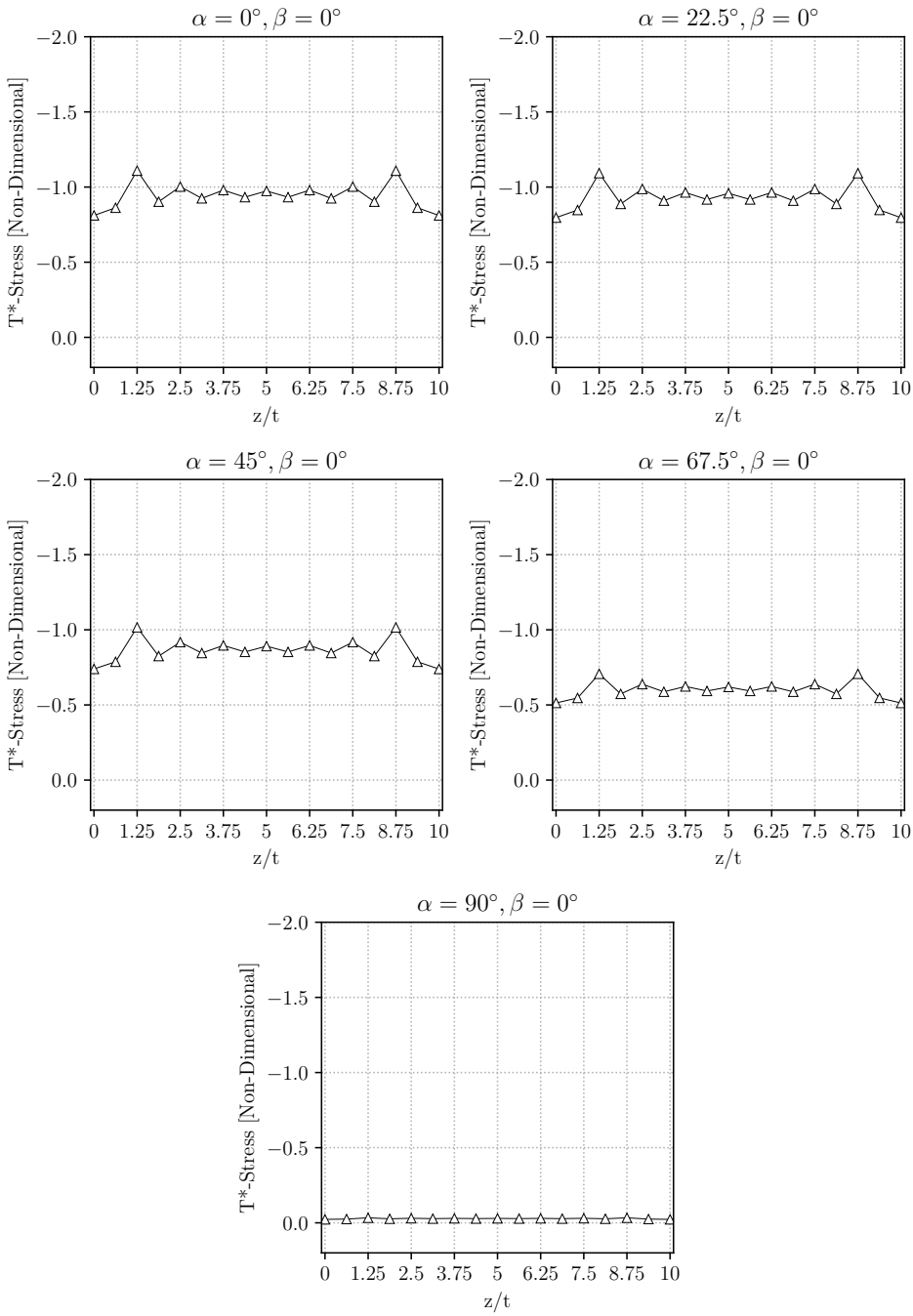

Figure 7.7: Plot of Dimensionless T-Stress along specimen thickness for Mixed Mode I/II.

7.3.2 T-Stress for Mixed Mode I/III

The plotted T^*-stress for the case of mixed mode I/III can be seen in figure 7.8. As the steps of β angle increases from $\beta = 22.5°$ to $\beta = 67.5°$, the T^* values increases. The value in the center node, $z/t = 5$, increases from -1.03, for $\beta = 22.5°$ to -1.5 for $\beta = 67.5°$. For all the loading cases of mode I/III in figure 7.8, a maximum T^* value can be found at the third node from both of the specimen surfaces, $z/t = 1.25$ and $z/t = 8.75$.

For the case of pure mode III, $\alpha = 0°/\beta = 90°$, the T^* values have a flat curve, with node values close to zero. This was also the case for the loading device position of $\alpha = 90°/\beta = 0°$, see figure 7.7.

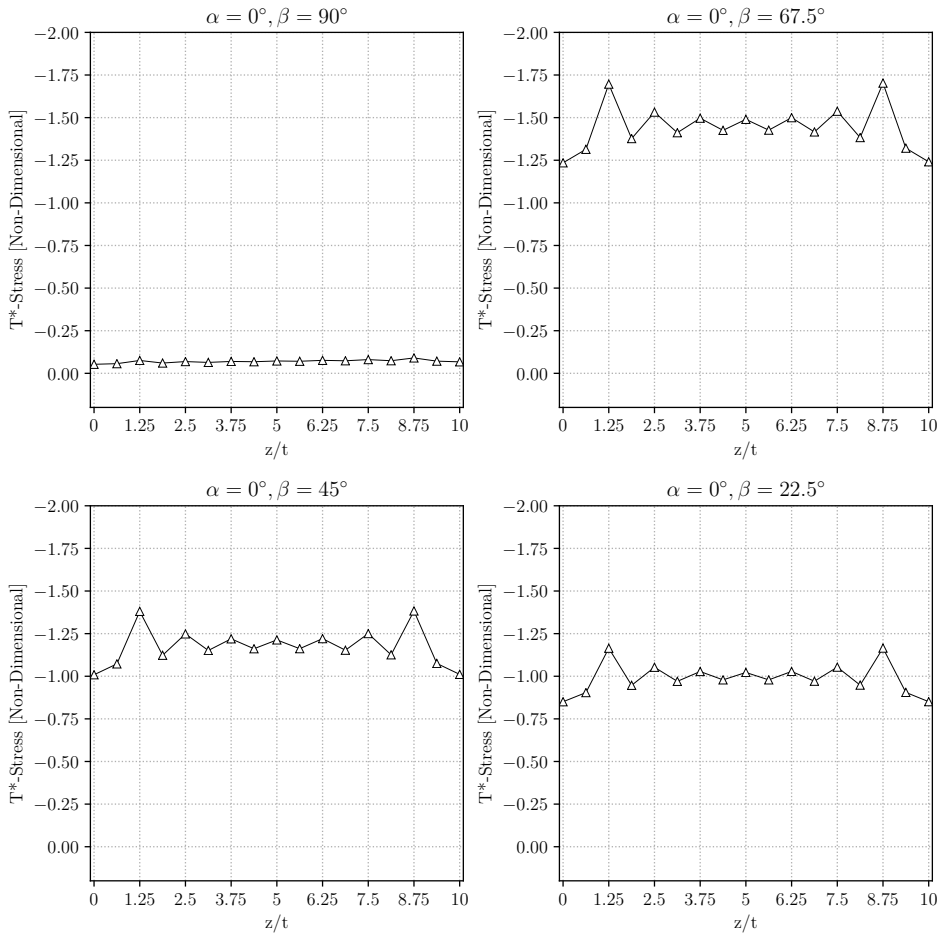

Figure 7.8: Plot of Dimensionless T-Stress along specimen thickness for Mixed Mode I/III.

7.3.3 T-Stress for Mixed Mode I/II/III

Figure 7.9 and 7.10 presents all the plots for T^*-stress along the specimen thickness, for the mixed mode I/II/III loading cases. For the case of $\alpha = 22.5°/\beta = 22.5°$, the T^* values were increasing for each step until $\alpha = 22.5°/\beta = 67.5°$. The T^*-stresses for the loading case of $\alpha = 22.5°/\beta = 90°$ shows a flat curve close to zero. These same trends were also seen for the remaining loading cases in figure 7.9 and 7.10. Decreasing T^* values from $\alpha = 45°/\beta = 67.5°$ to $\alpha = 45°/\beta = 22.5°$ and from $\alpha = 67.5°/\alpha = 67.5°$ to $\alpha = 67.5°/\beta = 22.5°$. Flat curves close to zero were also found for the mixed mode loading positions of $\alpha = 45°/\beta = 90°$ and $\alpha = 67.5°/\beta = 90°$.

Even though similar trends for mentioned loading cases where observed, the T^* values were not the same. The center node, $z/t = 5$, values for $\alpha = 22.5°/\beta = 67.5°$ was -1.4 and -0.71 for $\alpha = 67.5°/\beta = 67.5°$. This shows a decreasing T^* value for an increasing α angle.

In the loading case of mixed mode I/II/III, all three loading device positions with $\beta = 90°$ resulted in T^* values close to zero. The loading cases with $\beta = 90°$ can be categorized as pure mode III. The different α angles do not seem to affect the pure mode III, $\beta = 90°$, cases.

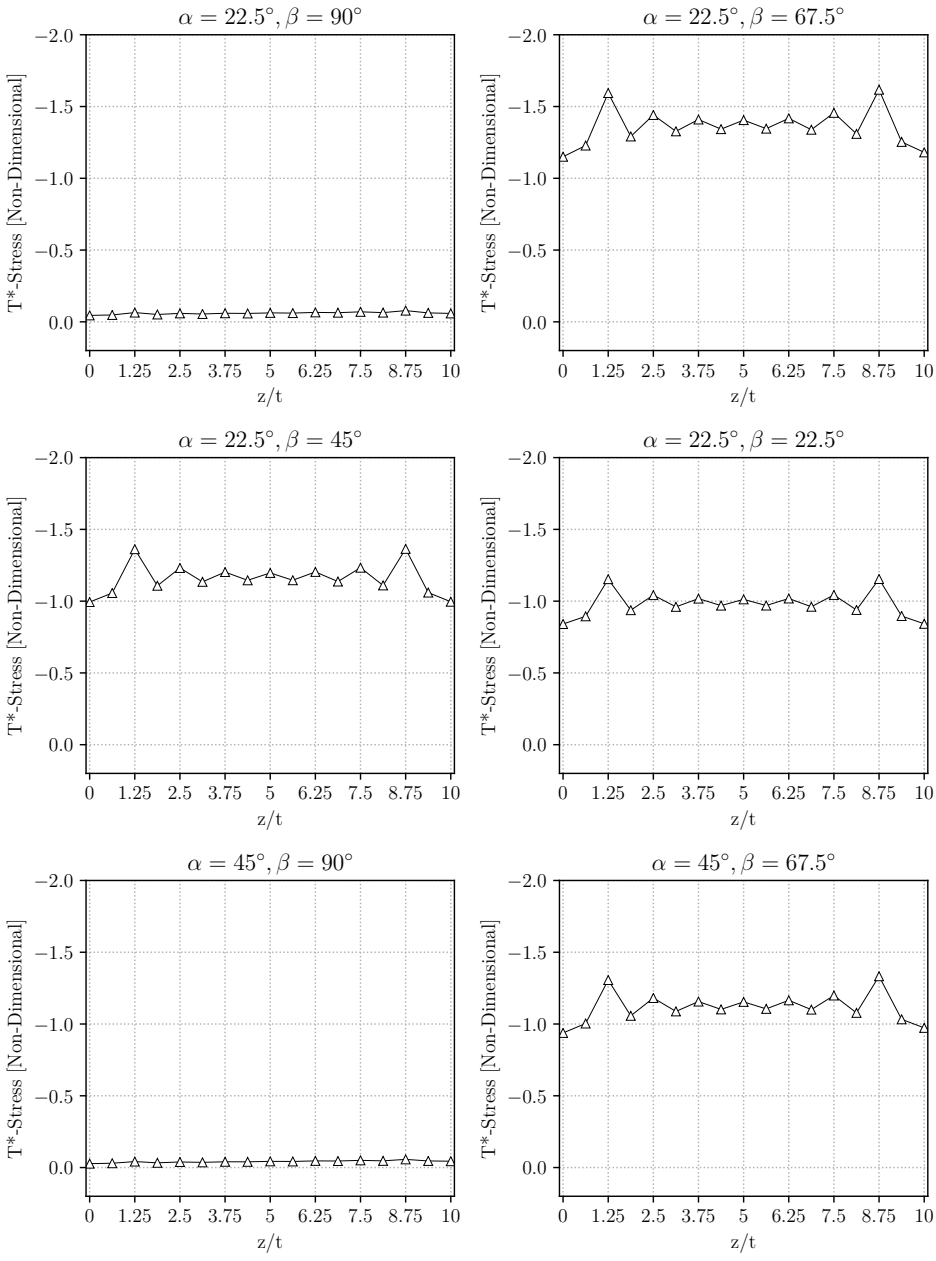

Figure 7.9: Plot of dimensionless T-stress along specimen thickness for Mixed Mode I/II/III.

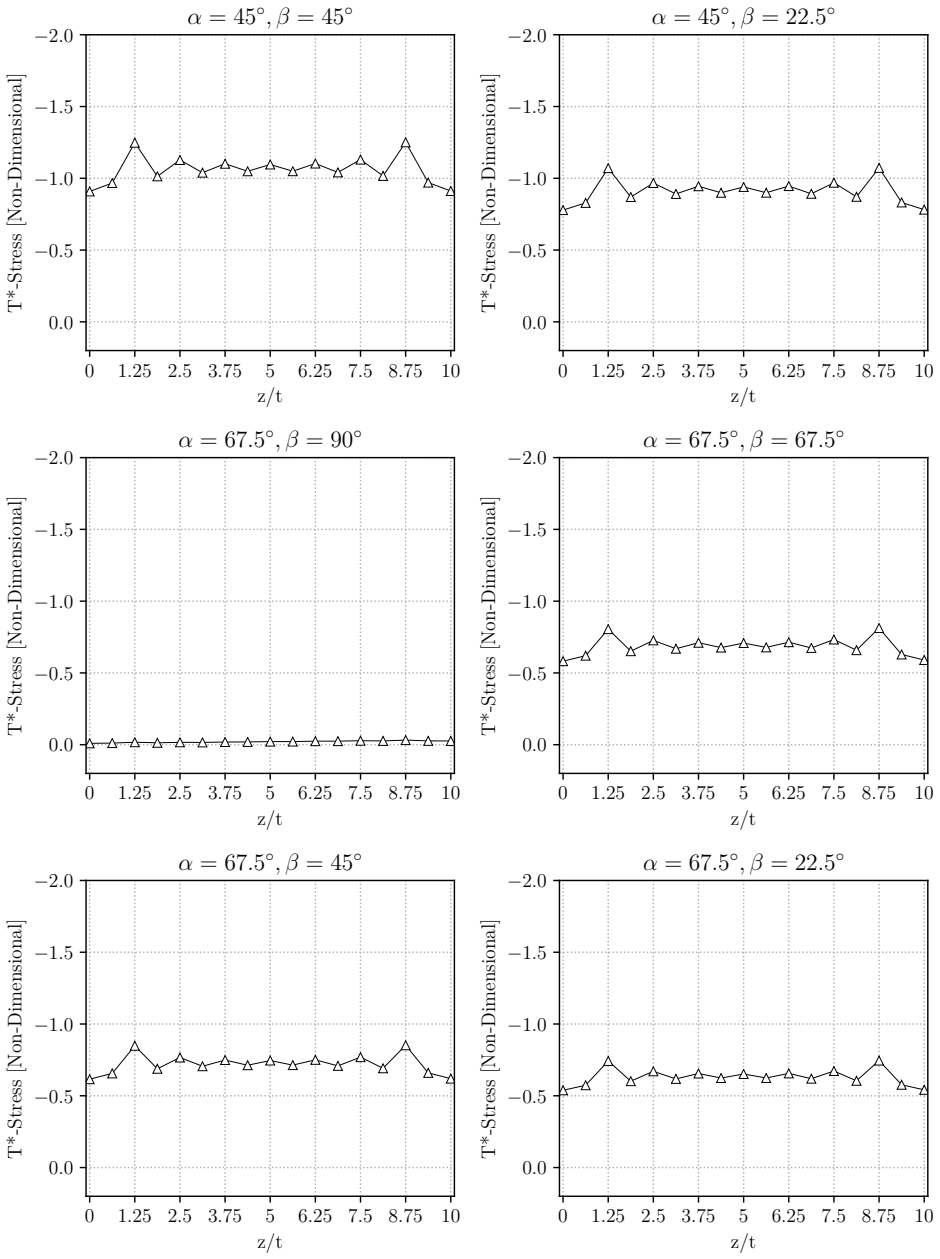

Figure 7.10: Continued - Plot of dimensionless T-stress along specimen thickness for Mixed Mode I/II/III.

7.3.4 T-Stress for Mixed Mode II/III

The T^* values across the specimen thickness for the mixed mode loading cases of II/III were presented in four plots, see figure 7.11. All of these plots have flat curves, with T^*-stresses close to zero. The loading device angles for these mixed mode positions, all include an α angle of 90°. The $\alpha = 90°/\beta = 0°$ case for mixed mode I/II in figure 7.7 also resulted in a similar plot. All of the presented values for the loading cases including $\beta = 90°$ resulted in close to zero T^*-stresses.

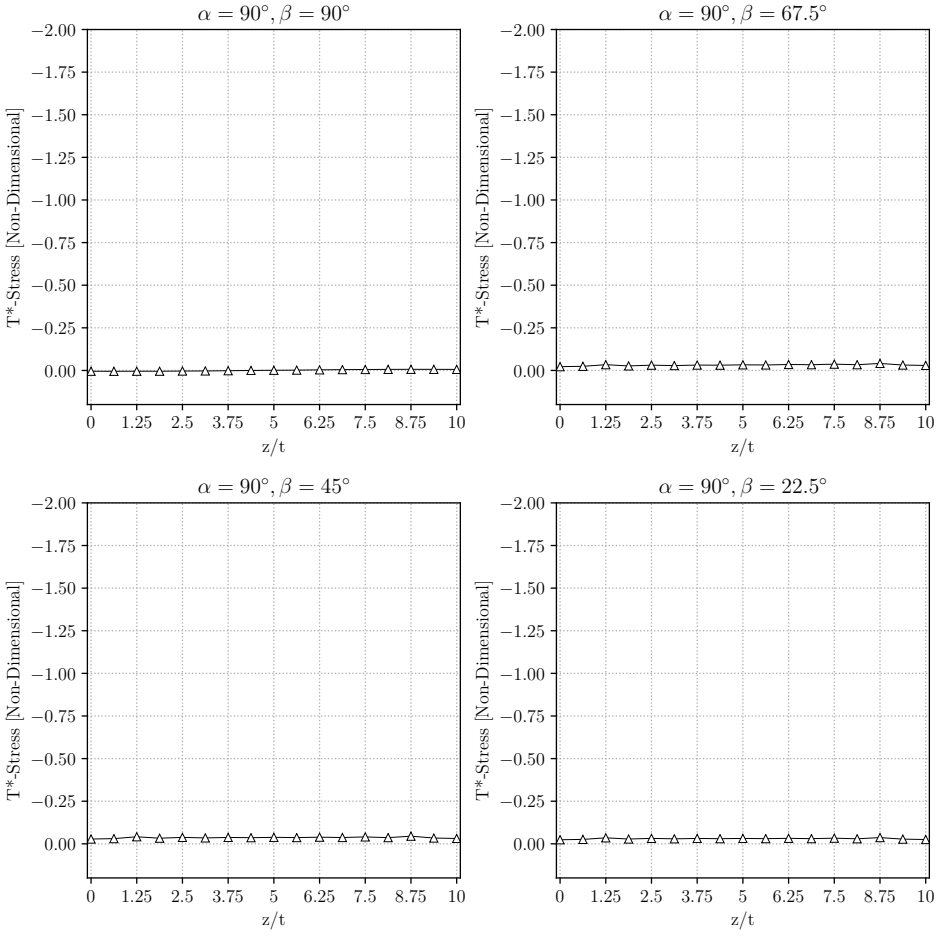

Figure 7.11: Plot of Dimensionless T-Stress along specimen thickness for Mixed Mode II/III.

7.4 Fracture Criteria & Test Results

This subsection will cover this thesis' presented fracture criteria and its respective test data. The criteria were used to predict different parameters. The first cases were in and out of plane angles of the fractured specimens. The second was the normalized stress intensity factors. These are critical stress intensity factors divided by mode I fracture toughness, K_{If}/K_{IC}, K_{IIf}/K_{IC} and K_{IIIf}/K_{IC}. The criteria used in this thesis were MTS, GMTS, and Richard [13, 14, 4]. When applying the geometry factors and T-stresses, the center node value, $z/t = 5$ were used. This is because of the plane strain condition. These criteria are further explained in chapter 2.6 and 5.4.

7.4.1 Mixed Mode I/II

The first comparison of fracture criteria and test data were the mixed mode case of I/II. Two plots are presented, see figures 7.12 and 7.13. Figure 7.12 shows the plot of in-plane crack initiation angle, θ_f, versus mixity parameter, M^e_{12}. The criteria show an in-plane angle of $-70°$ for pure mode II and $0°$ for pure mode I. The criteria shows increasing in-plane angles from pure mode I to II, presented as a curved plot. Both the MTS and GMTS criterion has similar behavior, but a slightly lower curve can be observed for the GMTS criterion. The test data consist of five points, representing the five loading device combinations for mixed mode I/II. The test data at the point of $\theta_f = 0°$ and $M^e_{12} = 1.0$ presents the loading case of pure mode I. The test data to the left, at the point of $\theta_f = -70°$ and $M^e_{12} = 0.0$, presents the loading case of pure mode II. The mixed mode test data shows similar curve as the MTS and GMTS criterion. However, the measured angles were found to be slightly below the criteria. As discussed in chapter 7.3.1, all of the obtained T- and T^*-stresses were of negative values. As presented in figure 2.7, a negative T-stress for the mixed mode case of I/II would result in a GMTS curve below the MTS curve. This was also discussed by Ayatollahi et al. [7, 14]. Therefore, the measured crack initiation angles below the MTS criterion could be expected because of the negative T values. The in-plane crack initiation angles, θ_f, were some of the easiest angles to measure, see chapter 6.3.3. However, there may be some deviation between the measured angles and the actual crack initiation angles. All of the measured angles and criteria values were also presented in table 6.

As seen in equations 2.36 and 2.37, the only thing that separates the GMTS criterion from the MTS criterion is the last term. This term includes the T-stress. With the low T-stresses obtained in this thesis, the T-stress terms of equation 2.36 and 2.37 were found to be small. The small values resulted in the terms including T-stress being close to zero. When this term was found to be close to zero, the GMTS criterion followed a similar path as the MTS criterion. The GMTS criterion for θ_f is shown as a dotted line in figure 7.12. The MTS criterion showed a good agreement with the test data for in-plane crack initiation angles for the mixed mode I/II cases. T^* values of greater magnitude would have given a GMTS curve with greater deviation from the MTS curve.

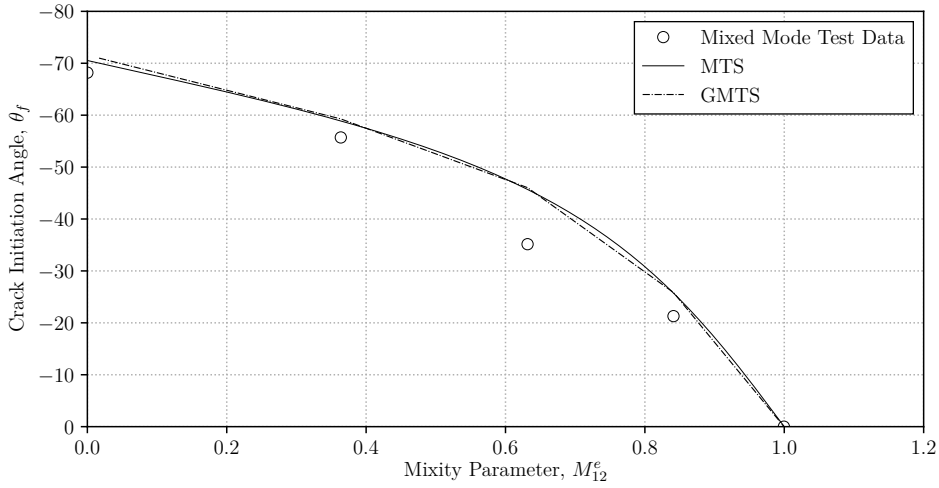

Figure 7.12: Plot of measured in plane crack initiation angle, θ_f, and the angle predictions of MTS and GMTS criterion.

The presented test data is similar to the data for AECT and AECS specimen presented by Aliha [29]. These data show a curve similar to MTS, slightly below the angles of the criterion. The presented T^* values for AECT and AECS specimens starts at 0 for pure mode I and ends at -4 for pure mode II. This results in a GMTS curve that deviates from the MTS curve [29].

Figure 7.13 presents the fracture limit plots for the mixed mode I/II loading cases. The presented plot shows normalized mode II, K_{II}/K_{IC}, on the y-axis and normalized mode I, K_I/K_{IC}, on the x-axis. The plotted criteria in this figure are GMTS, MTS and Richard. The dotted line presents the MTS criterion, the dashed/dotted line presents the GMTS criterion and the solid line presents the Richard criterion. Circular markers presents the normalized critical stress intensity factors, calculated from the mixed mode tensile tests. For each test point, the critical stress intensity factors were obtained by applying the fracture load and geometry factor to equation 2.47. This factor is then normalized by dividing with the fracture toughness, K_{IC}. The average of the the three different critical stress intensity factors can be found in table 5. Each loading device position have three test data points, which are spread in a linear form from the axis origin. For the loading case of pure mode I, the three normalized points were found at $K_I/K_{IC} = 1.11$, 0.99 and 0.89. For these three mode I cases, the K_{II}/K_{IC} values were found to be zero. For the loading case of pure mode II, the K_{II}/K_{IC} values were 2.02, 2.03 and 1.99. This value shows a critical stress intensity factor of pure mode II, K_{IIf}, being twice the magnitude as the critical stress intensity factor for pure mode I, K_{If}. Critical stress intensity factor for pure mode I is also called fracture toughness, K_{IC}. Test data in the

transition from pure mode I to II have a circular pattern, with a relatively small spread. Mixed mode cases with least spread in data were obtained for the loading positions of $\alpha = 22.5°/\beta = 0°$ and pure mode II. As discussed, the the T^* values for mixed mode I/II were found to be small, see chapter 7.3.1. T^* values for pure mode II were found to be close to zero, as shown in figure 7.7. This effect is shown on the GMTS curve in figure 7.13, where the curve ends at the same point for pure mode II as the MTS criterion. For larger T^* values, closer to pure mode I, the GMTS curve has a greater deviation from the MTS curve. The GMTS presents larger values of K_{II}/K_{IC} as excepted from the negative T-Stresses, see figure 2.7. However, the GMTS criterion was found to be below the mixed mode test data. In this case, the best fitting criterion was the one by Richard [3]. Where parameter $\alpha_1 = K_{IC}/K_{IIC}$ and $\alpha_2 = K_{IC}/K_{IIIC}$, see chapter 5.4 and table 5.

The obtained normalized fracture limit of $K_{II}/K_{IC} = 2.0$, for pure mode II, was higher than expected. In the works of Aliha, the highest value of K_{II}/K_{IC} for pure mode II was about 1.4. This was obtained for the AECT specimen [29]. Ayatollahi presented test results that had values of $K_{II}/K_{IC} = 0.4$ for pure mode II [20]. In this work, positive T^* values of 3.0 were obtained for pure mode II. This comparison presents a great variation of obtained K_{II}/K_{IC} relations for pure mode II, for different specimen types of PMMA. In another study by Aliha et al. [16] the values of K_{II}/K_{IC} varies from 0.3 to 1.7 for different specimen types of the same rock material. The referred test data also presents a great deviation from the MTS criterion.

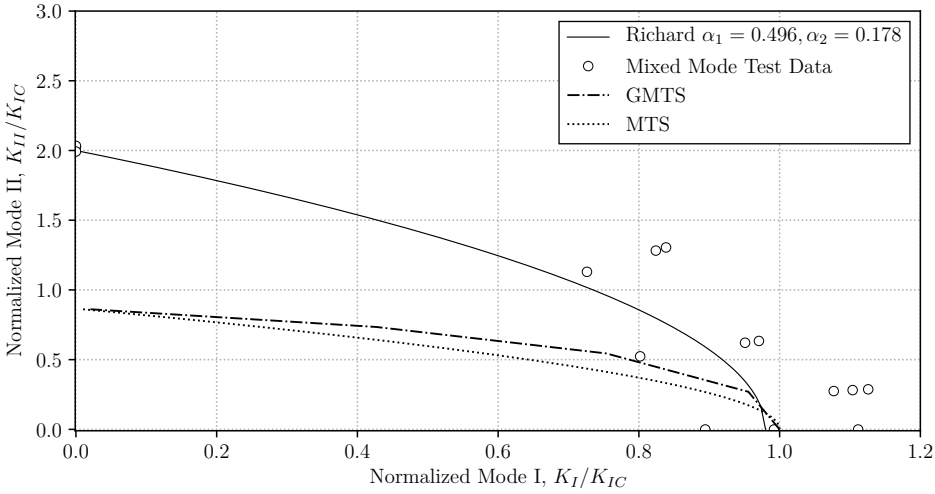

Figure 7.13: Fracture limit curves by the criteria of MTS, GMTS and Richard compared with mixed mode I/II test data.

7.4.2 Mixed Mode I/III

Figure 7.14 presents four plots. Mixed mode test data, GMTS criterion and MTS criterion for plane stress and plane strain. Measured angles for pure mode III shows an out of plane crack initiation angle of $-42.02°$. This angle is close to the predicted criterion angle of $-45°$. All of the exact measured angles and criterion predictions can be studied in table 6. Transitioning from pure mode II to I, the measured angles have a curved form ending in $\phi_f = 0°$ for $M^e_{13} = 1.0$.

The MTS curve for plane strain showed higher values than the plane stress curve. However, plots generated from GMTS criterion and MTS plane strain criterion were found to be close. Even though the curves were close, the GMTS criterion shows slightly lower values. This was expected from the negative T^* values [7]. The similar values of GMTS and MTS were also expected, due to the low obtained T^* values. The difference between the criterion procedure for plane strain and stress was explained in 5.4.

The GMTS criterion and MTS, for plane strain, both have a good fit with the measured angles from the mixed mode I/III test data. The test data with the highest deviation from the criteria was for the loading case of $\alpha = 0°/\beta = 67.5°$. In this loading position, the measured angle was $\phi_f = -46.71°$, and the predicted GMTS angle was $\phi_f = 37.52°$. This deviation can be a result of inaccuracy of the microscope angle measurements.

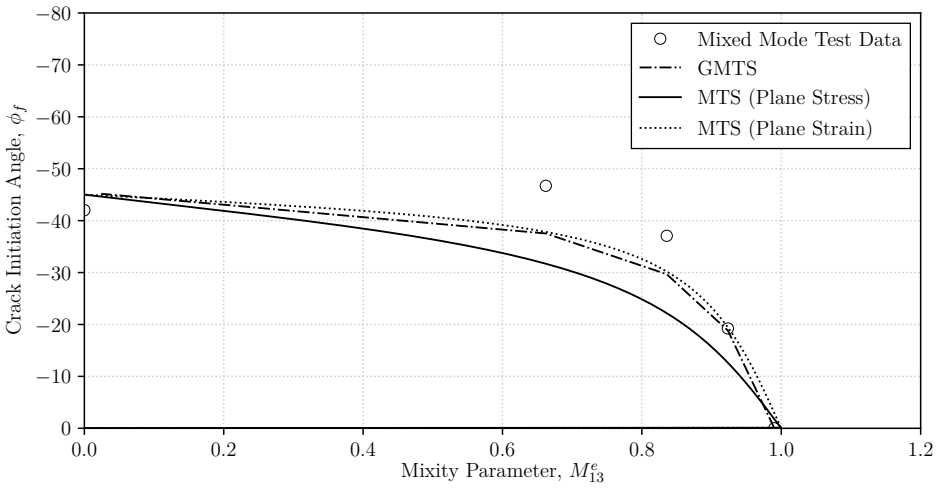

Figure 7.14: Plot of measured out of plane crack initiation angle, ϕ_f, and the angle predictions of MTS and GMTS criterion.

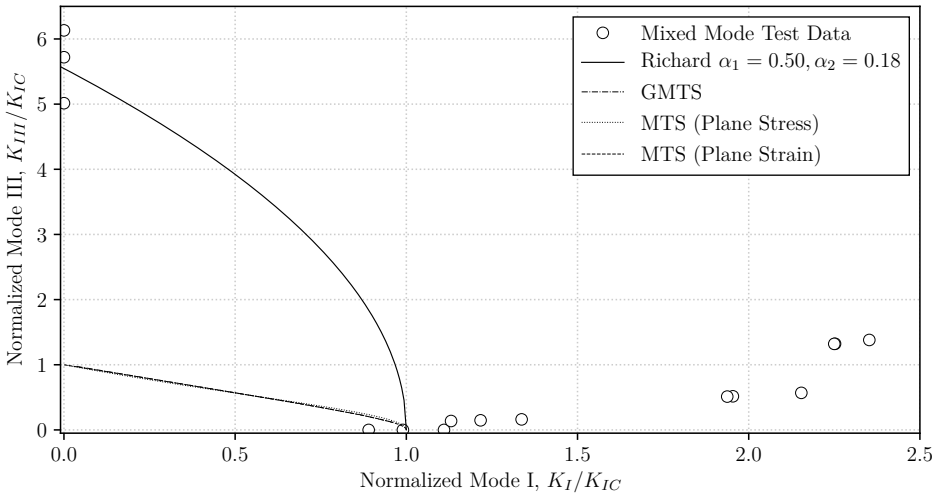

Figure 7.15: Fracture limit curves by the criteria of MTS, GMTS and Richard compared with mixed mode I/III test data.

Figure 7.15 shows the fracture limit for the mixed mode I/III loading cases. In the figure, six plots were presented. Two plots of the MTS criterion, one of GMTS, one for the Richard criterion and all the mixed mode I/III test data. MTS criterion was plotted for plane stress and plane strain. The two MTS plots and GMTS curves have similar forms, with estimated values of $K_{III}/K_{IC} = 1$ for pure mode III and $K_I/K_{IC} = 1.0$ for pure mode I. This curve is similar to the extended GMTS criterion for mixed mode I/III, obtained by Ayatollahi [7]. Richard's criterion, with $\alpha_1 = 0.50$ and $\alpha_2 = 0.18$, shows a $K_{III}/K_{IC} = 5.61$ for pure mode III and $K_I/K_{IC} = 1.0$ for pure mode I.

The test data of this thesis shows a good fit for the criterion predictions of pure mode I and pure mode III. However, the mixed mode test data transiting from mode I to mode III, did not seem to fit the criterion predictions. The loading cases of $\alpha = 0°/\beta = 22.5°$, $\alpha = 0°/\beta = 45°$ and $\alpha = 0°/\beta = 67.5°$ all seem to have values of greater magnitude for normalized mode I, K_I/K_{IC}. These high values originate from the large Y_I values and fracture loads for these loading positions, these can be seen in figure 7.2. Higher Y_I values and higher fracture loads, than for pure mode I, results in greater K_{If} values, see table 5. When the K_{If} values was greater than K_{IC}, the normalized K_I/K_{IC} values were found to be as high as 2.49 for $\beta = 67.5°$, see figure 7.15. The high Y_I values for mixed mode I/III can be due to some deviations, from the loading device experiments, with respect to the Abaqus model. The works of Saboori et al. [22] shows a mixed mode I/III fracture limit test data with normalized mode III values of 1.2 for pure mode III. In this work, a different specimen geometry and loading device was tested.

7.4.3 Mixed Mode II/III

The plots in figure 7.16 presents the measured in-plane crack initiation angle and the angles predicted by Richard criterion. This figure covers five loading device positions for the mixed mode II/III loading cases. This loading case results in two crack initiation angles, in-plane and out of plane. The out of plane angle can be studied in figure 7.17. Due to the two different angles, the microscope angle measuring was somewhat more difficult, see figure 6.14, 6.15 and 6.16.

The measured angles in figure 7.16 show a similar curve as the criterion of Richard. Out of the five test data, the measured angles for pure $M^e_{23} = 0.0$ and $M^e_{23} = 1.0$ had the best fit with the criterion of Richard. These are the mixed mode cases of pure mode II and III. The criterion predicts an in-plane angle of $\theta_f = 0°$ for pure mode III and $\theta_f = -71.32°$ for pure mode II. Which is similar to the MTS and GMTS prediction for mixed mode I/II.

Even with a similar curved form as the criterion, the test data were found to be of lower magnitude than the criterion predictions. Ayatollahi [7] presented a lower criteria curve for the in-plane crack initiation angle for mixed mode II/III loading cases. His work also shows that the simplified criterion by Richard is in good agreement with his extended GMTS criterion for the mixed mode II/III loading cases. The criterion shows to be in good agreement with Schöllmanns and Pooks three dimensional fracture criteria for in-plane angle [30, 4, 10].

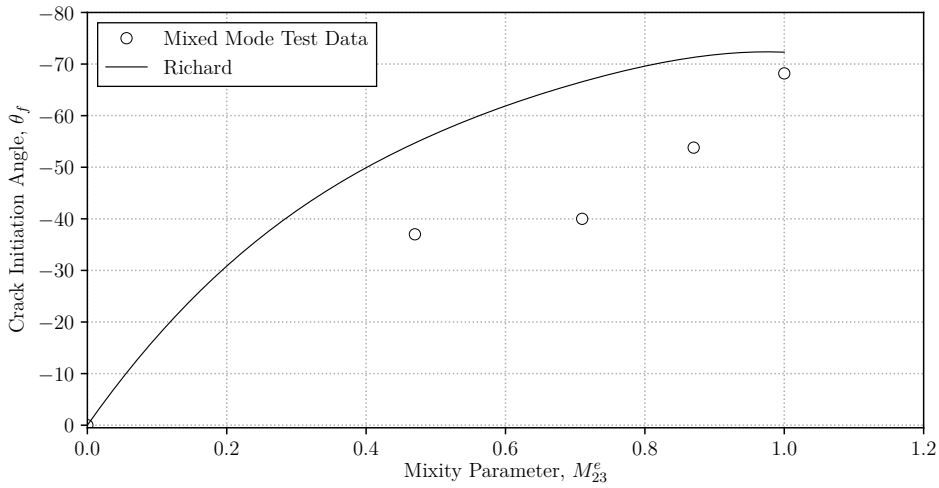

Figure 7.16: Plot of measured in plane crack initiation angle, θ_f, and the angle predictions of the Richard criterion.

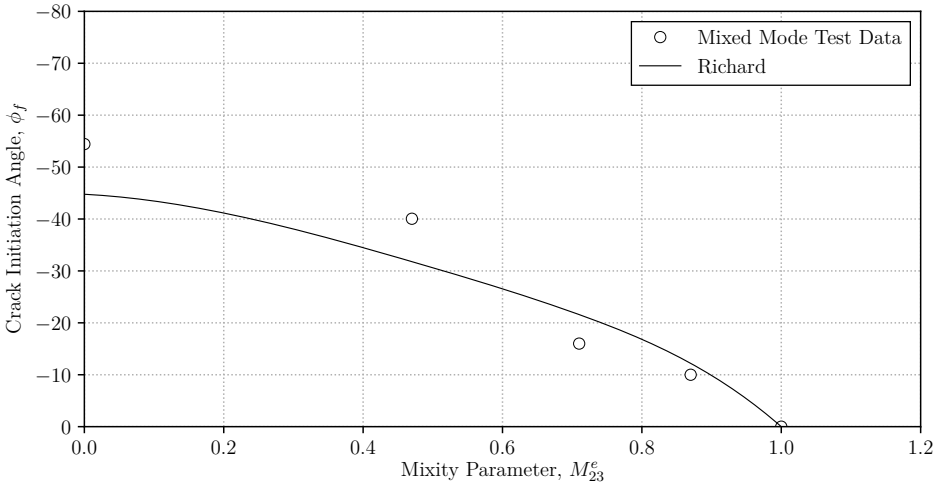

Figure 7.17: Plot of measured out of plane crack initiation angle, ϕ_f, and the angle predictions of the Richard criterion.

Figure 7.17 presents the Richard criterion for out of plane crack initiation angles, for mixed mode II/III loading cases. The criterion predicts an out of plane crack initiation angle of $\phi_f = 0°$ for pure mode II, and $\phi_f = -44.77°$ for pure mode III. Obtained measured data was found to be $\phi_f = -54.43°$ for pure mode III and $\phi_f = 0°$ for pure mode II.

Measured out of plane angles for the mixed mode II/III loading cases were found to be in a good agreement with the Richard criterion. The works of Ayatollahi showed higher values for negative T values [7]. The measured angles in this thesis show lower values than the Richard criterion for the loading cases of $\alpha = 90°/\beta = 22.5°$ and $\alpha = 90°/\beta = 45°$, and higher for $\alpha = 90°/\beta = 67.5°$ and $\alpha = 90°/\beta = 90°$. The Richard criterion of ϕ_f, for mixed mode II/III, were found to be in good agreement with the extended criterion of Ayatollahi and the three-dimensional criteria by Pook and Schöllmann [30, 7, 4, 10].

The mixed mode II/III fracture limit prediction can be studied in figure 7.18. In addition to the criteria predictions, mixed mode test data were plotted as circular markers. The five loading device positions, transitioning from pure mode II to III, can be seen as mixed mode data sets in pair of three markers. Richard's criterion shows a descending plot from pure mode II to III. For the criterion, with $\alpha_1 = 0.50$ and $\alpha_2 = 0.18$, the normalized mode II value of pure mode II was found to be 2.0, and the normalized mode III value for pure mode III were 5.6. The criterion with $\alpha_1 = 1.155$ and $\alpha_2 = 1.0$, shows descending curve from $K_{II}/K_{IC} = 0.8$ to $K_{III}/K_{IC} = 1.0$.

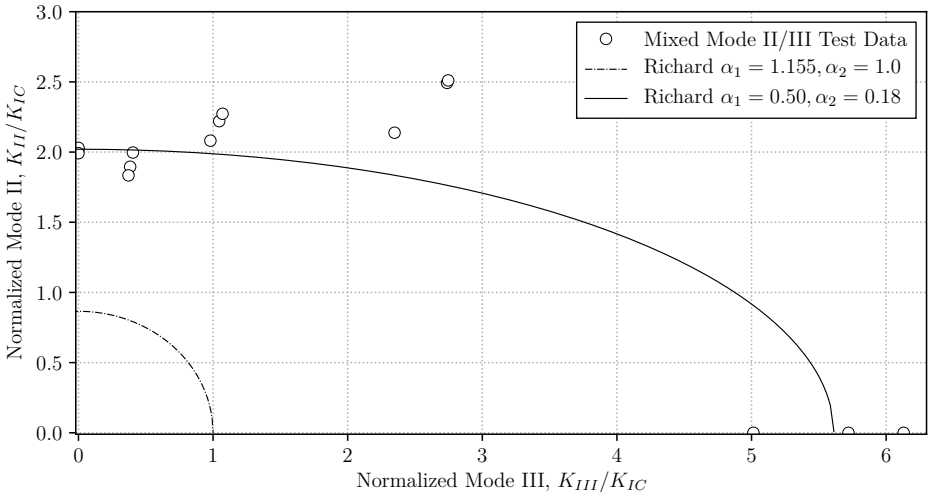

Figure 7.18: Fracture limit curves by the criterion of Richard compared with mixed mode II/III test data.

The plot in figure 7.18 shows a good agreement between the Richard criterion, $\alpha_1 = 0.50/\alpha_2 = 0.18$, and the mixed mode II/III test data. Where α_1 being K_{IC}/K_{IIC} and α_2 being K_{IC}/K_{IIIC}. The Richard criterion of $\alpha_1 = 1.155/\alpha_2 = 1.0$ was found to be very similar to the more complex criterion of Schöllmann [4, 10]. Which is also shown to be in good agreement with the MTS criterion [4]. The Richard $\alpha_1 = 1.155/\alpha_2 = 1.0$ criterion was also found to be in good agreement with the extended MTS criterion for mixed mode II/III, by Ayatollahi [7]. As mentioned, the Richard $\alpha_1 = 0.50/\alpha_2 = 0.18$ criterion shows a good agreement with the mixed mode test data. To calculate the correct α_1 and α_2 parameters, the fracture toughness for pure mode I, II and III were required. K_{IIC} and K_{IIIC} were not found to be as recognized as the well-known fracture toughness, K_{IC}. To calculate these, the fracture load for all three modes, with the respective specimen, is required. However, when comparing results with test data, all of the fracture loads are necessary regardless. For MTS and GMTS, only the K_{IC} is required.

As discussed in this thesis, the values of K_{IC} shows a great variation for different specimen geometries, for the same material [20, 25, 31]. One should therefore obtain own K_{IC} values. The MTS criterion shows a good fit with the measured test data of angles in this thesis. However, the criterion does not fit well with the values of normalized mode I, II and III values. The works of Aliha and Ayatollahi showed a good mixed mode test data fit with the GMTS criterion [16, 20]. In this works, a greater magnitude of T-stresses were obtained. Due to the low T values obtained in this thesis, the GMTS and MTS criterion did not show much deviation.

7.4.4 Comparison of Measured and Theoretical Predictions of Fracture Angles

Table 6 lists all of the measured angles, side by side with the angles calculated by criteria. For the cases of mixed mode I/II and I/III, the GMTS criterion was used. For the rest of the the criterion of Richard was used, see chapter 5.4 and 2.6. Most of the criteria predicted angles show a good agreement with the measurements. Largest deviation was found for the mixed mode I/II/III cases.

As mentioned earlier in this thesis, the combination of in and out of plane angles, made precise angle measurements difficult, see figure 6.14 and 6.23. For the cases of no twisting angle, the cracks showed a straight form. By increasing the amount of mode III to the loading case, the cracks gained more curve. This changing in crack angle, made it difficult to find the exact crack initiation angles for some loading cases, see chapter 6.3.

Table 6: Overview of α and β degree combinations for all loading cases.

Fracture Modes	Fixture Positions	Measure θ_f	Criterion θ_f	Measure ϕ_f	Criterion ϕ_f
I	$\alpha = 0°$, $\beta = 0°$	$0°$	$0°$	$0°$	$0°$
I/II	$\alpha = 22.5°$, $\beta = 0°$	$-21.29°$	$-25.84°$	$0°$	$0°$
I/II	$\alpha = 45.0°$, $\beta = 0°$	$-35.15°$	$-46.04°$	$0°$	$0°$
I/II	$\alpha = 67.5°$, $\beta = 0°$	$-55.71°$	$-59.28°$	$0°$	$0°$
II	$\alpha = 90.0°$, $\beta = 0°$	$-68.19°$	$-70.99°$	$0°$	$0°$
I/III	$\alpha = 0°$, $\beta = 22.5°$	$0°$	$0°$	$-19.23°$	$-18.8°$
I/III	$\alpha = 0°$, $\beta = 45.0°$	$0°$	$0°$	$-37.08°$	$-29.71°$
I/III	$\alpha = 0°$, $\beta = 67.5°$	$0°$	$0°$	$-46.71°$	$-37.52°$
II/III	$\alpha = 90°$, $\beta = 22.5°$	$-53.80°$	$-71.32°$	$-10.41°$	$-12.21°$
II/III	$\alpha = 90°$, $\beta = 45.0°$	$-40.35°$	$-66.57°$	$-16.02°$	$-21.59°$
II/III	$\alpha = 90°$, $\beta = 67.5°$	$-37.53°$	$-54.71°$	$-40.05°$	$31.79°$
I/II/III	$\alpha = 22.5°$, $\beta = 22.5°$	$-33.83°$	$-26.58°$	$-8°$	$-7.09°$
I/II/III	$\alpha = 22.5°$, $\beta = 45.0°$	$-18.04°$	$-23.21°$	$-36.61°$	$-13.48°$
I/II/III	$\alpha = 22.5°$, $\beta = 67.5°$	$-15.42°$	$-19.99°$	$-48.96°$	$-22.77°$
I/II/III	$\alpha = 45.0°$, $\beta = 22.5°$	$-45.99°$	$-44.45°$	$-9.36°$	$-7.29°$
I/II/III	$\alpha = 45.0°$, $\beta = 45.0°$	$-25.03°$	$-39.62°$	$-18.47°$	$-13.94°$
I/II/III	$\alpha = 45.0°$, $\beta = 67.5°$	$-17.52°$	$-33.71°$	$-44.39°$	$-23.69°$
I/II/III	$\alpha = 67.5°$, $\beta = 22.5°$	$-67.13°$	$-59.27°$	$-25.34°$	$-8.60°$
I/II/III	$\alpha = 67.5°$, $\beta = 45.0°$	$-32.91°$	$-53.56°$	$-13.67°$	$-16.15°$
I/II/III	$\alpha = 67.5°$, $\beta = 67.5°$	$-20.99°$	$-44.41°$	$-38.25°$	$-26.40°$
III	$\alpha = 0°$, $\beta = 90.0°$	$0°$	$0°$	$-42.02°$	$-45.17°$
III	$\alpha = 22.5°$, $\beta = 90.0°$	$0°$	$0°$	$-42.37°$	$-44.47°$
III	$\alpha = 45.0°$, $\beta = 90.0°$	$0°$	$-2.25°$	$-53.19°$	$-44.52°$
III	$\alpha = 67.5°$, $\beta = 90.0°$	$0°$	$-2.67°$	$-53.04°$	$-44.64°$
III	$\alpha = 90.0°$, $\beta = 90.0°$	$0°$	$-2.77°$	$-54.43°$	$44.77°$

7.4.5 Three Dimensional Mixed Mode Criterion

The three-dimensional criterion by Richard can be seen in figure 7.19. The plot shows the normalized mode II, K_{II}/K_{IC}, on its z-axis, normalized mode I, K_I/K_{IC}, on the y-axis and normalized mode III, K_{III}/K_{IC}, on the x-axis. In this criterion $\alpha_1 = 1.155$ and $\alpha_2 = 1.0$. These parameters result in a good agreement with the three-dimensional criterion of Schöllmann [10, 4]. The three-dimensional criterion of Schöllmann results in a good agreement with the extended GMTS criterion for mode I/II, I/III and II/III of Ayatollahi, with $B\alpha_r = 0$ (MTS) [7]. As discussed in chapter 7.4, the MTS criterion predictions were not found to be a good prediction for the test data obtained in this thesis. Richard compared the criterion, for $\alpha_1 = 1.155/\alpha_2 = 1.0$, with test results of different steels, and aluminum [32, 33]. In this work, most of the test data did not fit well with the Richard, $\alpha_1 = 1.155/\alpha_2 = 1.0$, criterion.

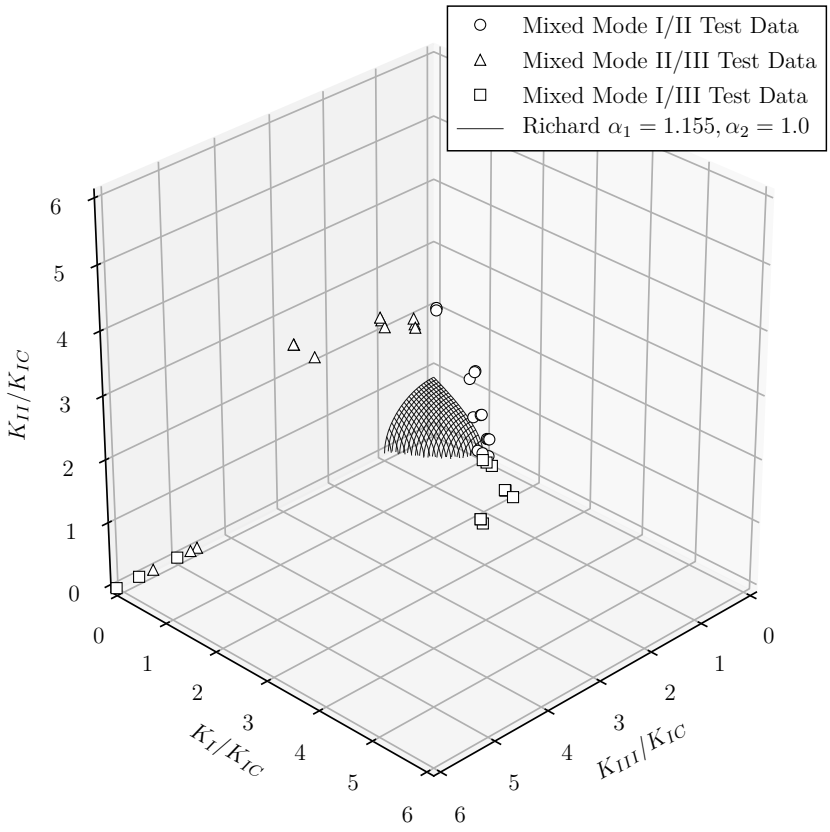

Figure 7.19: Plot of three dimensional mixed mode criterion of Richard, with $\alpha_1 = 1.155$ and $\alpha_2 = 1.0$, and mixed mode test data.

The three dimensional criterion by Richard, with parameters $\alpha_1 = 0.50$ and $\alpha_2 = 0.18$, can be seen in figure 7.20. The wire-frame presents the Richard criterion, and markers presents test data. In addition to the plot in figure 7.19, this plot includes the test data for mixed mode I/II/III. These can be seen as markers formed as diamonds. As expected from the two dimensional Richard criterion, see figure 7.13, 7.15 and 7.18, the parameters of $\alpha_1 = 0.50/\alpha_2 = 0.18$ presents a more accurate representation of the test data. In the works of Richard, a more accurate criterion estimate was obtained when replacing α_1 and α_2 with the relations K_{IC}/K_{IIC} and K_{IC}/K_{IIIC} [33, 21]. The python script used for these plots can be studied in appendix R.

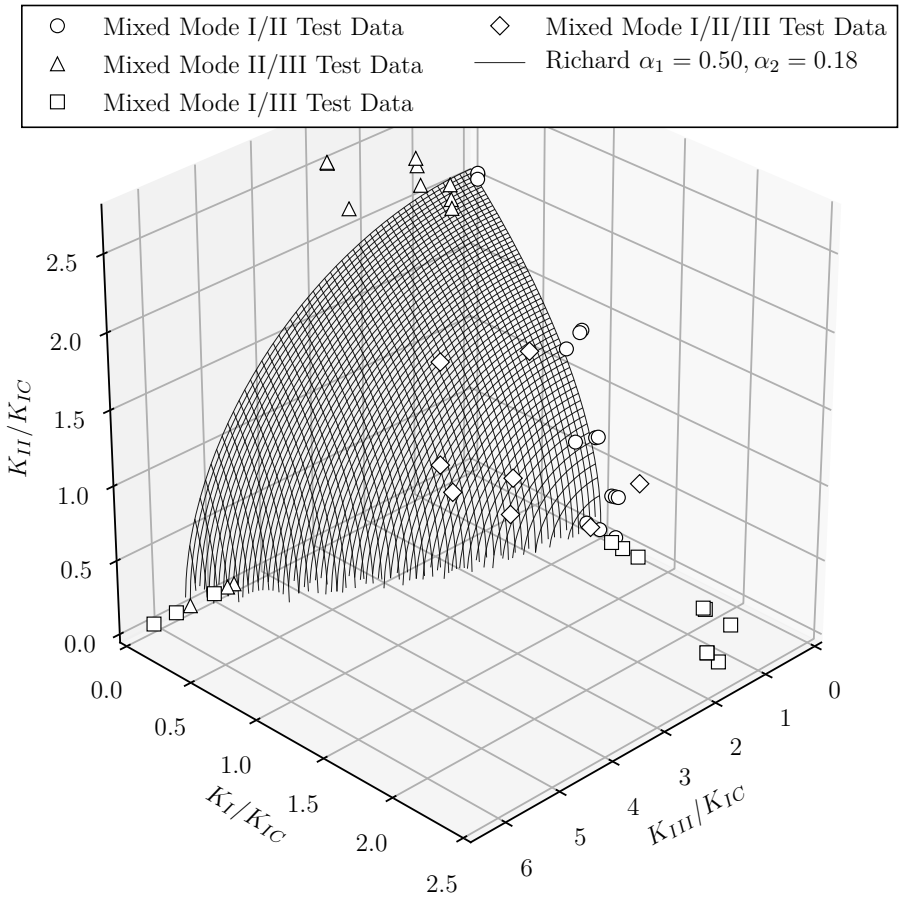

Figure 7.20: Plot of three dimensional mixed mode criterion of Richard, with $\alpha_1 = 0.50$ and $\alpha_2 = 0.18$, and mixed mode test data.

8 Conclusion

In this work, general mixed mode I/II/III fracture assessments were studied experimentally and theoretically. A new mixed mode I/II/III loading device was designed, manufactured and used for testing of pre-cracked CTS specimens. Experiments were conducted on all twenty-five combinations of the loading device, on specimens of PMMA. The presented mixed mode loading device allowed mixed mode I/II/III loading combinations in steps of 22.5°, for in and out of plane rotations. From the experimental procedure, fracture loads were obtained, and in and out of plane angles were measured. The theoretical study in this thesis consisted of numerical analyses, simulations, and fracture criteria.

The presented geometry factors in this thesis showed different values across the specimen thickness. Y_I values were in most loading cases found to be peaking at the specimen center, but Y_{II} and Y_{III} often had descending values from surface to surface. All of the geometry values were found to be symmetric about the specimen center. A coupling effect for Y_{II} and Y_{III} was found, the presence of Y_{II} lead to the presence of Y_{III} values and vice versa. Alternating values of T-stresses across the specimen thickness were also obtained. The peaking value was consistently the third node from the specimen surface. All values were found to be symmetric about the specimen center.

MTS and GMTS criteria were found to be accurate for predicting in-plane and out of plane crack initiation angles. Small deviations between GMTS and MTS were obtained, due to the low values of T-stresses. The criteria predicted slightly higher angles for mixed mode I/II and slightly lower angles for mixed mode I/III. The Richard criterion, with A = 140°, B = −70°, C = 78° and D = −33°, gave a good prediction for out of plane crack initiation angles for mixed mode II/III cases. The in-plane angle prediction resulted in slightly higher values than the measured angles. MTS and GMTS predictions for mixed mode fracture limits were found to be conservative. The fracture limit for pure mode II was found to be twice the magnitude as the predicted values. For the loading case of pure mode III, the obtained fracture limit was five times higher than for the MTS prediction. Richard's criterion was found to be a relatively good prediction method for the fracture limits, except from some of the cases of mixed mode I/III. Even with a better fit, the criterion predictions for the fracture limit were still found to be conservative in most mixed mode I/II/III loading cases. To present a satisfying prediction with the criterion of Richard, K_{IC}, K_{IIC} and K_{IIIC} are required. For the predictions of MTS and GMTS, only K_{IC} needs to be obtained.

9 Further Work

In this thesis, mixed mode I/II/III loading cases were studied experimentally and theoretically. Two loading devices were designed for the thesis, but only one of them were manufactured. It could be of interest to manufacture the second, AFM, loading device and compare mixed mode test results. In addition to another mixed mode loading device, other specimens could be tested as well. In this thesis, pre-cracked CTS specimens were used for testing. It would be interesting to also conduct testing of notched CTS specimens, with different notched radius for comparison. As illustrated by the GMTS criterion, low deviations from the MTS criterion were obtained due to the low T-stresses of pre-cracked CTS specimen. It would be of interest to test a specimen with a greater amount of T-stresses to get a better study of the GMTS criterion.

For the theoretical study in this thesis, mainly three fracture criteria were analyzed. These were MTS, GMTS and Richard's criterion. It would be of interest to study other criteria as well. For two-dimensional mixed mode cases, the ASED criterion could be analyzed. For the cases of three dimensional mixed mode loading, the criteria by Pook and Schöllmann could be added to the experimental data validation. In addition to the criteria, it could be of interest to study the numerical analysis of mixed mode I/III further, which gave values of great magnitude.

References

[1] T.L. Anderson. *Fracture Mechanics, Fundamentals and Applications*. Taylor and Francis Group, 6000 Broken Sound Parkway NW, Suite 300, third edition edition, July 2011. Book Number-13: 978-1-4200-5821-5.

[2] Norman E. Dowling. *Mechanical Behavior of Materials*. Pearson Education Limited, Edinburg Gate, Harlow, Essex CM20 2JE, England, fourth edition edition, 2012.

[3] N.-H. Schirmeisen H.A. Richard, B. Schramm. Cracks on mixed mode loading - theories, experiments, simulations. *International Journal of Fatigue*, page 11, October 2012.

[4] H. A. RICHARD, M. FULLAND, and M. SANDER. Theoretical crack path prediction. *Fatigue and Fracture of Engineering Materials and Structures*, 28(1-2):3–12, 1 2005.

[5] M. Kuna H.A. Richard. Theoretical and experimental study of superimposed fracture modes i, ii and iii. *Institute of Applied Mechanics, Department of Mechanical Engineering, University of Paderborn*, 35(6):949–960, 1990.

[6] M. L. Williams. The Bending Stress Distribution at the Base of a Stationary Crack. *Journal of Applied Mechanics*, 28(1):78, 1961.

[7] Majid R. Ayatollahi and Behnam Saboori. T-stress effects in mixed mode I/II/III brittle fracture. *Engineering Fracture Mechanics*, 144:32–45, 2015.

[8] Y.H. Tai, M.W. Brown, and J.R. Yates. A new solution for 3d crack extension based on linear elastic stress fields. *Engineering Fracture Mechanics*, 78(8):1602 – 1613, 2011. Multiaxial Fracture.

[9] L.P. Pook. The fatigue crack direction and threshold behaviour of mild steel under mixed mode i and iii loading. *International Journal of Fatigue*, 7(1):21 – 30, 1985.

[10] Matthias Schöllmann, Hans A. Richard, Gunter Kullmer, and Markus Fulland. A new criterion for the prediction of crack development in multiaxially loaded structures. *International Journal of Fracture*, 117(2):129–141, Sep 2002.

[11] F.-G. BUCHHOLZ, V. JUST, and H. A. RICHARD. Computational simulation and experimental findings of three-dimensional fatigue crack growth in a single-edge notched specimen under torsion loading. *Fatigue and Fracture of Engineering Materials and Structures*, 28(1-2):127–134, 1 2005.

[12] Jun Chang, Jin quan Xu, and Yoshiharu Mutoh. A general mixed-mode brittle fracture criterion for cracked materials. *Engineering Fracture Mechanics*, 73(9):1249 – 1263, 2006.

[13] F. Erdogan and G. C. Sih. On the Crack Extension in Plates Under Plane Loading and Transverse Shear. *Journal of Basic Engineering*, 85(4):519, 1963.

[14] D. J. Smith, M. R. Ayatollahi, and M. J. Pavier. The role of T-stress in brittle fracture for linear elastic materials under mixed-mode loading. *Fatigue and Fracture of Engineering Materials and Structures*, 24(2):137–150, 2001.

[15] M.R.M. Aliha and M.R. Ayatollahi. Analysis of fracture initiation angle in some cracked ceramics using the generalized maximum tangential stress criterion. *International Journal of Solids and Structures*, 49(13):1877 – 1883, 2012.

[16] M. R. M. Aliha, M. R. Ayatollahi, and J. Akbardoost. Typical upper bound–lower bound mixed mode fracture resistance envelopes for rock material. *Rock Mechanics and Rock Engineering*, 45(1):65–74, Jan 2012.

[17] M. R. M. Aliha, Gh. R. Hosseinpour, and M. R. Ayatollahi. Application of cracked triangular specimen subjected to three-point bending for investigating fracture behavior of rock materials. *Rock Mechanics and Rock Engineering*, 46(5):1023–1034, Sep 2013.

[18] M.R. Ayatollahi, M.R.M. Aliha, and H. Saghafi. An improved semi-circular bend specimen for investigating mixed mode brittle fracture. *Engineering Fracture Mechanics*, 78(1):110 – 123, 2011.

[19] Shu Liu, Yuh J. Chao, and Xiankui Zhu. Tensile-shear transition in mixed mode i/iii fracture. *International Journal of Solids and Structures*, 41(22):6147 – 6172, 2004.

[20] M.R. Ayatollahi, M.R.M. Aliha, and M.M. Hassani. Mixed mode brittle fracture in pmma, an experimental study using scb specimens. *Materials Science and Engineering: A*, 417(1):348 – 356, 2006.

[21] H.A. Richard and A. Eberlein. Material characteristics at 3D-mixed-mode-loadings. *Procedia Structural Integrity*, 2:1821–1828, 2016.

[22] M.R. Ayatollahi and Behnam Saboori. A new fixture for fracture tests under mixed mode i/iii loading. *European Journal of Mechanics - A/Solids*, 51:67 – 76, 2015.

[23] H.A. Richard and M. Kuna. Theoretical and experimental study of superimposed fracture modes i, ii and iii. *Engineering Fracture Mechanics*, 35(6):949 – 960, 1990.

[24] M. Sander and H.A. Richard. Experimental and numerical investigations on the influence of the loading direction on the fatigue crack growth. *International Journal of Fatigue*, 28(5):583 – 591, 2006. Selected papers from the 7th International Conference on Biaxial/Multiaxial Fatigue and Fracture (ICBMFF).

[25] S.M.J. Razavi, M.R. Ayatollahi, and F. Berto. A synthesis of geometry effect on brittle fracture. *Engineering Fracture Mechanics*, 187:94 – 102, 2018. SI: 50th Anniversary Issue.

[26] M.R. Ayatollahi, M. Rashidi Moghaddam, S.M.J. Razavi, and F. Berto. Geometry effects on fracture trajectory of pmma samples under pure mode-i loading. *Engineering Fracture Mechanics*, 163:449 – 461, 2016.

[27] ASM aerospace specification metals. *Titanium Ti-6Al-4V (Grade 5), Annealed*. ASM aerospace specification metals, 2014. Accessed 2018-03-20.

[28] Abaqus analysis user's manual. `http://abaqusdoc.ucalgary.ca/books/usb/default.htm?startat=book01.html`.

[29] M. R.M. Aliha, A. Bahmani, and Sh Akhondi. Mixed mode fracture toughness testing of PMMA with different three-point bend type specimens. *European Journal of Mechanics, A/Solids*, 58:148–162, 2016.

[30] Hans A. Richard, Markus Fulland, Fritz G. Buchholz, and Matthias Schollmann. 3D Fracture Criteria for Structures with Cracks. *Steel Research International*, 74(8):491–497, 2003.

[31] M. R. Ayatollahi, M. Rashidi Moghaddam, S. M.J. Razavi, and F. Berto. Geometry effects on fracture trajectory of PMMA samples under pure mode-I loading. *Engineering Fracture Mechanics*, 163:449–461, 2016.

[32] T. Vojtek, R. Pippan, A. Hohenwarter, L. Holàn, and J. Pokluda. Near-threshold propagation of mode ii and mode iii fatigue cracks in ferrite and austenite. *Acta Materialia*, 61(12):4625 – 4635, 2013.

[33] H.A. Richard, A. Eberlein, and G. Kullmer. Concepts and experimental results for stable and unstable crack growth under 3d-mixed-mode-loadings. *Engineering Fracture Mechanics*, 174:10 – 20, 2017. Special Issue on Multiaxial Fracture 2016.

Appendices

A Technical Drawing of AFM Specimen

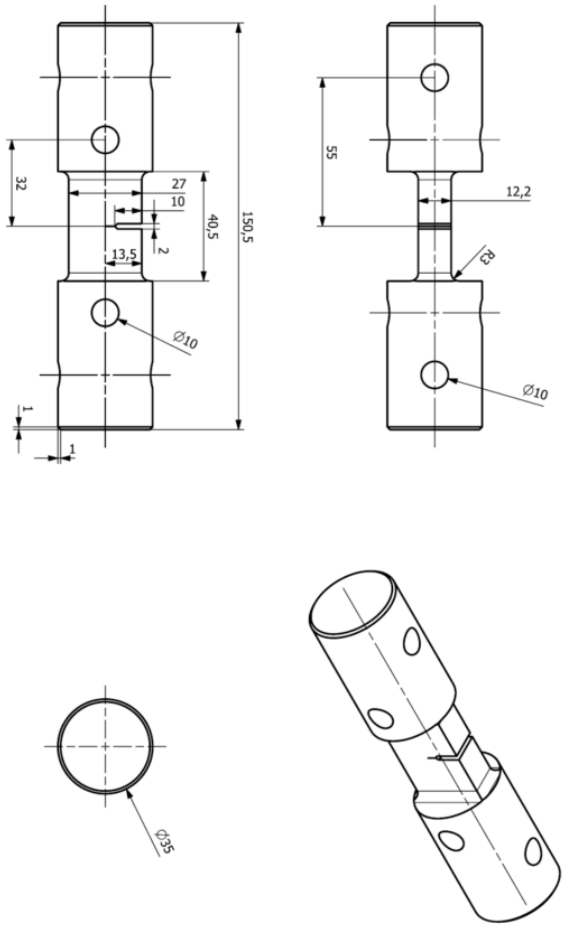

B Technical Drawing of AFM Fixture

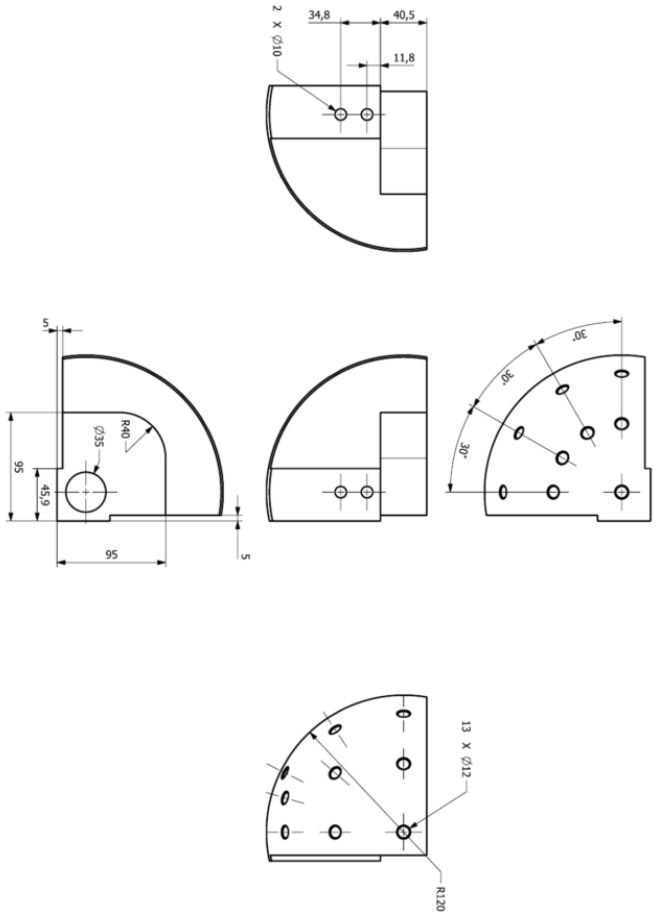

C Technical Drawing of CTS Specimen

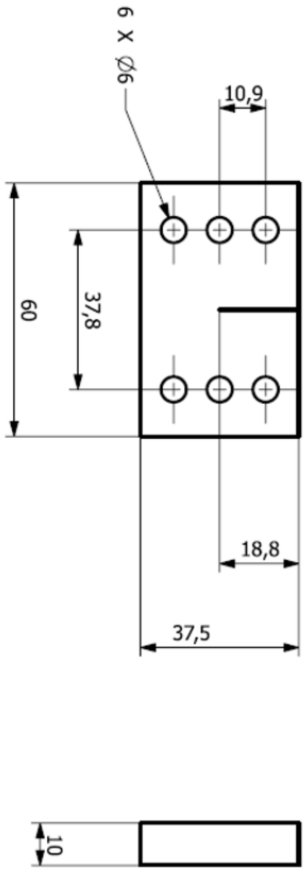

D Technical Drawing of mixed mode I/II/III C-fixture

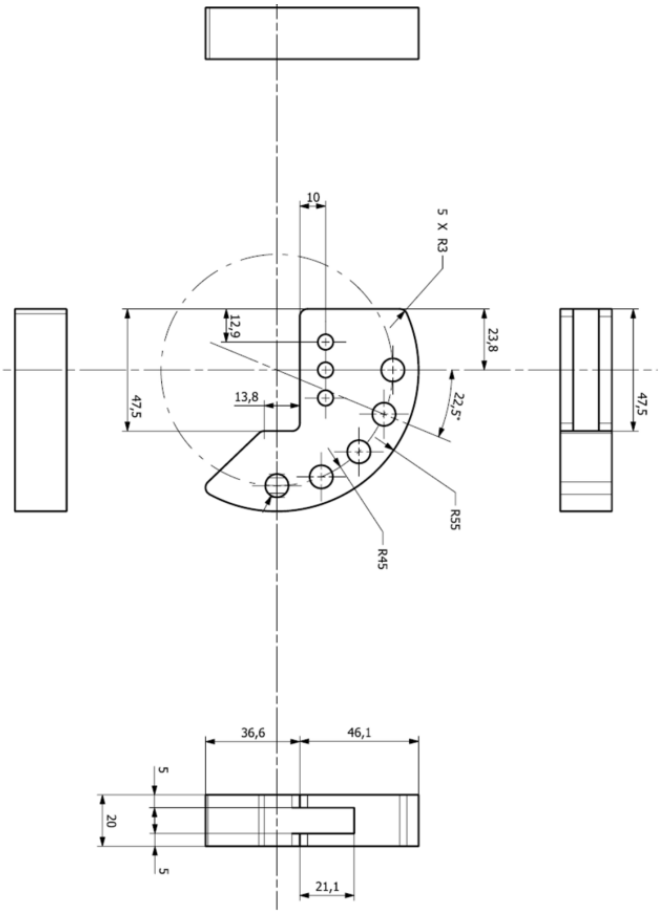

E Technical Drawing of mixed mode I/II/III J-fixture

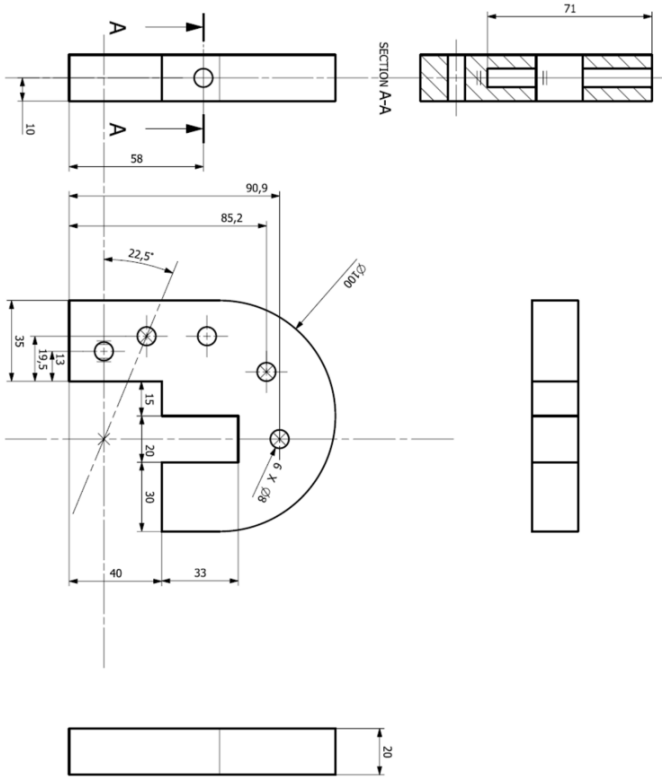

F Table of KI Values

	KI-Stress- 8 Mesh Thickness	1	2	3	4	5	6
Mode I / II	α = 0° , β = 0°	20.1800	21.8700	22.8300	22.6400	22.8600	22.8000
	α = 22,5° , β = 0°	20.0400	21.7200	22.6700	22.4900	22.7100	22.6500
	α = 45° , β = 0°	18.7300	20.3000	21.1900	21.0200	21.2300	21.1700
	α = 67,5° , β = 0°	13.1100	14.2200	14.8400	14.7200	14.8700	14.8200
	α = 90° , β = 0°	0.6676	0.7212	0.7508	0.7427	0.7481	0.7448
Mode I / III	α = 0° , β = 90°	1.5910	1.7180	1.7860	1.7650	1.7750	1.7620
	α = 0° , β = 67,5°	31.3100	33.9300	35.4200	35.1400	35.4800	35.3800
	α = 0° , β = 45°	25.2200	27.3300	28.3300	28.3000	28.5700	28.4900
	α = 0° , β = 22,5°	21.2900	23.0700	24.0800	23.8900	24.1200	24.0500
Mode I / II / III	α = 22,5° , β = 90°	1.3710	1.4810	1.5390	1.5210	1.5290	1.5180
	α = 22,5° , β = 67,5°	29.7100	32.2300	33.6800	33.4300	33.7800	33.7000
	α = 22,5° , β = 45°	24.9300	27.0200	28.2100	27.9800	28.2500	28.1700
	α = 22,5° , β = 22,5°	21.1300	22.9100	23.9100	23.7200	23.9500	23.8800
	α = 45° , β = 90°	0.9553	1.0310	1.0710	1.0580	1.0640	1.0550
	α = 45° , β = 67,5°	24.5300	26.6200	27.8300	27.6300	27.9200	27.8600
	α = 45° , β = 45°	22.9700	24.8900	25.9800	25.7700	26.0200	25.9500
	α = 45° , β = 22,5°	19.7200	21.3800	22.3200	22.1400	22.3600	22.2900
	α = 67,5° , β = 90°	0.5072	0.5429	0.5593	0.5487	0.5478	0.5387
	α = 67,5° , β = 67,5°	15.1300	16.4000	17.1100	16.9700	17.1300	17.0800
	α = 67,5° , β = 45°	15.7300	17.0500	17.8000	17.6300	17.8200	17.7700
	α = 67,5° , β = 22,5°	13.7800	14.9400	15.5900	15.4700	15.6200	15.5800
Mode II / III	α = 90° , β = 90°	0.0997	0.0948	0.0863	0.07.50	0.0649	0.0527
	α = 90° , β = 67,5°	0.7978	0.8541	0.8812	0.8650	0.8644	0.8528
	α = 90° , β = 45°	0.8737	0.9406	0.9756	0.9622	0.9661	0.9583
	α = 90° , β = 22,5°	0.7253	0.7823	0.8130	0.8031	0.8078	0.8028

7	8	9	10	11	12	13	14	15	16	17
22.8000	22.8300	22.8900	22.8300	22.8900	22.8000	22.8600	22.6400	22.8300	21.8700	20.1700
22.7300	22.6800	22.7400	22.6800	22.7300	22.6500	22.7100	22.4900	22.6700	21.7200	20.0400
21.2500	21.2000	21.2500	21.2000	21.2500	21.1700	21.2300	21.0200	21.1900	20.3000	18.7300
14.8800	14.8500	14.8800	14.8500	14.8800	14.8200	14.8700	14.7200	14.8400	14.2200	13.1200
0.7465	0.7444	0.7459	0.7443	0.7464	0.7447	0.7480	0.7426	0.7507	0.7211	0.6675
1.7620	1.7530	1.7500	1.7370	1.7370	1.7230	1.7200	1.6950	1.7020	1.6220	1.4890
35.5100	35.4300	35.5100	35.4200	35.5000	35.3600	35.4300	35.1100	35.3900	33.8900	31.2600
28.6000	28.5300	28.6000	28.5300	28.6000	28.4900	28.5700	28.2900	28.5200	27.3200	25.2100
24.1400	24.0900	24.1500	24.0900	24.1400	24.0500	24.1200	23.8900	24.0800	23.0700	21.2800
1.5180	1.5110	1.5070	1.4970	1.4960	1.4850	1.4810	1.4610	1.4660	1.3970	1.2830
33.8500	33.7900	33.9000	33.8300	33.9200	33.8100	33.9200	33.6100	33.9000	32.4800	29.9800
28.2800	28.2100	28.2800	28.2100	28.2700	28.1700	28.2500	27.9700	28.2000	27.0100	24.9200
23.9800	23.9200	23.9800	23.9200	23.9800	23.8900	23.9600	23.7200	23.9200	22.9200	21.1400
1.0550	1.0500	1.0470	1.0390	1.0390	1.0310	1.0280	1.0130	1.0160	0.9680	0.8884
27.9900	27.9500	28.0400	27.9900	28.0800	27.9900	28.0900	27.8300	28.0800	26.9100	24.8400
26.0500	25.9900	26.0500	25.9800	26.0400	25.9400	26.0200	25.7600	25.9700	24.8800	22.9500
22.3800	22.3300	22.3900	22.3300	22.3900	22.3000	22.3700	22.1500	22.3300	21.3900	19.7400
0.5351	0.5299	0.5241	0.5156	0.5128	0.5052	0.4990	0.4878	0.4855	0.4578	0.4155
17.1400	17.1000	17.1300	17.0900	17.1200	17.0500	17.0900	16.9200	17.0500	16.3300	15.0600
17.8400	17.7900	17.8400	17.7900	17.8300	17.7600	17.8100	17.6400	17.7800	17.0300	15.7100
15.6400	15.6000	15.6400	15.6000	15.6400	15.5800	15.6300	15.4800	15.6000	14.9500	13.7900
0.0429	0.0345	0.0232	0.0118	0.0035	-0.0064	-0.0183	-0.0287	-0.0396	-0.0499	-0.0581
0.8483	0.8404	0.8346	0.8253	0.8220	0.8134	0.8089	0.7958	0.7972	0.7575	0.6933
0.9576	0.9524	0.9509	0.9453	0.9453	0.9399	0.9402	0.9298	0.9363	0.8953	0.8251
0.8036	0.8004	0.8007	0.7977	0.7989	0.7959	0.7980	0.7909	0.7982	0.7651	0.7070

G Table of KII Values

	KI-Stress- 8 Mesh Thickness	1	2	3	4	5	6
Mode I / II	α = 0° , β = 0°	-0.0194	-0.0189	-0.0190	-0.0194	-0.0195	-0.0197
	α = 22,5° , β = 0°	6.8140	6.2120	6.0100	6.1470	6.1130	6.1600
	α = 45° , β = 0°	15.3500	13.9900	13.5400	13.8500	13.7700	13.8800
	α = 67,5° , β = 0°	25.6000	23.3400	22.5800	23.1000	22.9700	23.1500
	α = 90° , β = 0°	31.4300	28.6600	27.7300	28.3600	28.2000	28.4200
Mode I / III	α = 0° , β = 90°	52.1100	31.3800	17.3500	15.4200	10.1200	7.7570
	α = 0° , β = 67,5°	23.0000	13.8200	7.6200	6.7700	4.4280	3.3880
	α = 0° , β = 45°	8.3250	5.0020	2.7540	2.4460	1.5970	1.2200
	α = 0° , β = 22,5°	3.2290	1.9420	1.0710	0.9505	0.6208	0.4736
Mode I / II / III	α = 22,5° , β = 90°	52.5900	31.8100	17.7800	15.8600	10.5500	8.1960
	α = 22,5° , β = 67,5°	34.6600	23.9700	17.0400	16.3300	13.7800	12.7300
	α = 22,5° , β = 45°	16.9400	12.6400	9.9670	9.7910	8.8320	8.4770
	α = 22,5° , β = 22,5°	10.5900	8.5620	7.4050	7.4160	7.0230	6.9120
	α = 45° , β = 90°	52.9200	32.1100	18.0600	16.1400	10.8300	8.4750
	α = 45° , β = 67,5°	48.2000	35.1600	26.9300	26.2800	23.3000	22.1500
	α = 45° , β = 45°	28.7200	22.7200	19.1800	19.1200	17.8900	17.5100
	α = 45° , β = 22,5°	20.2700	17.1200	15.4700	15.6300	15.1000	15.0100
	α = 67,5° , β = 90°	53.1000	32.2700	18.2000	16.2900	10.9700	8.6150
	α = 67,5° , β = 67,5°	60.5000	45.0800	35.5000	34.8500	31.4100	30.1200
	α = 67,5° , β = 45°	42.9800	34.7300	30.0100	30.0500	28.4500	27.9900
	α = 67,5° , β = 22,5°	32.1500	27.5400	25.2100	25.5300	24.8200	24.7400
Mode II / III	α = 90° , β = 90°	53.2200	32.3600	18.2800	16.3600	11.0300	8.6640
	α = 90° , β = 67,5°	66.3600	49.7400	39.4600	38.8000	35.1100	33.7500
	α = 90° , β = 45°	50.9400	41.3900	35.9800	36.0600	34.2300	33.7300
	α = 90° , β = 22,5°	38.9500	33.4800	30.7500	31.1600	30.3300	30.2600

7	8	9	10	11	12	13	14	15	16	17
-0.0199	-0.0200	-0.0201	-0.0203	-0.0203	-0.0204	-0.0204	-0.0205	-0.0204	-0.0207	-0.0216
6.1510	6.1710	6.1590	6.1710	6.1500	6.1590	6.1120	6.1460	6.0090	6.2100	6.8110
13.8600	13.9000	13.8800	13.9000	13.8600	13.8800	13.7700	13.8500	13.5400	13.9900	15.3500
23.1100	23.1900	23.1500	23.1900	23.1100	23.1500	22.9700	23.1000	22.5800	23.3400	25.6000
28.3800	28.4700	28.4200	28.4700	28.3800	28.4200	28.2000	28.3600	27.7300	28.6600	31.4300
4.6860	2.4040	-0.0003	-2.4060	-4.6870	-7.7590	-10.1200	-15.4200	-17.3500	-31.3800	-52.1100
2.0340	1.0300	-0.0293	-1.0890	-2.0930	-3.4470	-4.4860	-6.8280	-7.6770	-13.8800	-23.0500
0.7286	0.3643	-0.0197	-0.4038	-0.7679	-1.2590	-1.6360	-2.4850	-2.7920	-5.0400	-8.3640
0.2822	0.1399	-0.0100	-0.1600	-0.3022	-0.4935	-0.6406	-0.9702	-1.0910	-1.9610	-3.2480
5.1250	2.8450	0.4408	-1.9630	-4.2440	-7.3150	-9.6770	-14.9800	-16.9200	-30.9300	-51.6100
11.2600	10.2200	9.0620	7.9420	6.8340	5.3950	4.2110	1.7520	0.6391	-5.6960	-14.6100
7.9340	7.5630	7.1330	6.7290	6.3110	5.7890	5.3260	4.4440	3.9320	1.7490	-1.1580
6.6940	6.5600	6.3850	6.2340	6.0580	5.8600	5.6510	5.3270	5.0350	4.3170	3.5410
5.4020	3.1210	0.7135	-1.6920	-3.9770	-7.0490	-9.4160	-14.7200	-16.6600	-30.6700	-51.3300
20.4500	19.2700	17.9300	16.6500	15.3500	13.7000	12.2800	9.4930	8.0460	0.9934	-8.5510
16.8200	16.3900	15.8400	15.3500	14.8100	14.1800	13.5500	12.5000	11.7300	9.2330	6.3190
14.7300	14.3800	14.3500	14.1800	13.9400	13.7000	13.3900	13.0200	12.5400	11.8300	11.4800
5.3370	3.2530	0.8415	-1.5670	-3.8560	-6.9330	-9.3040	-14.6100	-16.5600	-30.5700	-51.2400
28.1700	26.8300	25.2800	23.8200	22.3200	20.4400	18.7700	15.6000	13.8300	5.9000	-4.5830
27.1000	26.5600	25.8500	25.2300	24.5200	23.7100	22.8600	21.5400	20.4300	17.4000	14.1900
24.3600	24.1900	23.8800	23.6600	23.3300	23.0300	22.5900	22.1300	21.3900	20.6300	20.6700
5.5770	3.2850	0.8647	-1.5530	-3.8500	-6.9350	-9.3150	-14.6300	-16.5900	-30.6200	-51.3000
31.6500	30.2200	28.5600	27.0000	25.3900	23.3800	21.5800	18.2000	16.2700	7.8540	-3.1880
32.7200	32.1100	31.3000	30.6000	29.7800	28.8600	27.8900	26.3900	25.0900	21.7200	18.2800
29.8300	29.6300	29.2800	29.0300	28.6400	28.3000	27.7800	27.2700	26.3800	25.5600	25.8000

H Table of KIII Values

	KIII-Stress- 8 Mesh Thickness	1	2	3	4	5	6
Mode I / II	α = 0° , β = 0°	-0.0072	-0.0034	-0.0007	-0.0006	0.0002	0.0002
	α = 22,5° , β = 0°	3.1280	2.0040	1.2070	1.0460	0.7142	0.5438
	α = 45° , β = 0°	7.0440	4.5120	2.7150	2.3520	1.6060	1.2230
	α = 67,5° , β = 0°	11.7500	7.5220	4.5250	3.9210	2.6770	2.0380
	α = 90° , β = 0°	14.4200	9.2340	5.5540	4.8120	3.2850	2.5010
Mode I / III	α = 0° , β = 90°	37.5000	37.1100	39.7700	41.9400	43.9300	45.0900
	α = 0° , β = 67,5°	16.5700	16.4200	17.6000	18.5600	19.4500	19.9600
	α = 0° , β = 45°	6.0020	5.9470	6.3780	6.7250	7.0470	7.2330
	α = 0° , β = 22,5°	2.3260	2.3030	2.4680	2.6020	2.7260	2.7980
Mode I / II / III	α = 22,5° , β = 90°	37.7200	37.2500	39.8500	42.0000	43.9800	45.1200
	α = 22,5° , β = 67,5°	22.3300	20.5000	20.5800	21.3700	21.8200	22.1200
	α = 22,5° , β = 45°	10.1400	8.7710	8.3110	8.5010	8.4650	8.4690
	α = 22,5° , β = 22,5°	5.7750	4.5820	3.9340	3.9130	3.7040	3.6050
	α = 45° , β = 90°	37.8700	37.3500	39.9100	42.0600	44.0200	45.1500
	α = 45° , β = 67,5°	29.5200	26.0400	25.1700	25.8800	26.0100	26.1400
	α = 45° , β = 45°	16.1000	13.1300	11.6500	11.7100	11.2800	11.1000
	α = 45° , β = 22,5°	10.4500	7.7970	6.1620	5.9690	5.3660	5.0670
	α = 67,5° , β = 90°	37.9600	37.4100	39.9500	42.0900	44.0500	45.1800
	α = 67,5° , β = 67,5°	36.2500	31.3900	29.7800	30.4700	30.3600	30.3800
	α = 67,5° , β = 45°	23.4800	18.6500	16.0400	15.9600	15.1300	14.7300
	α = 67,5° , β = 22,5°	16.2500	11.8500	9.0480	8.6630	7.5990	7.0670
Mode II / III	α = 90° , β = 90°	38.0200	37.4500	39.9900	42.1300	44.0800	45.2200
	α = 90° , β = 67,5°	39.5000	34.0300	32.0900	32.7900	32.5800	32.5700
	α = 90° , β = 45°	27.6300	21.7900	18.5700	18.4300	17.3700	16.8700
	α = 90° , β = 22,5°	19.5800	14.1900	10.7400	10.2400	8.9230	8.2610

7	8	9	10	11	12	13	14	15	16	17
0.0003	0.0003	0.0002	0.0002	0.0002	0.0004	0.0004	0.0012	0.0013	0.0042	0.0083
0.3286	0.1712	0.0003	-0.1707	-0.3279	-0.5433	-0.7135	-1.0450	-1.2060	-2.0040	-3.1280
0.7384	0.3846	0.0002	-0.3845	-0.7380	-1.2230	-1.6050	-2.3520	-2.7140	-4.5110	-7.0460
1.2300	0.6409	0.0001	-0.6410	-1.2300	-2.0380	-2.6760	-3.9210	-4.5240	-7.5230	-11.7500
1.5100	0.7862	-0.0001	-0.7869	-1.5100	-2.5010	-3.2840	-4.8130	-5.5530	-9.2350	-14.4300
46.2700	46.6700	47.0700	46.6700	46.2700	45.0900	43.9300	41.9400	39.7700	37.1100	37.5200
20.4900	20.6600	20.8400	20.6600	20.4900	19.9600	19.4300	18.5700	17.6100	16.4300	16.6000
7.4220	7.4860	7.5500	7.4850	7.4210	7.2320	7.0460	6.7260	6.3780	5.9530	6.0200
2.8700	2.8950	2.9190	2.8940	2.8690	2.7960	2.7240	2.6000	2.4660	2.3040	2.3320
46.2900	46.6700	47.0000	46.6500	46.2400	45.0500	43.8800	41.8600	39.6800	36.9600	37.2900
22.3600	22.3200	22.2500	21.8100	21.3900	20.5200	19.7200	18.2900	17.0300	14.6000	13.1400
8.4250	8.3120	8.1840	7.9160	7.6650	7.2100	6.8110	6.0800	5.5170	4.1290	2.8950
3.4610	3.3250	3.1750	2.9710	2.7810	2.4780	2.2230	1.7450	1.4330	0.4274	-0.7097
46.3100	46.6900	47.0700	46.6500	46.2300	45.0300	43.8500	41.8200	39.6300	36.8800	37.1700
26.1600	25.9200	25.6400	24.9300	24.2500	22.9800	21.8600	19.8100	18.1600	14.3900	11.3300
10.8000	10.4800	10.1300	9.6010	9.1120	8.3050	7.6180	6.3360	5.4570	2.8320	0.0247
4.6650	4.3330	3.9690	3.5370	3.1380	2.5370	2.0440	1.1030	0.5465	-1.5360	-4.1230
46.3300	46.7100	47.0800	46.6600	46.2400	45.0300	43.8500	41.8100	39.6200	36.8600	37.1200
30.2400	29.8400	29.3900	28.4400	27.5500	25.9300	24.5100	21.9100	19.8900	14.9600	10.6000
14.1600	13.6100	13.0000	12.1800	11.4100	10.1800	9.1480	7.2060	5.9340	1.8510	-2.7580
6.3640	5.8000	5.1830	4.4770	3.8260	2.8620	2.0760	0.5718	-0.2890	-3.6750	-7.9920
46.3700	46.7400	47.1200	46.6900	46.2700	45.0700	43.8800	41.8400	39.6500	36.8900	37.1600
32.3600	31.8900	31.3700	30.3100	29.3200	27.5400	25.9800	23.1200	20.9300	15.4600	10.5300
16.1500	15.4800	14.7400	13.7400	12.8200	11.3600	10.1400	7.8300	6.3370	1.4530	-4.1320
7.3890	6.6940	5.9340	5.0730	4.2780	3.1080	2.1560	0.3295	-0.7059	-4.8340	-10.1300

I Table of YI Values

	YI-Stress- & Mesh Thickness	1	2	3	4	5	6
Mode I / II	α = 0° , β = 0°	0.9848	1.0672	1.1141	1.1048	1.1156	1.1126
	α = 22,5° , β = 0°	0.9779	1.0599	1.1063	1.0975	1.1082	1.1053
	α = 45° , β = 0°	0.9140	0.9906	1.0341	1.0258	1.0360	1.0331
	α = 67,5° , β = 0°	0.6398	0.6939	0.7242	0.7183	0.7256	0.7232
	α = 90° , β = 0°	0.0326	0.0352	0.0366	0.0362	0.0365	0.0363
Mode I / III	α = 0° , β = 90°	0.0776	0.0838	0.0872	0.0861	0.0866	0.0860
	α = 0° , β = 67,5°	1.5279	1.6558	1.7285	1.7148	1.7314	1.7265
	α = 0° , β = 45°	1.2307	1.3337	1.3922	1.3810	1.3942	1.3903
	α = 0° , β = 22,5°	1.0389	1.1258	1.1751	1.1658	1.1770	1.1736
Mode I / II / III	α = 22,5° , β = 90°	0.0669	0.0723	0.0751	0.0742	0.0746	0.0741
	α = 22,5° , β = 67,5°	1.4498	1.5728	1.6436	1.6314	1.6484	1.6445
	α = 22,5° , β = 45°	1.2166	1.3186	1.3766	1.3654	1.3786	1.3747
	α = 22,5° , β = 22,5°	1.0311	1.1180	1.1668	1.1575	1.1687	1.1653
	α = 45° , β = 90°	0.0466	0.0503	0.0523	0.0516	0.0519	0.0515
	α = 45° , β = 67,5°	1.1970	1.2990	1.3581	1.3483	1.3625	1.3595
	α = 45° , β = 45°	1.1209	1.2146	1.2678	1.2576	1.2698	1.2663
	α = 45° , β = 22,5°	0.9623	1.0433	1.0892	1.0804	1.0912	1.0877
	α = 67,5° , β = 90°	0.0248	0.0265	0.0273	0.0268	0.0267	0.0263
	α = 67,5° , β = 67,5°	0.7383	0.8003	0.8350	0.8281	0.8359	0.8335
	α = 67,5° , β = 45°	0.7676	0.8320	0.8686	0.8613	0.8696	0.8672
	α = 67,5° , β = 22,5°	0.6725	0.7291	0.7608	0.7549	0.7622	0.7603
Mode II / III	α = 90° , β = 90°	0.0049	0.0046	0.0042	0.0037	0.0032	0.0026
	α = 90° , β = 67,5°	0.0389	0.0417	0.0430	0.0422	0.0422	0.0416
	α = 90° , β = 45°	0.0426	0.0459	0.0476	0.0470	0.0471	0.0468
	α = 90° , β = 22,5°	0.0354	0.0382	0.0397	0.0392	0.0394	0.0392

7	8	9	10	11	12	13	14	15	16	17
1.1170	1.1141	1.1170	1.1141	1.1170	1.1126	1.1156	1.1048	1.1141	1.0672	0.9843
1.1092	1.1068	1.1097	1.1068	1.1092	1.1053	1.1082	1.0975	1.1063	1.0599	0.9779
1.0370	1.0345	1.0370	1.0345	1.0370	1.0331	1.0360	1.0258	1.0341	0.9906	0.9140
0.7261	0.7247	0.7261	0.7247	0.7261	0.7232	0.7256	0.7183	0.7242	0.6939	0.6402
0.0364	0.0363	0.0364	0.0363	0.0364	0.0363	0.0365	0.0362	0.0366	0.0352	0.0326
0.0860	0.0855	0.0854	0.0848	0.0848	0.0841	0.0839	0.0827	0.0831	0.0792	0.0727
1.7329	1.7290	1.7329	1.7285	1.7324	1.7255	1.7299	1.7133	1.7270	1.6538	1.5255
1.3957	1.3922	1.3957	1.3922	1.3957	1.3903	1.3942	1.3805	1.3918	1.3332	1.2302
1.1780	1.1756	1.1785	1.1756	1.1780	1.1736	1.1770	1.1638	1.1751	1.1258	1.0384
0.0741	0.0737	0.0735	0.0731	0.0730	0.0725	0.0723	0.0713	0.0715	0.0682	0.0626
1.6519	1.6489	1.6543	1.6509	1.6533	1.6499	1.6553	1.6401	1.6543	1.5850	1.4630
1.3800	1.3766	1.3800	1.3766	1.3796	1.3747	1.3786	1.3649	1.3761	1.3181	1.2161
1.1702	1.1673	1.1702	1.1673	1.1702	1.1658	1.1692	1.1575	1.1673	1.1185	1.0316
0.0515	0.0512	0.0511	0.0507	0.0507	0.0503	0.0502	0.0494	0.0496	0.0472	0.0434
1.3659	1.3639	1.3683	1.3659	1.3703	1.3659	1.3708	1.3581	1.3703	1.3132	1.2122
1.2712	1.2683	1.2712	1.2678	1.2707	1.2659	1.2698	1.2571	1.2673	1.2141	1.1199
1.0921	1.0897	1.0926	1.0897	1.0926	1.0882	1.0916	1.0809	1.0897	1.0438	0.9633
0.0261	0.0259	0.0256	0.0252	0.0250	0.0247	0.0244	0.0238	0.0237	0.0223	0.0203
0.8364	0.8345	0.8359	0.8340	0.8354	0.8320	0.8340	0.8257	0.8320	0.7969	0.7349
0.8706	0.8681	0.8706	0.8681	0.8701	0.8667	0.8691	0.8608	0.8677	0.8311	0.7666
0.7632	0.7613	0.7632	0.7613	0.7632	0.7603	0.7627	0.7554	0.7613	0.7295	0.6729
0.0021	0.0017	0.0011	0.0006	0.0002	-0.0003	-0.0009	-0.0014	-0.0019	-0.0024	-0.0028
0.0414	0.0410	0.0407	0.0403	0.0401	0.0397	0.0395	0.0388	0.0389	0.0370	0.0338
0.0467	0.0465	0.0464	0.0461	0.0461	0.0459	0.0459	0.0454	0.0457	0.0437	0.0403
0.0392	0.0391	0.0391	0.0389	0.0390	0.0388	0.0389	0.0386	0.0390	0.0373	0.0345

J Table of YII Values

	YII-Stress- & Mesh Thickness	1	2	3	4	5	6
Mode I / II	α = 0° , β = 0°	-0.0009	-0.0009	-0.0009	-0.0009	-0.0010	-0.0010
	α = 22,5° , β = 0°	0.3325	0.3031	0.2933	0.3000	0.2983	0.3006
	α = 45° , β = 0°	0.7491	0.6827	0.6607	0.6759	0.6720	0.6773
	α = 67,5° , β = 0°	1.2493	1.1390	1.1019	1.1273	1.1209	1.1297
	α = 90° , β = 0°	1.5338	1.3986	1.3532	1.3839	1.3761	1.3869
Mode I / III	α = 0° , β = 90°	2.5429	1.5313	0.8467	0.7525	0.4938	0.3785
	α = 0° , β = 67,5°	1.1224	0.6744	0.3719	0.3304	0.2161	0.1653
	α = 0° , β = 45°	0.4063	0.2441	0.1344	0.1194	0.0779	0.0595
	α = 0° , β = 22,5°	0.1576	0.0948	0.0523	0.0464	0.0303	0.0231
Mode I / II / III	α = 22,5° , β = 90°	2.5664	1.5523	0.8677	0.7740	0.5148	0.4000
	α = 22,5° , β = 67,5°	1.6914	1.1697	0.8315	0.7969	0.6725	0.6212
	α = 22,5° , β = 45°	0.8267	0.6168	0.4864	0.4778	0.4310	0.4137
	α = 22,5° , β = 22,5°	0.5168	0.4178	0.3614	0.3619	0.3427	0.3373
	α = 45° , β = 90°	2.5825	1.5669	0.8813	0.7876	0.5285	0.4136
	α = 45° , β = 67,5°	2.3521	1.7158	1.3142	1.2824	1.1370	1.0809
	α = 45° , β = 45°	1.4015	1.1087	0.9360	0.9330	0.8730	0.8545
	α = 45° , β = 22,5°	0.9892	0.8354	0.7549	0.7627	0.7369	0.7325
	α = 67,5° , β = 90°	2.5912	1.5748	0.8881	0.7949	0.5353	0.4204
	α = 67,5° , β = 67,5°	2.9524	2.1999	1.7324	1.7007	1.5328	1.4698
	α = 67,5° , β = 45°	2.0974	1.6948	1.4645	1.4664	1.3883	1.3659
	α = 67,5° , β = 22,5°	1.5689	1.3439	1.2302	1.2458	1.2112	1.2073
Mode II / III	α = 90° , β = 90°	2.5971	1.5791	0.8921	0.7984	0.5383	0.4228
	α = 90° , β = 67,5°	3.2383	2.4273	1.9256	1.8934	1.7133	1.6470
	α = 90° , β = 45°	2.4858	2.0198	1.7558	1.7397	1.6704	1.6460
	α = 90° , β = 22,5°	1.9007	1.6338	1.5006	1.5206	1.4801	1.4767

7	8	9	10	11	12	13	14	15	16	17
-0.0010	-0.0010	-0.0010	-0.0010	-0.0010	-0.0010	-0.0010	-0.0010	-0.0010	-0.0010	-0.0011
0.3002	0.3011	0.3006	0.3011	0.3001	0.3006	0.2983	0.2999	0.2982	0.3030	0.3324
0.6764	0.6783	0.6773	0.6783	0.6764	0.6773	0.6720	0.6759	0.6607	0.6827	0.7491
1.1278	1.1317	1.1297	1.1317	1.1278	1.1297	1.1209	1.1273	1.1019	1.1390	1.2493
1.3849	1.3893	1.3869	1.3893	1.3849	1.3869	1.3761	1.3839	1.3532	1.3986	1.5338
0.2287	0.1173	0.0000	-0.1174	-0.2287	-0.3786	-0.4938	-0.7525	-0.8467	-1.5313	-2.5429
0.0993	0.0503	-0.0014	-0.0531	-0.1021	-0.1682	-0.2189	-0.3332	-0.3746	-0.6773	-1.1248
0.0356	0.0178	-0.0010	-0.0197	-0.0375	-0.0614	-0.0798	-0.1213	-0.1362	-0.2459	-0.4082
0.0138	0.0068	-0.0005	-0.0078	-0.0147	-0.0241	-0.0313	-0.0473	-0.0532	-0.0957	-0.1585
0.2501	0.1388	0.0215	-0.0958	-0.2071	-0.3570	-0.4722	-0.7310	-0.8257	-1.5094	-2.5185
0.5495	0.4987	0.4422	0.3876	0.3335	0.2633	0.2055	0.0855	0.0312	-0.2780	-0.7130
0.3872	0.3691	0.3481	0.3284	0.3080	0.2825	0.2599	0.2169	0.1929	0.0853	-0.0565
0.3267	0.3201	0.3116	0.3042	0.2956	0.2860	0.2758	0.2600	0.2467	0.2107	0.1728
0.2636	0.1523	0.0348	-0.0826	-0.1941	-0.3440	-0.4595	-0.7183	-0.8130	-1.4967	-2.5049
0.9979	0.9404	0.8750	0.8125	0.7491	0.6685	0.5993	0.4633	0.3926	0.0485	-0.4173
0.8208	0.7998	0.7730	0.7491	0.7227	0.6920	0.6612	0.6100	0.5724	0.4506	0.3084
0.7188	0.7115	0.7003	0.6920	0.6803	0.6685	0.6534	0.6354	0.6119	0.5773	0.5602
0.2702	0.1587	0.0411	-0.0765	-0.1882	-0.3383	-0.4540	-0.7130	-0.8081	-1.4918	-2.5005
1.3747	1.3093	1.2336	1.1624	1.0892	0.9975	0.9160	0.7613	0.6749	0.2879	-0.2236
1.3225	1.2961	1.2615	1.2312	1.1966	1.1570	1.1156	1.0511	0.9970	0.8491	0.6925
1.1887	1.1805	1.1653	1.1546	1.1385	1.1238	1.1024	1.0799	1.0438	1.0067	1.0087
0.2722	0.1603	0.0422	-0.0758	-0.1879	-0.3384	-0.4546	-0.7139	-0.8096	-1.4942	-2.5034
1.5445	1.4747	1.3937	1.3176	1.2390	1.1409	1.0531	0.8881	0.7940	0.3833	-0.1556
1.5967	1.5669	1.5274	1.4933	1.4532	1.4083	1.3610	1.2878	1.2244	1.0599	0.8921
1.4557	1.4439	1.4288	1.4166	1.3976	1.3810	1.3556	1.3308	1.2873	1.2473	1.2590

K Table of YIII Values

	YIIIStress- 8 Mesh Thickness	1	2	3	4	5	6
Mode I / II	α = 0° , β = 0°	-0.0004	-0.0002	0.0000	0.0000	0.0000	0.0000
	α = 22,5° , β = 0°	0.1526	0.0978	0.0589	0.0510	0.0349	0.0265
	α = 45° , β = 0°	0.3437	0.2202	0.1325	0.1148	0.0784	0.0597
	α = 67,5° , β = 0°	0.5734	0.3671	0.2208	0.1913	0.1306	0.0995
	α = 90° , β = 0°	0.7037	0.4506	0.2710	0.2348	0.1603	0.1220
Mode I / III	α = 0° , β = 90°	1.8300	1.8109	1.9407	2.0466	2.1438	2.2004
	α = 0° , β = 67,5°	0.8086	0.8013	0.8589	0.9057	0.9491	0.9740
	α = 0° , β = 45°	0.2929	0.2902	0.3112	0.3282	0.3439	0.3530
	α = 0° , β = 22,5°	0.1135	0.1124	0.1204	0.1270	0.1330	0.1365
Mode I / II / III	α = 22,5° , β = 90°	1.8407	1.8178	1.9447	2.0496	2.1462	2.2018
	α = 22,5° , β = 67,5°	1.0897	1.0004	1.0043	1.0428	1.0648	1.0794
	α = 22,5° , β = 45°	0.4948	0.4280	0.4056	0.4148	0.4131	0.4133
	α = 22,5° , β = 22,5°	0.2818	0.2236	0.1920	0.1910	0.1808	0.1759
	α = 45° , β = 90°	1.8480	1.8227	1.9476	2.0525	2.1481	2.2033
	α = 45° , β = 67,5°	1.4406	1.2707	1.2283	1.2629	1.2693	1.2756
	α = 45° , β = 45°	0.7857	0.6407	0.5685	0.5714	0.5505	0.5417
	α = 45° , β = 22,5°	0.5100	0.3805	0.3007	0.2913	0.2619	0.2473
	α = 67,5° , β = 90°	1.8524	1.8256	1.9495	2.0540	2.1496	2.2048
	α = 67,5° , β = 67,5°	1.7690	1.5318	1.4532	1.4869	1.4815	1.4825
	α = 67,5° , β = 45°	1.1458	0.9101	0.7827	0.7788	0.7383	0.7188
	α = 67,5° , β = 22,5°	0.7930	0.5783	0.4415	0.4227	0.3708	0.3449
Mode II / III	α = 90° , β = 90°	1.8553	1.8275	1.9515	2.0559	2.1511	2.2067
	α = 90° , β = 67,5°	1.9276	1.6606	1.5660	1.6001	1.5899	1.5894
	α = 90° , β = 45°	1.3483	1.0633	0.9062	0.8994	0.8476	0.8232
	α = 90° , β = 22,5°	0.9555	0.6925	0.5241	0.4997	0.4354	0.4031

7	8	9	10	11	12	13	14	15	16	17
0.0000	0.0000	0.0000	0.0000	0.0000	0.0000	0.0000	0.0001	0.0001	0.0002	0.0004
0.0160	0.0084	0.0000	-0.0083	-0.0160	-0.0265	-0.0348	-0.0510	-0.0389	-0.0978	-0.1526
0.0360	0.0188	0.0000	-0.0188	-0.0360	-0.0597	-0.0783	-0.1148	-0.1324	-0.2201	-0.3438
0.0600	0.0313	0.0000	-0.0313	-0.0600	-0.0995	-0.1306	-0.1913	-0.2208	-0.3671	-0.5734
0.0737	0.0384	0.0000	-0.0384	-0.0737	-0.1220	-0.1603	-0.2349	-0.2710	-0.4507	-0.7042
2.2579	2.2775	2.2970	2.2775	2.2579	2.2004	2.1438	2.0466	1.9407	1.8109	1.8309
0.9999	1.0082	1.0170	1.0082	0.9999	0.9740	0.9491	0.9062	0.8594	0.8018	0.8101
0.3622	0.3653	0.3684	0.3653	0.3621	0.3529	0.3438	0.3282	0.3112	0.2905	0.2938
0.1401	0.1413	0.1424	0.1412	0.1400	0.1364	0.1329	0.1269	0.1203	0.1124	0.1138
2.2589	2.2775	2.2936	2.2765	2.2565	2.1984	2.1413	2.0427	1.9364	1.8036	1.8197
1.0912	1.0892	1.0858	1.0643	1.0438	1.0014	0.9623	0.8925	0.8311	0.7125	0.6412
0.4111	0.4056	0.3994	0.3863	0.3740	0.3518	0.3324	0.2967	0.2692	0.2015	0.1413
0.1689	0.1623	0.1549	0.1450	0.1357	0.1209	0.1085	0.0852	0.0699	0.0209	-0.0346
2.2599	2.2784	2.2970	2.2765	2.2560	2.1974	2.1398	2.0408	1.9339	1.7997	1.8139
1.2766	1.2649	1.2512	1.2166	1.1834	1.1214	1.0668	0.9667	0.8862	0.7022	0.5529
0.5270	0.5114	0.4943	0.4685	0.4447	0.4053	0.3718	0.3092	0.2663	0.1382	0.0012
0.2276	0.2114	0.1937	0.1726	0.1531	0.1238	0.0997	0.0538	0.0267	-0.0750	-0.2012
2.2609	2.2794	2.2975	2.2770	2.2565	2.1974	2.1398	2.0403	1.9334	1.7987	1.8114
1.4757	1.4562	1.4342	1.3879	1.3444	1.2654	1.1961	1.0692	0.9706	0.7300	0.5173
0.6910	0.6642	0.6344	0.5944	0.5568	0.4968	0.4464	0.3516	0.2896	0.0903	-0.1346
0.3106	0.2830	0.2529	0.2185	0.1867	0.1397	0.1013	0.0279	-0.0141	-0.1793	-0.3900
2.2628	2.2809	2.2994	2.2784	2.2579	2.1994	2.1413	2.0418	1.9349	1.8002	1.8134
1.5791	1.5562	1.5308	1.4791	1.4308	1.3439	1.2678	1.1282	1.0214	0.7544	0.5139
0.7881	0.7534	0.7193	0.6705	0.6256	0.5344	0.4948	0.3821	0.3092	0.0709	-0.2016
0.3606	0.3267	0.2896	0.2476	0.2088	0.1517	0.1052	0.0161	-0.0344	-0.2359	-0.4943

L Table of T-Stress

	T-Stress- 8 Mesh Thickness	1	2	3	4	5	6
Mode I / II	α = 0° , β = 0°	-2.1630	-2.2090	-2.9570	-2.4070	-2.6740	-2.4660
	α = 22,5° , β = 0°	-2.1240	-2.2590	-2.9130	-2.3670	-2.6320	-2.4250
	α = 45° , β = 0°	-1.9720	-2.0990	-2.7100	-2.2000	-2.4470	-2.2540
	α = 67,5° , β = 0°	-1.3680	-1.4570	-1.8850	-1.5290	-1.7020	-1.5670
	α = 90° , β = 0°	-0.0610	-0.0664	-0.0892	-0.0716	-0.0809	-0.0741
Mode I / III	α = 0° , β = 90°	-0.1413	-0.1511	-0.2012	-0.1609	-0.1839	-0.1707
	α = 0° , β = 67,5°	-3.2930	-3.5040	-4.5240	-3.6720	-4.0860	-3.7640
	α = 0° , β = 45°	-2.6900	-2.8600	-3.6820	-2.9950	-3.3290	-3.0700
	α = 0° , β = 22,5°	-2.2680	-2.4110	-3.1050	-2.5250	-2.8070	-2.5870
Mode I / II / III	α = 22,5° , β = 90°	-0.1197	-0.1278	-0.1719	-0.1368	-0.1572	-0.1457
	α = 22,5° , β = 67,5°	-3.0670	-3.2750	-4.2510	-3.4440	-3.8430	-3.5390
	α = 22,5° , β = 45°	-2.6500	-2.8180	-3.6320	-2.9530	-3.2830	-3.0260
	α = 22,5° , β = 22,5°	-2.2420	-2.3850	-3.0750	-2.4990	-2.7790	-2.5610
	α = 45° , β = 90°	-0.0726	-0.0801	-0.1110	-0.0882	-0.1033	-0.0966
	α = 45° , β = 67,5°	-2.5010	-2.6760	-3.4840	-2.8190	-3.1500	-2.9010
	α = 45° , β = 45°	-2.4230	-2.5780	-3.3280	-2.7030	-3.0070	-2.7710
	α = 45° , β = 22,5°	-2.0760	-2.2100	-2.8550	-2.3180	-2.5790	-2.3760
	α = 67,5° , β = 90°	-0.0249	-0.0300	-0.0434	-0.0354	-0.0442	-0.0423
	α = 67,5° , β = 67,5°	-1.5510	-1.6540	-2.1470	-1.7370	-1.9380	-1.7830
	α = 67,5° , β = 45°	-1.6410	-1.7490	-2.2620	-1.8350	-2.0440	-1.8820
	α = 67,5° , β = 22,5°	-1.4350	-1.5290	-1.9800	-1.6050	-1.7880	-1.6470
Mode II / III	α = 90° , β = 90°	0.0125	0.0132	0.0121	0.0121	0.0095	0.0079
	α = 90° , β = 67,5°	-0.0592	-0.0646	-0.0990	-0.0707	-0.0825	-0.0761
	α = 90° , β = 45°	-0.0752	-0.0816	-0.1105	-0.0882	-0.1006	-0.0926
	α = 90° , β = 22,5°	-0.0638	-0.0695	-0.0939	-0.0751	-0.0853	-0.0783

7	8	9	10	11	12	13	14	15	16	17
-2.6120	-2.4870	-2.5970	-2.4870	-2.6120	-2.4660	-2.6740	-2.4070	-2.9560	-2.2990	-2.1620
-2.5700	-2.4460	-2.5550	-2.4460	-2.5700	-2.4250	-2.6320	-2.3670	-2.9120	-2.2660	-2.1230
-2.3890	-2.2740	-2.3760	-2.2740	-2.3890	-2.2540	-2.4470	-2.2000	-2.7090	-2.0990	-1.9710
-1.6610	-1.5810	-1.6520	-1.5810	-1.6610	-1.5670	-1.7020	-1.5290	-1.8850	-1.4580	-1.3670
-0.0791	-0.0751	-0.0787	-0.0751	-0.0791	-0.0741	-0.0808	-0.0716	-0.0891	-0.0664	-0.0609
-0.1860	-0.1815	-0.1934	-0.1886	-0.2031	-0.1963	-0.2148	-0.1972	-0.2408	-0.1906	-0.1797
-3.9910	-3.8010	-3.9730	-3.8040	-3.9990	-3.7760	-4.1000	-3.6880	-4.5400	-3.5220	-3.3090
-3.2520	-3.0970	-3.2330	-3.0980	-3.2550	-3.0740	-3.3340	-3.0020	-3.6880	-2.8670	-2.6960
-2.7410	-2.6100	-2.7260	-2.6100	-2.7420	-2.5890	-2.8090	-2.5280	-3.1070	-2.4140	-2.2690
-0.1595	-0.1560	-0.1665	-0.1625	-0.1754	-0.1700	-0.1860	-0.1713	-0.2086	-0.1662	-0.1564
-3.7590	-3.5800	-3.7480	-3.5890	-3.7800	-3.5690	-3.8830	-3.4920	-4.3120	-3.3430	-3.1480
-3.2070	-3.0540	-3.1910	-3.0550	-3.2100	-3.0310	-3.2880	-2.9590	-3.6380	-2.8260	-2.6560
-2.7140	-2.5840	-2.7000	-2.5850	-2.7160	-2.5630	-2.7820	-2.5030	-3.0780	-2.3900	-2.2460
-0.1074	-0.1066	-0.1150	-0.1133	-0.1239	-0.1214	-0.1337	-0.1245	-0.1519	-0.1228	-0.1177
-3.0840	-2.9380	-3.0780	-2.9480	-3.1070	-2.9340	-3.1960	-2.8740	-3.5540	-2.7540	-2.5950
-2.9370	-2.7970	-2.9230	-2.7980	-2.9410	-2.7760	-3.0140	-2.7110	-3.3350	-2.5870	-2.4310
-2.5190	-2.3980	-2.5060	-2.3990	-2.5220	-2.3790	-2.5840	-2.3230	-2.8600	-2.2180	-2.0840
-0.0496	-0.0515	-0.0572	-0.0579	-0.0654	-0.0661	-0.0737	-0.0703	-0.0854	-0.0708	-0.0695
-1.8940	-1.8040	-1.8880	-1.8080	-1.9040	-1.7970	-1.9540	-1.7560	-2.1670	-1.6760	-1.5730
-1.9970	-1.9010	-1.9880	-1.9030	-2.0010	-1.8890	-2.0510	-1.8440	-2.2720	-1.7390	-1.6520
-1.7470	-1.6630	-1.7380	-1.6640	-1.7490	-1.6510	-1.7930	-1.6120	-1.9870	-1.5380	-1.4440
0.0042	0.0003	-0.0025	-0.0050	-0.0092	-0.0126	-0.0146	-0.0166	-0.0177	-0.0174	-0.0163
-0.0840	-0.0822	-0.0880	-0.0857	-0.0929	-0.0897	-0.0984	-0.0896	-0.1097	-0.0846	-0.0780
-0.1000	-0.0962	-0.1016	-0.0978	-0.1042	-0.0990	-0.1081	-0.0971	-0.1197	-0.0910	-0.0839
-0.0842	-0.0804	-0.0846	-0.0811	-0.0860	-0.0811	-0.0885	-0.0789	-0.0979	-0.0736	-0.0676

M Table of Dimensionless T Values

	T* - 8 mesh thickness	1	2	3	4	5	6
Mode I / II	α = 0° , β = 0°	-0,811125	-0,862125	-1,108875	-0,902625	-1,00275	-0,92475
	α = 22,5° , β = 0°	-0,7965	-0,847125	-1,092375	-0,887625	-0,987	-0,909375
	α = 45° , β = 0°	-0,7395	-0,787125	-1,01625	-0,825	-0,917625	-0,84525
	α = 67,5° , β = 0°	-0,513	-0,546375	-0,706875	-0,573375	-0,63825	-0,587625
	α = 90° , β = 0°	-0,0228684625	-0,02489475	-0,03345	-0,02684175	-0,030321	-0,02778188
Mode I / III	α = 0° , β = 90°	-0,0529875	-0,0566625	-0,07545	-0,0603375	-0,0689625	-0,0640125
	α = 0° , β = 67,5°	-1,234875	-1,314	-1,6965	-1,377	-1,53225	-1,4115
	α = 0° , β = 45°	-1,00875	-1,0725	-1,38075	-1,123125	-1,248375	-1,15125
	α = 0° , β = 22,5°	-0,8505	-0,904125	-1,164375	-0,946875	-1,052625	-0,970125
Mode I / II / III	α = 22,5° , β = 90°	-0,0448875	-0,047925	-0,0644625	-0,0513	-0,05895	-0,0546375
	α = 22,5° , β = 67,5°	-1,150125	-1,228125	-1,594125	-1,2915	-1,441125	-1,327125
	α = 22,5° , β = 45°	-0,9937,5	-1,05675	-1,362	-1,107375	-1,231125	-1,13475
	α = 22,5° , β = 22,5°	-0,84075	-0,894375	-1,153125	-0,937125	-1,042125	-0,960375
	α = 45° , β = 90°	-0,0270221625	-0,030031875	-0,041625	-0,033308025	-0,0387375	-0,036223313
	α = 45° , β = 67,5°	-0,937875	-1,0035	-1,3065	-1,057125	-1,18125	-1,087875
	α = 45° , β = 45°	-0,908625	-0,96675	-1,248	-1,013625	-1,127625	-1,039125
	α = 45° , β = 22,5°	-0,7785	-0,83287,5	-1,070625	-0,86925	-0,967125	-0,891
	α = 67,5° , β = 90°	-0,0093146875	-0,011235375	-0,01703625	-0,013273875	-0,01657125	-0,015286363
	α = 67,5° , β = 67,5°	-0,581625	-0,62025	-0,805125	-0,651375	-0,72675	-0,668625
	α = 67,5° , β = 45°	-0,615375	-0,65587,5	-0,84825	-0,688125	-0,7665	-0,70575
	α = 67,5° , β = 22,5°	-0,538125	-0,573375	-0,7425	-0,601875	-0,6705	-0,617625
Mode II / III	α = 90° , β = 90°	0,0046728875	0,00493387,5	0,004534125	0,004542	0,0035534025	0,00297971
	α = 90° , β = 67,,5°	-0,022194	-0,02421,75	-0,03376125	-0,02650612,5	-0,030928125	-0,028533038
	α = 90° , β = 45°	-0,028185	-0,030614625	-0,041437,5	-0,033076125	-0,037725	-0,03170888
	α = 90° , β = 22,5°	-0,0239163,75	-0,02604825	-0,03,522	-0,028162125	-0,03199875	-0,02936963

7	8	9	10	11	12	13	14	15	16	17
-0.9795	-0.932625	-0.973875	-0.932625	-0.9795	-0.92475	-1.00275	-0.902625	-1.1085	-0.862125	-0.81075
-0.96375	-0.91725	-0.958125	-0.91725	-0.96375	-0.90975	-0.987	-0.887625	-1.092	-0.8475	-0.796125
-0.893875	-0.85275	-0.891	-0.85275	-0.893875	-0.84525	-0.917625	-0.825	-1.013875	-0.787125	-0.739125
-0.622875	-0.592875	-0.6195	-0.592875	-0.622875	-0.587625	-0.63825	-0.573375	-0.706875	-0.5467.5	-0.512625
-0.029679375	-0.0281475	-0.029515.5	-0.028146	-0.029678625	-0.027776625	-0.030314625	-0.026834625	-0.033426	-0.024883.5	-0.022839375
-0.06075	-0.06806.25	-0.072525	-0.070725	-0.076162.5	-0.073612.5	-0.080.55	-0.07395	-0.0903	-0.071475	-0.067387.5
-1.496625	-1.425375	-1.489875	-1.4265	-1.499625	-1.416	-1.5375	-1.383	-1.7025	-1.32075	-1.240875
-1.2195	-1.161375	-1.213125	-1.16175	-1.220625	-1.15275	-1.25025	-1.12575	-1.383	-1.075125	-1.011
-1.027875	-0.97875	-1.02225	-0.97875	-1.02825	-0.970875	-1.053375	-0.948	-1.165125	-0.90525	-0.850875
-0.598125	-0.0585	-0.0624375	-0.0600375	-0.065775	-0.06375	-0.06975	-0.0642375	-0.078225	-0.062325	-0.05865
-1.409625	-1.3425	-1.4055	-1.345875	-1.4175	-1.338375	-1.456125	-1.3095	-1.617	-1.253625	-1.1805
-1.202625	-1.14525	-1.196625	-1.145625	-1.20375	-1.136625	-1.233	-1.109625	-1.36425	-1.0575	-0.996
-1.01775	-0.969	-1.0125	-0.960375	-1.0185	-0.961125	-1.04325	-0.938625	-1.15425	-0.89625	-0.84225
-0.040275	-0.039975	-0.043125	-0.0424875	-0.0461625	-0.045525	-0.050137.5	-0.0466875	-0.059625	-0.04605	-0.0441375
-1.1565	-1.10175	-1.15425	-1.1055	-1.165125	-1.10025	-1.1985	-1.07775	-1.33275	-1.03275	-0.973125
-1.101375	-1.048875	-1.096125	-1.04925	-1.102875	-1.041	-1.13025	-1.016625	-1.250625	-0.970125	-0.911625
-0.944625	-0.89925	-0.93975	-0.899625	-0.94575	-0.892125	-0.969	-0.871125	-1.0725	-0.83175	-0.7815
-0.018.39138	-0.01931175	-0.02143875	-0.02169525	-0.02453813	-0.02478488	-0.02763488	-0.026373	-0.03201563	-0.02654175	-0.02605763
-0.71025	-0.6765	-0.708	-0.678	-0.714	-0.673875	-0.73275	-0.6585	-0.812625	-0.6285	-0.589875
-0.748875	-0.712875	-0.7455	-0.713625	-0.750375	-0.708375	-0.769125	-0.6915	-0.852	-0.639625	-0.6195
-0.655125	-0.628625	-0.65175	-0.624	-0.655875	-0.619125	-0.672375	-0.6045	-0.745125	-0.5675	-0.5415
0.000158711	0.00010843	-0.000093026	-0.00188494	-0.00343818	-0.00473363	-0.00546525	-0.006223738	-0.00664125	-0.0065085	-0.00612075
-0.031.50938	-0.030831	-0.03299.55	-0.03213338	-0.03484.65	-0.03363188	-0.03688388	-0.0336165	-0.041137.5	-0.0317295	-0.02926838
-0.0375	-0.0360585	-0.0381	-0.03666863	-0.039075	-0.037111.3	-0.040537.5	-0.036424.13	-0.044887.5	-0.034347.5	-0.031475.63
-0.031.57275	-0.03013763	-0.03173363	-0.03040463	-0.03224925	-0.0303945	-0.03320.55	-0.029.5995	-0.03671138	-0.02758163	-0.02536275

N Python Script For Mixed Mode I/II Crack Angle Plots

```
import matplotlib.pyplot as plt
import numpy as np
import math
from numpy import genfromtxt
import matplotlib
from matplotlib.backends.backend_pdf import PdfPages

matplotlib.rcParams['text.latex.preamble']=[r"\usepackage{lmodern}", r
                                    "\usepackage[utf8x]{inputenc}", r"\
                                    usepackage[T1]{fontenc}" ]

params = {'text.usetex' : True,
          'font.size' : 11,
          'font.family' : 'lmodern',
          'text.latex.unicode': True,
          }

matplotlib.rcParams.update(params)

x = np.arange(0 , -80, -0.01) # Grid of 0.01 spacing from -2 to 10
pi = math.pi
B0 = 0
#B02 = 0.2
#B04 = 0.3

#A = [0.01681432, 0.363683038, 0.631648616, 0.84103086,0.999440392]
A = [0, 0.363683038, 0.631648616, 0.84103086,0.999440392]
B = [-68.19        , -55.71        , -35.15         , -21.29        , 0
                                          ]

C = [0.01681432, 0.363683038, 0.631648616, 0.84103086,0.999440392]
D = [ -70.99379237, -59.27677991, -46.03887117, -25.84751055,-0.
                                    038512885]

cos2 = np.cos(((x*pi)/180)/2)
sin2 = np.sin(((x*pi)/180)/2)
cos = np.cos((x*pi)/180)
sin = np.sin((x*pi)/180)

a = ( (3*cos) - 1 )  /  (sin)
b =  (8/3) * B0     * (cos/cos2)
b2 = (8/3) * 0.2    * (cos/cos2)
b3 = (8/3) * 0.375  * (cos/cos2)
b4 = (8/3) * -0.2   * (cos/cos2)
b5 = (8/3) * -0.4   * (cos/cos2)
b6 = (8/3) * -0.6   * (cos/cos2)
b005 =  (8/3) * -0.05     * (cos/cos2)

sqrt_ab = np.sqrt(a**2 + b**2 +1)
sqrt_ab2 = np.sqrt(  a**2 - b**2 + 1  )
#ab3 = (a**2 - b**2) / (-a -b * sqrt_ab2)
```

```
Me005 = (2 / pi) * ( np.arctan(  (a**2 - b005**2)  / (-a-b005 * (np.
                                  sqrt(  a**2 - b005**2 + 1  ) ) )  )
                                  )
Me  = (2 / pi) * ( np.arctan(  (a**2 - b**2)  / (-a-b * (np.sqrt(  a**
                                  2 - b**2 + 1  ) ) )  ) )
Me2 = (2 / pi) * ( np.arctan(  (a**2 - b2**2) / (-a-b2 * (np.sqrt(  a
                                  **2 - b2**2 + 1  ) ) )  ) )
Me3 = (2 / pi) * ( np.arctan(  (a**2 - b3**2) / (-a-b3 * (np.sqrt(  a
                                  **2 - b3**2 + 1  ) ) )  ) )
Me4 = (2 / pi) * ( np.arctan(  (a**2 - b4**2) / (-a-b4 * (np.sqrt(  a
                                  **2 - b4**2 + 1  ) ) )  ) )
Me5 = (2 / pi) * ( np.arctan(  (a**2 - b5**2) / (-a-b5 * (np.sqrt(  a
                                  **2 - b5**2 + 1  ) ) )  ) )
Me6 = (2 / pi) * ( np.arctan(  (a**2 - b6**2) / (-a-b6 * (np.sqrt(  a
                                  **2 - b6**2 + 1  ) ) )  ) )

f = plt.figure(figsize=(8,4))

plt.plot(A, B, ls="None",label = 'Mixed Mode Test Data', marker="o",
                                  markersize=6 , markerfacecolor='
                                  white' ,markeredgewidth=0.5, c='k'
                                  ,)

plt.plot(Me,  x, linestyle='-', c='k', label=r" MTS", linewidth=0.5)


plt.plot(C,  D, linestyle='-.', c='k', label=r'GMTS', linewidth=0.6, )
                                   #GMTS


#plt.plot(Me005, x, linestyle='-', marker='o' , markersize=4.5 ,
                                  markerfacecolor='red'   ,
                                  markeredgewidth=0.5 , markevery=130
                                  , c='k', label=r'$ B \alpha =   0.2
                                   $', linewidth=0.75,)
#plt.plot(Me2, x, linestyle='-', marker='o' , markersize=4.5 ,
                                  markerfacecolor='k'   ,
                                  markeredgewidth=0.5 , markevery=130
                                  , c='k', label=r"$ B \alpha =   0.2
                                   $", linewidth=0.75,)
#plt.plot(Me3, x, linestyle='-', marker='s' , markersize=4 ,
                                  markerfacecolor='k'     ,
                                  markeredgewidth=0.5 , markevery=130
                                  , c='k', label=r'$ B \alpha =   0.
                                  375 $', linewidth=0.75,)
#plt.plot(Me4, x, linestyle='-', marker='o' , markersize=5 ,
                                  markerfacecolor='white' ,
                                  markeredgewidth=0.5 , markevery=130
                                  ,c='k', label=r'$ B \alpha = - 0.2
                                  $', linewidth=0.75,)
#plt.plot(Me5, x, linestyle='-', marker='s' , markersize=4 ,
                                  markerfacecolor='white' ,
                                  markeredgewidth=0.5 , markevery=130
                                  ,c='k', label=r'$ B \alpha = - 0.4
                                  $', linewidth=0.75,)
```

```
#plt.plot(Me6, x, linestyle='-', marker='^' , markersize=5 ,
                                    markerfacecolor='white' ,
                                    markeredgewidth=0.5 , markevery=130
                                    ,c='k', label=r'$ B \alpha = - 0.6
                                    $', linewidth=0.75,)

plt.gca().invert_yaxis()
plt.gca().set_xlim([0,1.2])
plt.gca().set_ylim([0,-80])
plt.ylabel(r"Crack Initiation Angle,  $\theta_{f}$ ")
plt.xlabel(r"Mixity Parameter, $ M^{e}_{12} $ ")
plt.legend(loc='lower left')
plt.grid(True, linestyle=':')
legend = plt.legend(frameon = 1, fancybox=False, framealpha=1)
frame = legend.get_frame()
frame.set_facecolor('white')
frame.set_edgecolor('k')
frame.set_linewidth(0.7)

plt.savefig("Theta_I_II_TESTDATA.pdf", bbox_inches='tight')

plt.show()
```

O Python Script For Mixed Mode I/II Fracture Limit Plots

```
import matplotlib.pyplot as plt
import numpy as np
import math
from numpy import genfromtxt
import matplotlib

matplotlib.rcParams['text.latex.preamble']=[r"\usepackage{lmodern}", r
                                    "\usepackage[utf8x]{inputenc}", r"\
                                    usepackage[T1]{fontenc}" ]

params = {'text.usetex' : True,
          'font.size' : 11,
          'font.family' : 'lmodern',
          'text.latex.unicode': True,
          }

matplotlib.rcParams.update(params)

x = np.arange(0 , -70.5, -0.1)
pi = math.pi
B0 = 0
#B02 = 0.2
#B04 = 0.3

cos2 = np.cos(((x*pi)/180)/2)
sin2 = np.sin(((x*pi)/180)/2)
cos = np.cos((x*pi)/180)
sin = np.sin((x*pi)/180)
tan2 = np.tan(((x*pi)/180)/2)

a = ( (3*cos) - 1 )  /  (sin)
b =  (8/3) * B0    * (cos/cos2)
b2 = (8/3) * 0.2   * (cos/cos2)
b3 = (8/3) * 0.375 * (cos/cos2)
b4 = (8/3) * -0.2  * (cos/cos2)
b5 = (8/3) * -0.4  * (cos/cos2)
b6 = (8/3) * -0.6  * (cos/cos2)
sqrt_ab  = np.sqrt(a**2 + b**2 +1)
sqrt_ab2 = np.sqrt(a**2 + b2**2 +1)
sqrt_ab3 = np.sqrt(a**2 + b3**2 +1)
sqrt_ab4 = np.sqrt(a**2 + b4**2 +1)
sqrt_ab5 = np.sqrt(a**2 + b5**2 +1)
sqrt_ab6 = np.sqrt(a**2 + b6**2 +1)
sqrt_ab22 = np.sqrt(  a**2 - b**2 + 1  )
#ab3 = (a**2 - b**2) / (-a -b * sqrt_ab2)
c = -3 * tan2

z = (-a-(b* sqrt_ab)) / ((a**2 - b**2))
e = -4 * B0 * tan2 * sin2

z2 = (-a-(b2* sqrt_ab2)) / ((a**2 - b2**2))
e2 = -4 * 0.2 * tan2 * sin2
```

```
z3 = (-a-(b3* sqrt_ab3)) / ((a**2 - b3**2))
e3 = -4 * 0.375 * tan2 * sin2

z4 = (-a-(b4* sqrt_ab4)) / ((a**2 - b4**2))
e4 = -4 * -0.2 * tan2 * sin2

z5 = (-a-(b5* sqrt_ab5)) / ((a**2 - b5**2))
e5 = -4 * -0.4 * tan2 * sin2

z6 = (-a-(b6* sqrt_ab6)) / ((a**2 - b6**2))
e6 = -4 * -0.6 * tan2 * sin2


KI  = 1 / ( cos2**3 * ( 1 + c * z - e * np.sqrt(1+z**2) ) )
KII = z / ( cos2**3 * ( 1 + c * z - e * np.sqrt(1+z**2) ) )

KI2  = 1  / ( cos2**3 * ( 1 + c * z2 - e2 * np.sqrt(1+z2**2) ) )
KII2 = z2 / ( cos2**3 * ( 1 + c * z2 - e2 * np.sqrt(1+z2**2) ) )

KI3  = 1  / ( cos2**3 * ( 1 + c * z3 - e3 * np.sqrt(1+z3**2) ) )
KII3 = z3 / ( cos2**3 * ( 1 + c * z3 - e3 * np.sqrt(1+z3**2) ) )

KI4  = 1  / ( cos2**3 * ( 1 + c * z4 - e4 * np.sqrt(1+z4**2) ) )
KII4 = z4 / ( cos2**3 * ( 1 + c * z4 - e4 * np.sqrt(1+z4**2) ) )

KI5  = 1  / ( cos2**3 * ( 1 + c * z5 - e5 * np.sqrt(1+z5**2) ) )
KII5 = z5 / ( cos2**3 * ( 1 + c * z5 - e5 * np.sqrt(1+z5**2) ) )

KI6  = 1  / ( cos2**3 * ( 1 + c * z6 - e6 * np.sqrt(1+z6**2) ) )
KII6 = z6 / ( cos2**3 * ( 1 + c * z6 - e6 * np.sqrt(1+z6**2) ) )

## J KIC
A = [ 1.111544218,  0.894316805,  0.991982611, 0, 0, 0, 0.838557639, 0
                                  .726204302, 0.824063064, 0.
                                  801800136, 0.950865039, 0.970586684
                                  , 1.076899049, 1.103757686, 1.
                                  125892908]
B = [-0.000977081, -0.000786131, -0.000871983, 2.024892132, 2.0330665,
                                   1.992755189, 1.304610844, 1.
                                  129813816, 1.28206048, 0.523716983,
                                   0.62108267, 0.633964385, 0.
                                  274642702    , 0.281492488, 0.
                                  287137657 ]

E = [0.904618352, 0.72783015, 0.807314419, 0.043535219, 0.043710968, 0
                                  .042844274, 0.68245115,0.59101359,0
                                  .670654896,0.65253645,0.773851324,
                                  0.789901574,0.876422753, 0.
                                  898281367]
F = [-0.000795187,-0.000639785,-0.000709654,1.647936767,1.654589388,1.
                                  621782459,1.061743557,0.919486869,1
                                  .043391185,0.426221455,0.505461477,
                                  0.515945122,0.22351502,0.229089646
                                  ]
```

```
C = [ 1.00000032, 0.955558889, 0.753748061, 0.426828315, 0.020575759 ]
D = [ -0.000827828, 0.269614007, 0.544472129, 0.734328285, 0.861342695
                                    ]

t = np.linspace(-1, 0.98, 300)

r = np.sqrt( ( 4-(4*t) / (0.98)  ) )

f = plt.figure(figsize=(8,4))

#plt.plot(Ktest1,  Ktest2, linestyle='-', c='k', label=r'$ B \alpha =
                                    0 $', linewidth=0.5)
plt.plot(t,r,linestyle='-', c='k', label=r'Richard $\alpha_{1} = 0.496
                                    , \alpha_{2} = 0.178 $', linewidth=
                                    0.6)


plt.plot(A, B, ls="None",label = 'Mixed Mode Test Data', marker="o",
                                    markersize=5 , markerfacecolor='
                                    white' ,markeredgewidth=0.5, c='k'
                                    ,)
#plt.plot(E, F, ls="None",label = 'Mixed Mode Test Data', marker="^",
                                    markersize=4 , markerfacecolor='
                                    white' ,markeredgewidth=0.5, c='k
                                    ',)
plt.plot(C,  D, linestyle='-.', c='k', label=r'GMTS', linewidth=1, )
plt.plot(KI,  KII, linestyle=':', c='k', label=r' MTS', linewidth=1, )
#plt.plot(KI2, KII2, linestyle='-', marker='o' , markersize=4.5 ,
                                    markerfacecolor='k'   ,
                                    markeredgewidth=0.5, markevery=20,
                                    c='k', label=r'$ B \alpha =   0.2 $
                                    ', linewidth=0.75,)
#plt.plot(KI3, KII3, linestyle='-', marker='s' , markersize=4 ,
                                    markerfacecolor='k'     ,
                                    markeredgewidth=0.5 , c='k', label=
                                    r'$ B \alpha =   0.375 $',
                                    linewidth=0.75,)
#plt.plot(KI4, KII4, linestyle='-', marker='o' , markersize=5 ,
                                    markerfacecolor='white' ,
                                    markeredgewidth=0.5,  markevery=8 ,
                                     c='k', label=r'$ B \alpha = - 0.2
                                    $', linewidth=0.75,)
#plt.plot(KI5, KII5, linestyle='-', marker='s' , markersize=4 ,
                                    markerfacecolor='white' ,
                                    markeredgewidth=0.5 , markevery=8 ,
                                     c='k', label=r'$ B \alpha = - 0.4
                                    $', linewidth=0.75,)
#plt.plot(KI6, KII6, linestyle='-', marker='^' , markersize=5 ,
                                    markerfacecolor='white' ,
                                    markeredgewidth=0.5 , markevery=8 ,
                                    c='k', label=r'$ B \alpha = - 0.6 $
                                    ', linewidth=0.75,)


plt.gca().invert_yaxis()
plt.gca().set_xlim([-0.001,1.2])
```

```
plt.gca().set_ylim([-0.01,3])
plt.ylabel(r'Normalized Mode II,  $ K_{II} / K_{IC}$ ')
plt.xlabel(r'Normalized Mode I,   $ K_{I}  / K_{IC}$ ')
plt.grid(True, linestyle=':')
legend = plt.legend(frameon = 1, fancybox=False, framealpha=1)
frame = legend.get_frame()
frame.set_facecolor('white')
frame.set_edgecolor('k')
frame.set_linewidth(0.7)

plt.savefig("K_I_II_TESTDATA.pdf", bbox_inches='tight')

plt.show()
```

P Python Script For Mixed Mode I/III Crack Angle Plots

```
import matplotlib.pyplot as plt
import numpy as np
import math
from numpy import genfromtxt
import matplotlib

matplotlib.rcParams['text.latex.preamble']=[r"\usepackage{lmodern}", r
                                    "\usepackage[utf8x]{inputenc}", r"\
                                    usepackage[T1]{fontenc}" ]

params = {'text.usetex' : True,
          'font.size' : 11,
          'font.family' : 'lmodern',
          'text.latex.unicode': True,
          }

matplotlib.rcParams.update(params)


plt.rcParams['grid.alpha'] = 1
plt.rcParams['grid.color'] = "#cccccc"

A = [0.024143993, 0.923423517, 0.835689684, 0.662136782, 0.99]
B = [-42.02       , -19.23       , -37.08        , - 46.71       , -0
                                    ]

C = [0.99,0.923423517,  0.835689684, 0.662136782, 0.024143993 ]
D = [ -0.038512885 , -18.82641591,-29.68205096 ,-37.53015091, -45.
                                    17161807 ]

x = np.arange(0 , -70.5, -0.1) # Grid of 0.01 spacing from -2 to 10
pi = math.pi
B0 = 0
v = 0.35
#B02 = 0.2
#B04 = 0.3

cos2 = np.cos(((x*pi)/180)*2)
sin2 = np.sin(((x*pi)/180)*2)
cos = np.cos((x*pi)/180)
sin = np.sin((x*pi)/180)
tan2 = np.tan(((x*pi)/180)/2)

Me =  (2/pi) * np.arctan( (-2*cos2) / sin )

Me2 = (2/pi) * np.arctan( 2/ ( np.tan(((x*pi)/180)*2) * (2*v - 1) ) )


f = plt.figure(figsize=(8,4))

plt.plot(C,  D, linestyle='--', c='k', label=r'GMTS', linewidth=0.5, )
                                    #GMTS
```

```
plt.plot(A, B, ls="None",label = 'Mixed Mode Test Data', marker="o",
                                    markersize=6 , markerfacecolor='
                                    white' ,markeredgewidth=0.5, c='k'
                                    ,)

plt.plot(Me, x, linestyle='-', c='k', label=r'MTS (Plane Stress) ',
                                    linewidth=0.5)
plt.plot(Me2, x, linestyle=':', c='k', label=r'MTS (Plane Strain)',
                                    linewidth=0.75,)

plt.gca().invert_yaxis()
plt.gca().set_xlim([0,1.2])
plt.gca().set_ylim([0,-80])
plt.ylabel(r'Crack Initiation Angle,  $\phi_{f}$ ')
plt.xlabel(r'Mixity Parameter, $ M^{e}_{13} $ ')
plt.legend(loc='lower left')
plt.grid(True, linestyle=':')


legend = plt.legend(frameon = 1, fancybox=False, framealpha=1)
frame = legend.get_frame()
frame.set_facecolor('white')
frame.set_edgecolor('k')
frame.set_linewidth(0.7)


plt.savefig("Theta_I_III_TESTDATA.pdf", bbox_inches='tight')

plt.show()
```

Q Python Script For Mixed Mode I/III Fracture Limit Plots

```
import matplotlib.pyplot as plt
import numpy as np
import math
from numpy import genfromtxt
import matplotlib

import subprocess

###FONT SETUP
#matplotlib.rcParams['mathtext.fontset'] = 'stix'
#matplotlib.rcParams['font.family'] = 'STIXGeneral'
#matplotlib.pyplot.title(r'ABC123 vs $\mathrm{ABC123}^{123}$')
####


plt.rcParams['grid.alpha'] = 1
plt.rcParams['grid.color'] = "#cccccc"

plt.rcParams['text.latex.preamble']=[r"\usepackage{lmodern}"]
#Options
params = {'text.usetex' : True,
          'font.size' : 11,
          'font.family' : 'lmodern',
          'text.latex.unicode': True,
          }

plt.rcParams.update(params)


A = [ 1.11,0.89,0.99,0          , 0          , 0          , 1.
                                    336726596, 1.216868273, 1.130682478
                                    , 1.953731944, 1.937279662, 2.
                                    153666337, 2.352231729, 2.252176913
                                    , 2.249900729 ]
B = [ 0   ,0   ,0   ,6.131755706, 5.719717566, 5.014213785, 0.
                                    161569562, 0.147082339, 0.1366651
                                    , 0.515757908, 0.511414736, 0.
                                    568537792, 1.38047055 , 1.321750686
                                    , 1.320414846 ]

C = [0.036768501, 0.689267153, 0.869332424, 0.960421104]
D = [0.974867142, 0.403952147, 0.229012625, 0.115950058]



x = np.arange(0 , -45, -0.01) # Grid of 0.01 spacing from -2 to 10
pi = math.pi
B0 = 0
v = 0.35
#B02 = 0.2
#B04 = 0.3
t = np.linspace(-1, 1, 300)
```

```
cos2 = np.cos(((x*pi)/180)*2)
sin2 = np.sin(((x*pi)/180)*2)
cos = np.cos((x*pi)/180)
sin = np.sin((x*pi)/180)
tan2 = np.tan(((x*pi)/180)*2)

r = np.sqrt( (4- (4*t)) / (0.13) )

Me = (2/pi) * np.arctan( (-2*cos2) / sin )


K1MTS = 1 / (   ( cos ) - ( (sin * sin2) / (-2 * cos2) )   )
K3MTS = 1 / ( (-2* cos2 / sin) - sin2   )

KI_0 = 1 / ( (cos**2) - ( ( tan2 * (2*v -1) * sin2 ) /2 )  + ( 2 * v *
                                    sin**2 ) )
KIII_0 = 1 /  ( ( (2 * (cos**2) ) / ( tan2 * (2*v-1) ) ) + ( ( 4*v * (
                                   sin**2) ) / ( tan2 * ( (2 *v) -1) )
                                     ) - sin2    )


f = plt.figure(figsize=(8,4))

plt.plot(A, B, ls="None",label = 'Mixed Mode Test Data', marker="o",
                                   markersize=6 , markerfacecolor='
                                   white' ,markeredgewidth=0.5, c='k'
                                   ,)
plt.plot(t,r,linestyle='-', c='k', label=r'Richard $\alpha_{1} = 0.50,
                                    \alpha_{2} = 0.18 $', linewidth=0.
                                   6)
plt.plot(C,  D, linestyle='-.', c='k', label=r'GMTS', linewidth=0.5, )
plt.plot(K1MTS,  K3MTS, linestyle=':', c='k', label=r'MTS (Plane
                                   Stress) ', linewidth=0.5)
plt.plot(KI_0,  KIII_0, linestyle='--', c='k', label=r'MTS (Plane
                                   Strain) ', linewidth=0.5)
#plt.plot(KI_0, KIII_0, linestyle=':', marker='o' , markersize=4.5 ,
                                   markerfacecolor='white'   ,
                                   markeredgewidth=0.5, markevery=100,
                                    c='k', label=r'$ B \alpha =   0  $
                                    (Plane Strain) ', linewidth=0.75,)
#plt.plot(KI3, KII3, linestyle='-', marker='s' , markersize=4 ,
                                   markerfacecolor='k'     ,
                                   markeredgewidth=0.5 , c='k', label=
                                   r'$ B \alpha =   0.375 $',
                                   linewidth=0.75,)
#plt.plot(KI4, KII4, linestyle='-', marker='o' , markersize=5 ,
                                   markerfacecolor='white' ,
                                   markeredgewidth=0.5,  markevery=8 ,
                                    c='k', label=r'$ B \alpha = - 0.2
                                   $', linewidth=0.75,)
#plt.plot(KI5, KII5, linestyle='-', marker='s' , markersize=4 ,
                                   markerfacecolor='white' ,
                                   markeredgewidth=0.5 , markevery=8 ,
                                    c='k', label=r'$ B \alpha = - 0.4
                                   $', linewidth=0.75,)
```

```
#plt.plot(KI6, KII6, linestyle='-', marker='^' , markersize=5 ,
                                    markerfacecolor='white' ,
                                    markeredgewidth=0.5 , markevery=8 ,
                                    c='k', label=r'$ B \alpha = - 0.6 $
                                    ', linewidth=0.75,)


#plt.gca().invert_yaxis()
plt.gca().set_xlim([-0.01,2.5])
plt.gca().set_ylim([-0.05,6.5])

#plt.gca().set_xlim([-0.01,1.1])
#plt.gca().set_ylim([-0.05,1.1])

plt.ylabel(r'Normalized Mode III,  $ K_{III} / K_{IC}$ ')
plt.xlabel(r'Normalized Mode I, $ K_{I} / K_{IC}$ ')
plt.legend(loc='upper right', frameon=True).get_frame().set_edgecolor(
                                    'k')
plt.grid(True, linestyle=':')
legend = plt.legend(frameon = 1, fancybox=False, framealpha=1)
frame = legend.get_frame()
frame.set_facecolor('white')
frame.set_edgecolor('k')
frame.set_linewidth(0.7)


#plt.savefig("K_I_III_TESTDATA.pdf", bbox_inches='tight')

plt.show()
```

R Python Script For Three-Dimensional Richard Criterion

```
import matplotlib as plt
from mpl_toolkits.mplot3d import Axes3D
import numpy as np
import matplotlib.pyplot as plt
import pylab
import scipy
import matplotlib

matplotlib.rcParams['text.latex.preamble']=[r"\usepackage{lmodern}", r
                                    "\usepackage[utf8x]{inputenc}", r"\
                                    usepackage[T1]{fontenc}" ]

params = {'text.usetex' : True,
          'font.size' : 11,
          'font.family' : 'lmodern',
          'text.latex.unicode': True,
          }

matplotlib.rcParams.update(params)

fig = plt.figure(figsize = (7, 7))
ax = fig.gca(projection='3d')

A = [ 1.111544218,  0.894316805,  0.991982611, 0.053493632, 0.
                                    053709582, 0.052644637, 0.838557639
                                    , 0.726204302, 0.824063064, 0.
                                    801800136, 0.950865039, 0.970586684
                                    , 1.076899049, 1.103757686, 1.
                                    125892908]
B = [0           , 0           , 0           , 2.024892132, 2.0330665,
                                     1.992755189, 1.304610844, 1.
                                    129813816, 1.28206048, 0.523716983,
                                     0.62108267, 0.633964385, 0.
                                    274642702    , 0.281492488, 0.
                                    287137657 ]
C = [0        , 0         , 0         , 0           , 0         , 0
                                    , 0           , 0         , 0
                                            , 0       ,  0       , 0
                                           , 0             , 0
                                    , 0]

D = [ 0           , 0           , 0           , 1.895418023, 1.996767496,
                                     1.834027641, 2.220125775, 2.
                                    081226443, 2.272753189, 2.492993292
                                    , 2.137855032,2.500409935 ]
E = [4.644961061 , 5.460748305, 4.767531798, 0.384132874, 0.404672757,
                                     0.371691258, 1.0455161, 0.
                                    980104721, 1.070299745, 2.738277296
                                    , 2.348197211, 2.746423657  ]
F = [0        , 0         , 0         , 0           , 0         , 0
                                    , 0           , 0         , 0
                                    , 0         ,  0        , 0
```

```
                                        ]

G = [ 0           , 0           , 0           , 1.336726596, 1.216868273,
                                     1.130682478, 1.953731944, 1.
                                    937279662, 2.153666337, 2.352231729
                                    , 2.252176913, 2.249900729 ]
H = [ 6.131755706, 5.719717566, 5.014213785, 0.161569562, 0.147082339,
                                     0.1366651  , 0.515757908, 0.
                                    511414736, 0.568537792, 1.38047055
                                    , 1.321750686, 1.320414846 ]
I = [0        , 0         , 0         , 0           , 0         , 0
                                    , 0           , 0         , 0
                                    , 0         ,  0        , 0
                                        ]

J = [0.185773577,0.079965391,0.053474155,1.169966461,1.182980523,0.
                                    793439555,1.745670835,1.430518873,1
                                    .170262109,1.942424082, 1.695922817
                                    ]

K = [0.05433908,0.054494085,0.085858618,0.311519427,0.758185373,1.
                                    211466534,0.440306579,0.869843338,1
                                    .695699301,0.519240325, 1.08444708]

L = [5.793867375,3.595005689,4.80359327,0.154905901,0.209702979,0.
                                    262940998,0.505182819,0.556282387,0
                                    .852769474,1.274894862, 1.550765372
                                    ]

x = np.linspace(0, 6.5, 300)
y = np.linspace(0, 1, 300)

[x, y] = scipy.meshgrid(x, y)

#z = np.sqrt( (4* (1-y-(x**2))) / (5.336)  )
z = np.sqrt( ( 4 - (4*y) - (0.13* (x**2) ) ) / (0.96)  )

ax.plot(C,A,B, ls="None",label = 'Mixed Mode I/II Test Data', marker="
                                    o", markersize=6 , markerfacecolor=
                                    'white' ,markeredgewidth=0.5, c='k'
                                    ,)
ax.plot(E,F,D, ls="None",label = 'Mixed Mode II/III Test Data', marker
                                    ="^", markersize=6 ,
                                    markerfacecolor='white' ,
                                    markeredgewidth=0.5, c='k',)
ax.plot(H,G,I, ls="None",label = 'Mixed Mode I/III Test Data', marker=
                                    "s", markersize=6 , markerfacecolor
                                    ='white' ,markeredgewidth=0.5, c='k
                                    ',)
ax.plot(J,K,L, ls="None",label = 'Mixed Mode I/II/III Test Data',
                                    marker="D", markersize=5.6 ,
                                    markerfacecolor='white' ,
                                    markeredgewidth=0.5, c='k',)

ax.plot_wireframe(x, y, z, label = r'Richard $\alpha_{1} = 0.50, \
                                    alpha_{2} = 0.18 $', rstride=5,
```

```
                                    cstride=5, alpha=0.9 , color= 'k',
                                    edgecolor = 'k', linewidth=0.4,
                                    linestyle = '-')
#ax.plot(X, Y, linestyle = '-', color= 'k', linewidth = 0.8)

ax.zaxis.set_rotate_label(False) # To disable automatic label rotation

ax.set_xlabel('${K_{III} / K_{IC}}$')
ax.set_ylabel('$K_{I} / K_{IC}$')
ax.set_zlabel('$K_{II} / K_{IC}$', rotation=90)

#ax.set_title('Hokstad')

ax.set_xlim3d(0, 6.5)
ax.set_ylim3d(0, 2.5)
ax.set_zlim3d(0, 2.75)

#ax.legend(borderpad=0.3, frameon=True).get_frame().set_edgecolor('k')
#ax.legend()
legend = ax.legend(frameon = 1, fancybox=False, framealpha=1, ncol=2,
                                    loc='upper right')
frame = legend.get_frame()
frame.set_facecolor('white')
frame.set_edgecolor('k')
frame.set_linewidth(0.7)

ax.azim = 45
#ax.elev = -45

plt.savefig("3dplot_newKic.pdf", bbox_inches='tight')

pylab.show()
```